

A COMPARISON AND OUTLINE OF TOLERANCES IN  
PERFORMING OPTICAL TIME DIVISION MULTIPLEXING  
USING ELECTRO-ABSORPTION MODULATORS

by

MARK OWSIAK

A thesis submitted to the  
Department of Electrical and Computer Engineering  
in conformity with the requirements for  
the degree of Master of Applied Science

Queen's University  
Kingston, Ontario, Canada

May 2010

Copyright © Mark Owsiak, 2010

# Abstract

As high bandwidth applications continue to emerge, investigation in technologies that will increase transmission capacity become necessary. Of these technologies, Optical Time Division Multiplexing (OTDM) has been presented as a possible solution, supporting a next generation bit rate of 160 Gbit/s. To perform the demultiplexing task, the use of tandem electro-absorption modulators (EAMs) has been widely studied, and due to its benefits was chosen as the topology of this thesis.

To create an effective model of an OTDM system, the vector based mathematical simulation tool MatLab is used. Care was taken to create an accurate representation of an OTDM system, including: the development of a realistic pulse shape, the development of a true pseudo-random bit sequence in all transmitted channels, the optimization of the gating function, and the representation of system penalty.

While posing impressive bit rates, various sources of system performance degradation pose issues in an OTDM system, owing to its ultra-narrow pulse widths. The presence of dispersion, timing jitter, polarization mode dispersion, and nonlinear effects, can sufficiently degrade the quality of the received data. This thesis gives a clear guideline to the tolerance an OTDM system exhibits to each of the aforementioned sources of system penalty. The theory behind each impairment is thoroughly discussed and simulated using MatLab. From the simulated results, a finite degree

of sensitivity to each source of system penalty is realized. These contributions are of particular importance when attempting to implement an OTDM system in either the laboratory, or the field.

# Acknowledgments

I would like to dedicate this thesis to my family. The unwavering support and encouragement of: my parents, Mary and Joe Owskiak, my sister and her husband, Erika and Mike Clements, my grandmother Maria Nariwonczyk, and my aunt Margret Nariwonczyk, has made this work possible. I would like to add to this dedication my deceased grandparents, Teresa and Kazimierz Owskiak and Stephan Nariwonczyk, for helping shape my mind towards education in my early years.

I would like to thank the members of the Lightwave System Research Laboratory at Queen's University. In particular I would like to express my appreciation to Chris Ito, David Krause, and Iannick Monfils. The discussions, and simply time spent with them, provided a foundation for the work presented in this document. I am privileged to have had the opportunity to work with them.

Lastly, I would like to thank my supervisor, Dr. John Cartledge for our constructive conversations, his helpful suggestions, and patient direction. His advice and guidance have added depth and reinforcement to this thesis and my own abilities.

# Table of Contents

|   |             |
|---|-------------|
| <b>Abstract</b>   | <b>i</b>    |
| <b>Acknowledgments</b>  | <b>iii</b>  |
| <b>Table of Contents</b>  | <b>iv</b>   |
| <b>List of Figures</b>  | <b>viii</b> |
| <b>List of Acronyms</b>   | <b>xiv</b>  |
| <b>Chapter 1: Introduction</b> . . . . .  | <b>1</b>    |
| 1.1 Problem Statement . . . . .   | 1           |
| 1.2 Available Technologies . . . . .  | 4           |
| 1.2.1 Introduction . . . . .  | 4           |
| 1.2.2 Four-Wave Mixing in Semi-Conductor Optical Amplifiers . . .                       | 5           |
| 1.2.3 Semi-Conductor Optical Amplifier based Symmetric Mach-Zehnder<br>Switch . . . . . | 8           |
| 1.2.4 Gain Transparent Nonlinear Optical Interferometer . . . . .                       | 10          |
| 1.2.5 Travelling-Wave Electro-Absorption Modulator . . . . .                            | 14          |
| 1.2.6 Electro-Absorption Modulator and Phase Lock Loop . . . . .                        | 17          |
| 1.3 EAMs for Practical Implementation . . . . .   | 20          |

|   |               |
|---|---------------|
| <b>Chapter 2: Simulated System Architecture . . . . .</b> | <b>23</b>     |
| 2.1 Introduction . . . . .                                | 23            |
| 2.2 Measures of System Performance . . . . .              | 24            |
| 2.2.1 Introduction . . . . .                              | 24            |
| 2.2.2 Eye-Opening Factor Penalty . . . . .                | 24            |
| 2.2.3 Eye-Opening Penalty . . . . .                       | 28            |
| 2.2.4 Power Penalty . . . . .                             | 29            |
| 2.3 Transmitter Design . . . . .                          | 34            |
| 2.3.1 Introduction . . . . .                              | 34            |
| 2.3.2 Simulated Implementation . . . . .                  | 35            |
| 2.3.3 Generating an OTDM Signal . . . . .                 | 37            |
| 2.4 Fiber Model . . . . .                                 | 40            |
| 2.4.1 Introduction . . . . .                              | 40            |
| 2.4.2 Simulated Fiber Spans . . . . .                     | 41            |
| 2.5 Demultiplexer Design . . . . .                        | 46            |
| 2.5.1 Introduction . . . . .                              | 46            |
| 2.5.2 EAM Gate Model . . . . .                            | 47            |
| 2.5.3 Optimization of Gates . . . . .                     | 54            |
| 2.6 Receiver Design . . . . .                             | 56            |
| 2.6.1 Introduction . . . . .                              | 56            |
| 2.6.2 System Implementation . . . . .                     | 57            |
| 2.7 Defining System Performance . . . . .                 | 59            |
| <br><b>Chapter 3: Transmission Impairments . . . . .</b>  | <br><b>63</b> |
| 3.1 Introduction . . . . .                                | 63            |

|   |  |           |
|---|--|-----------|
| 3.2   | Dispersion . . . . .                   | 64        |
| 3.2.1   | Background . . . . .                   | 64        |
| 3.2.2   | Compensation Methodology . . . . .     | 66        |
| 3.3   | Jitter . . . . .                       | 69        |
| 3.3.1   | Background . . . . .                   | 69        |
| 3.4   | Polarization Mode Dispersion . . . . . | 72        |
| 3.4.1   | Background . . . . .                   | 72        |
| 3.5   | Non-Linear Effects . . . . .           | 74        |
| 3.5.1   | Background . . . . .                   | 74        |
| <b>Chapter 4: Simulation Results &amp; Discussion . . . . .</b> |  | <b>77</b> |
| 4.1   | Introduction . . . . .                 | 77        |
| 4.2   | Global Operating Conditions . . . . .  | 77        |
| 4.3   | Dispersion . . . . .                   | 78        |
| 4.3.1   | Introduction . . . . .                 | 78        |
| 4.3.2   | System Tolerance . . . . .             | 78        |
| 4.4   | Jitter . . . . .                       | 97        |
| 4.4.1   | Introduction . . . . .                 | 97        |
| 4.4.2   | System Tolerance . . . . .             | 98        |
| 4.5   | Polarization Mode Dispersion . . . . . | 106       |
| 4.5.1   | Introduction . . . . .                 | 106       |
| 4.5.2   | System Tolerance . . . . .             | 106       |
| 4.6   | Non-Linear Effects . . . . .           | 112       |
| 4.6.1   | Introduction . . . . .                 | 112       |
| 4.6.2   | System Tolerance . . . . .             | 112       |

|   |            |
|---|------------|
| <b>Chapter 5: Conclusions</b> . . . . . | <b>119</b> |
| 5.1 Thesis Contributions . . . . .      | 119        |
| 5.2 The Future of OTDM . . . . .        | 121        |
| <b>Bibliography</b> . . . . .           | <b>122</b> |

# List of Figures

|     |   |    |
|-----|---|----|
| 1.1 | Graphical representation of the generation of optical time division multiplexing (OTDM) signals. . . . .  | 3  |
| 1.2 | Schematic of planar lightwave circuit (PLC) used to perform demultiplexing by utilizing four wave mixing (FWM) in semi-conductor optical amplifiers (SOAs). . . . . | 6  |
| 1.3 | Spectrum resulting after FWM product is generated (before optical bandpass filter (OBPF)). . . . .  | 7  |
| 1.4 | Schematic representing the utilization of a symmetric Mach-Zehnder (SMZ) for use in demultiplexing OTDM signals. . . . .  | 9  |
| 1.5 | gain transparent ultrafast-nonlinear interferometer (GT-UNI) used in demultiplexing 160 Gbit/s OTDM signals. . . . .  | 11 |
| 1.6 | Schematic representation of demultiplexing from 40 Gbit/s to 10 Gbit/s using a travelling wave electro-absorption modulator (TW-EAM). . .                           | 15 |
| 1.7 | Schematic representation of demultiplexing from 160 Gbit/s to 10 Gbit/s using two TW-EAMs. . . . .  | 16 |
| 1.8 | Configuration of a concatenated EAM scheme to demultiplex 160 Gbit/s OTDM Signals. . . . .  | 17 |
| 1.9 | Driving waveform showing a strong 10 GHz component on a 40 GHz sinusoid. . . . .  | 18 |

|      |  |    |
|------|--|----|
| 2.1  | Visual depiction of how the EOF is determined. . . . .   | 26 |
| 2.2  | Visual depiction of how the EOP is determined. . . . .   | 27 |
| 2.3  | Visual aid of how the receiver sensitivity is calculated. . . . .  | 30 |
| 2.4  | Visual depiction of separating the inner sampled data of the eye-diagram. . . . .  | 31 |
| 2.5  | Schematic of simulated transmitter design. . . . .   | 36 |
| 2.6  | Hyperbolic secant and gaussian pulse shape comparison. . . . .   | 37 |
| 2.7  | Diagram of resulting bit-sequence after interleaving 16 tributary sigals. . . . .  | 39 |
| 2.8  | Graphical representation of using 4:1 multiplexors to bit-interleave and<br>maintain a PRBS signal. . . . .  | 39 |
| 2.9  | Graphically shows how a series of 2:1 multiplexors with appropriate<br>signal delays maintain a PRBS signal. . . . .   | 40 |
| 2.10 | Visual aid in describing the split-step Fourier method. . . . .  | 44 |
| 2.11 | Schematic for driving EAMs with different frequencies. . . . .   | 46 |
| 2.12 | Schematic for driving EAMs with a sum of frequencies. . . . .  | 47 |
| 2.13 | Absorption characteristics for: (a) 40 GHz EAM (b) 10 GHz EAM. . . . .   | 49 |
| 2.14 | Back-to-back OTDM Signal, 40 GHz and 10 GHz EAM optimal switch-<br>ing windows. . . . .  | 50 |
| 2.15 | (a) Penalty (EOFP) that arises from varying $A_1$ and $B_1$ with $D_2(t)$ set<br>with optimal values. (b) Example of change in 40 GHz EAM switching<br>window (Peak Voltage = 0.6 V, Reverse Bias = 1.7 V). (c) Electrical<br>eye-diagram. . . . . | 51 |

|      |  |    |
|------|--|----|
| 2.16 | (a) Penalty (EOFP) that arises from varying $A_2$ and $B_2$ with $D_1(t)$ set with optimal values. (b) Example of change in 10 GHz EAM switching window (Peak Voltage = 0.7 V, Reverse Bias = 1.45 V). (c) Electrical eye-diagram. . . . . | 52 |
| 2.17 | Effect on EOF by varying driving waveform amplitude. . . . .   | 55 |
| 2.18 | Effect on EOF by varying driving waveform phase. . . . .   | 55 |
| 2.19 | Effect on EOF by varying driving waveform bias. . . . .  | 56 |
| 2.20 | Schematic of simulated receiver design. . . . .  | 57 |
| 2.21 | Penalty agreement when measuring residual dispersion. . . . .  | 60 |
| 2.22 | Penalty agreement when measuring dispersion slope. . . . .   | 61 |
| 3.1  | The effect of SMF dispersion slope on the optical signal spectrum of 160 Gbit/s and 10 Gbit/s bit rates. . . . .   | 65 |
| 3.2  | Visual representation and values for perfect dispersion and dispersion slope compensation. . . . .   | 69 |
| 4.1  | Back-to-back eye-diagram. . . . .  | 83 |
| 4.2  | Penalty (EOP) due to changes of residual dispersion. . . . .   | 83 |
| 4.3  | Electrical eye-diagram evolution with an equivalent residual dispersion of: (a) 0.86 ps/nm, (b) 1.29 ps/nm, (c) 1.71 ps/nm, (d) 2.14 ps/nm, (e) 2.57 ps/nm, and (f) 3.0 ps/nm. . . . .   | 84 |
| 4.4  | From left to right: optical eye-diagrams taken before the demultiplexer, after the demultiplexer, followed by the electrical eye-diagram, for a residual dispersion of: (a) 0.86 ps/nm , (b) 1.29 ps/nm, and (c) 1.71 ps/nm. . . . .       | 85 |

|      |   |    |
|------|---|----|
| 4.5  | From left to right: back-to-back (B2B) optical eye-diagrams taken before the demultiplexer, after the demultiplexer, followed by the electrical B2B eye-diagram. . . . .  | 86 |
| 4.6  | From left to right: optical time-domain OTDM signal taken before and after the demultiplexer, for a residual dispersion of: (a) 0.86 ps/nm , (b) 1.29 ps/nm, and (c) 1.71 ps/nm. . . . .  | 87 |
| 4.7  | Time domain 160 Gbit/s OTDM signal, and both EAM switching windows. . . . .   | 88 |
| 4.8  | Electrical eye-diagram evolution with an equivalent dispersion slope length product of: (a) 1.43 ps/nm <sup>2</sup> , (b) 2.14 ps/nm <sup>2</sup> , (c) 2.86 ps/nm <sup>2</sup> , (d) 3.57 ps/nm <sup>2</sup> , (e) 4.29 ps/nm <sup>2</sup> , and (f) 5.00 ps/nm <sup>2</sup> . . . . . | 89 |
| 4.9  | Penalty (EOP) due to increased residual dispersion slope. . . . .   | 90 |
| 4.10 | From left to right: optical eye-diagrams taken before the demultiplexer, after the demultiplexer, followed by the electrical eye-diagram, for a dispersion slope length product of: (a) 2.14 ps/nm <sup>2</sup> , (b) 2.86 ps/nm <sup>2</sup> , (c) 3.57 ps/nm <sup>2</sup> . . . . .   | 91 |
| 4.11 | From left to right: optical time-domain OTDM signal taken before and after the demultiplexer, for a dispersion slope length product of: (a) 2.14 ps/nm <sup>2</sup> , (b) 2.86 ps/nm <sup>2</sup> , (c) 3.57 ps/nm <sup>2</sup> . . . . .   | 92 |
| 4.12 | Visual representation of perfectly compensated dispersion curve. Lengths of SMF and DCF are 50 km and 14.583 km respectively. . . . .   | 94 |
| 4.13 | Electrical eye-diagrams for: (a) uncompensated signal after 50 km of single-mode fiber (SMF), and (b) fully dispersion compensated received electrical signal. . . . .  | 94 |

|      |   |     |
|------|---|-----|
| 4.14 | Penalty (EOP) due to change in length of DCF. . . . .   | 96  |
| 4.15 | Jitter is simulated by altering the sampling time of the decision threshold.  | 99  |
| 4.16 | Penalty (EOP) due to sampling the eye-diagram at various times. . .   | 100 |
| 4.17 | Electrical eye-diagram evolution with $T_s$ in the amount of: (a) 0.781 ps, (b) 1.172 ps, (c) 1.562 ps, (d) 1.758 ps, (e) 1.953 ps, and (f) 2.148 ps.   | 101 |
| 4.18 | From left to right: optical eye-diagrams taken before the demultiplexer, after the demultiplexer, followed by the electrical eye-diagram, for $T_s$ equal to: (a) 1.562 ps, (b) 1.758 ps, (c) 1.953 ps. . . . .                                 | 102 |
| 4.19 | From left to right: optical time-domain OTDM signal taken before and after the demultiplexer, for $T_s$ equal to: (a) 1.562 ps, (b) 1.758 ps, (c) 1.953 ps. . . . .   | 103 |
| 4.20 | Penalty (EOP) due to change in $T_s$ on the demultiplexing EAM gates.   | 105 |
| 4.21 | Illustration showing the delay in arrival time associated with PMD. .   | 107 |
| 4.22 | Penalty (EOP) due to increased amount of PMD. . . . .   | 108 |
| 4.23 | Electrical eye-diagrams, taken after the receiver, for a shift of the perpendicularly travelling mode by: (a) 0.39 ps, (b) 0.78 ps, (c) 1.17 ps, (d) 1.56 ps, (e) 1.95 ps, and (f) 2.73 ps. . . . .   | 109 |
| 4.24 | From left to right: optical eye-diagrams taken before the demultiplexer, after the demultiplexer, followed by the electrical eye-diagram, for a shift of the perpendicularly travelling mode by: (a) 0.78 ps, (b) 1.95 ps, (c) 2.73 ps. . . . . | 110 |
| 4.25 | From left to right: optical time-domain OTDM signal taken before and after the demultiplexer, for a shift of the perpendicularly travelling mode by: (a) 0.78 ps, (b) 1.95 ps, (c) 2.73 ps. . . . .   | 111 |

|      |   |     |
|------|---|-----|
| 4.26 | Diagram outlining the placement of amplifiers in a typical fiber transmission link. . . . . | 114 |
| 4.27 | Resulting values of $G_1$ due to changes of $P_{in,SMF}$ and $P_{in,DCF}$ . . . . .         | 116 |
| 4.28 | Resulting values of $G_2$ due to changes of $P_{in,SMF}$ and $P_{in,DCF}$ . . . . .         | 116 |
| 4.29 | Penalty (EOP) due to changes in both SMF and DCF input powers. . . . .                      | 118 |

# List of Acronyms

|             |                                       |
|-------------|---------------------------------------|
| <b>WDM</b>  | wavelength division multiplexing      |
| <b>OTDM</b> | optical time division multiplexing    |
| <b>DFB</b>  | distributed feedback                  |
| <b>RZ</b>   | return-to-zero                        |
| <b>FWHM</b> | full width at half maximum            |
| <b>ISI</b>  | inter-symbol interference             |
| <b>ETDM</b> | electrical time division multiplexing |
| <b>PMD</b>  | polarization mode dispersion          |
| <b>FWM</b>  | four wave mixing                      |
| <b>SOA</b>  | semi-conductor optical amplifier      |
| <b>PLC</b>  | planar lightwave circuit              |
| <b>CW</b>   | continuous waveform                   |
| <b>MMI</b>  | multi-mode-interface                  |

|               |   |
|---------------|---|
| <b>OBPF</b>   | optical bandpass filter                             |
| <b>ASE</b>    | amplified spontaneous emission                      |
| <b>SMZ</b>    | symmetric Mach-Zehnder                              |
| <b>MLLD</b>   | mode-locked laser diode                             |
| <b>PC</b>     | polarization controller                             |
| <b>BER</b>    | bit-error rate                                      |
| <b>PLL</b>    | phase-locked loop                                   |
| <b>PRBS</b>   | pseudo-random bit sequence                          |
| <b>PDL</b>    | polarization dependent loss                         |
| <b>SMF</b>    | single-mode fiber                                   |
| <b>GT-UNI</b> | gain transparent ultrafast-nonlinear interferometer |
| <b>EDFA</b>   | erbium doped fiber amplifier                        |
| <b>PBS</b>    | polarization beam splitter                          |
| <b>hibi</b>   | highly birefringent                                 |
| <b>MQW</b>    | multiple quantum well                               |
| <b>UNI</b>    | ultrafast-nonlinear interferometer                  |
| <b>BPF</b>    | bandpass filter                                     |
| <b>CD</b>     | chromatic dispersion                                |

|               |  |
|---------------|--|
| <b>S</b>      | dispersion slope                             |
| <b>DCF</b>    | dispersion compensating fiber                |
| <b>TW-EAM</b> | travelling wave electro-absorption modulator |
| <b>EAM</b>    | electro-absorption modulator                 |
| <b>RMS</b>    | root-mean-square                             |
| <b>E-O</b>    | electro-optic                                |
| <b>EDFA</b>   | erbium-doped fiber amplifier                 |
| <b>EOFP</b>   | eye-opening factor penalty                   |
| <b>EOP</b>    | eye-opening penalty                          |
| <b>PP</b>     | power penalty                                |
| <b>B2B</b>    | back-to-back                                 |
| <b>EOF</b>    | eye-opening factor                           |
| <b>NRZ</b>    | non-return-to-zero                           |
| <b>SPM</b>    | self phase modulation                        |
| <b>EO</b>     | eye-opening                                  |
| <b>EC</b>     | eye-closure                                  |
| <b>MZM</b>    | Mach Zehnder modulator                       |
| <b>DCM</b>    | dispersion compensating module               |

|                |                                    |
|----------------|------------------------------------|
| <b>FT</b>      | Fourier transform                  |
| <b>SNR</b>     | signal-to-noise ratio              |
| <b>OSNR</b>    | optical signal-to-noise ratio      |
| <b>NZDSF</b>   | non-zero dispersion shifted fiber  |
| <b>RDS</b>     | relative dispersion slope          |
| <b>CDR</b>     | clock-and-data recovery            |
| <b>RJ</b>      | random jitter                      |
| <b>DJ</b>      | deterministic jitter               |
| <b>SRS</b>     | stimulated Raman scattering        |
| <b>SBS</b>     | stimulated Brillouin scattering    |
| <b>XPM</b>     | cross-phase modulation             |
| <b>TX</b>      | transmitter                        |
| <b>RX</b>      | receiver                           |
| <b>JT</b>      | jitter tolerance                   |
| <b>DGD</b>     | differential group delay           |
| <b>NDSF</b>    | non-zero dispersion shifted fiber  |
| <b>CS-RZ</b>   | carrier-suppressed return-to-zero  |
| <b>RZ-DPSK</b> | RZ-differential-phase-shift-keying |

# Chapter 1

## Introduction

### 1.1 Problem Statement

The telecommunications industry has flourished in recent years as the requirements demanded by an ever growing list of high-bandwidth services continues to grow. Of these applications, most prominent is clearly the Internet and the services that are provided to users through its infrastructure. Once used most frequently for the transmission of conventional web sites, software, data and email, the evolving digital world has given it new purposes: downloading music, streaming video, and recently, telephone conversations through internet based phone companies. It has become clear to both researchers and investors alike that due to this increase there is a requirement for new technologies capable of supporting these demands[1].

Several technologies have been investigated in recent years to satisfy this increased demand in bandwidth. The most popular of these are wavelength division multiplexing (WDM), and 40 Gbit/s infrastructures, while optical time division

multiplexing (OTDM) techniques have not been as widely developed. In WDM, several optical signals are transmitted over a single fiber utilizing different wavelengths. By 2001, transmissions of up to 10 Tbit/s using 256 channels were demonstrated over distances of 200 km[2]. In 2008, a bit-rate of 25.6 Tbit/s was achieved over three 80 km spans of single-mode fiber (SMF) and 160 WDM channels[3]. The ultimate capacity of WDM systems is dependant upon how closely channels may be spaced within the wavelength domain[2]. Limiting factors of WDM performance include the stability and tunability of distributed feedback (DFB) lasers, signal degradation due to nonlinear effects, and various sources of interchannel crosstalk[2]. WDM has had a great degree of success in laboratories and is widely deployed commercially.

With WDM engaged in the frequency domain, OTDM focuses on increasing transmission capacity by multiplexing tributary optical signals in the time domain. A representation of how OTDM signals are constructed is shown in Figure 1.1. Several tributary signals are interleaved together by time-shifting very low duty-cycle pulses, and superimposing them on top of each other, forming the composite signal. Each channel is shifted by an amount of  $(n-1)/NB$ , for  $n=1,\dots,N$ , where  $N$  denotes the number of tributary signals and  $B$  is the tributary bit rate[2]. The resulting OTDM bit rate is simply the product of  $N$  and  $B$ . It is clear that the duty cycle of the tributary signals should be chosen such that each bit would occupy one bit period of the desired OTDM bit rate ( $NB$ ). Before reaching their respective destinations, each tributary signal must be demultiplexed from the OTDM signal and converted back to its tributary bit rate. Due to the high bandwidth demands of an OTDM system, the return-to-zero (RZ) format must be used. The spacing between neighbouring bits of the OTDM signal is often chosen to four times the full width at half

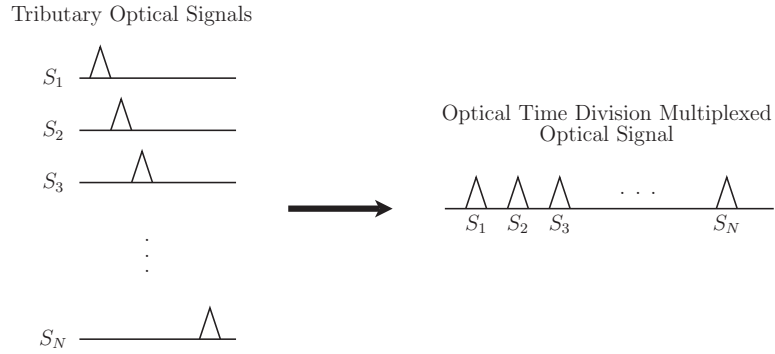


Figure 1.1: Graphical representation of the generation of OTDM signals.

maximum (FWHM) of the optical pulse at the desired bit rate[2]. Due to the high bandwidth nature of OTDM, inter-symbol interference (ISI) would occur for very short lengths of fiber as a result of dispersion. Transmission is only possible when the optical fiber is coupled with some method of dispersion compensation.

Although the methodology of OTDM may sound similar to that of electrical time division multiplexing (ETDM), it poses a different set of problems that must be thoroughly investigated to be effective. At such high bit rates, fiber dispersion becomes a limiting factor and must be mitigated. Other limiting factors include polarization mode dispersion (PMD), fiber non-linearity, and jitter associated with both the demultiplexing and clock recovery units.

A commonly investigated OTDM bit rate is 160 Gbit/s, as it is considered to be the next generation bit rate in optical communications[1]. In this thesis, the 160 Gbit/s data will be comprised of 16 very low duty cycle ( $\approx 2.2\%$ ) tributary signals at 10 Gbit/s. This combination of signals has been widely studied using various technologies capable of demultiplexing the OTDM signal. It is also possible to achieve 160 Gbit/s by using 4 OTDM channels at a tributary rate of 40 Gbit/s. This may be

more common in recent studies as 40 Gbit/s has become increasingly the standard. Of the demultiplexing techniques, five will be discussed in this chapter, outlining their methodology, topology, as well as advantages and disadvantages of each. Clearly a reduced number of components is of great interest as it reduces both the cost and complexity of the resulting system[4]. To achieve this high bandwidth transmission, the synchronization of the clock with the data is essential. This is true in all OTDM demultiplexing technologies as it ultimately determines how well the tributary 10 Gbit/s optical signals are extracted from the multiplexed data.

From the forthcoming discussion of the various OTDM demultiplexing technologies, a clear choice based on advantages in terms of ease of integration (how well can the technology be integrated with existing networks), cost (in terms of complexity or number of components), and performance will be made. The remainder of this document will comprise of testing OTDM demultiplexing against various sources of system impairment. The research that leads to these conclusions is being done in an effort to provide a better blueprint and guideline as to the performance of the technology in question. This investigation is necessary because of the fine constraints of an OTDM system, as well as various installation and environmental difficulties that may arise in a commercial deployment.

## **1.2 Available Technologies**

### **1.2.1 Introduction**

With the large amount of OTDM research being performed, several different methods have been proposed to achieve the performance required of such a system. For these

various techniques, important considerations are performance, complexity, and degree of control. Each method essentially performs the same task using a different set of tools, resulting in different consequences. They must gate the appropriate bits from a high speed OTDM signal such that one of the tributary signals becomes incident on the receiver.

Five of these available technologies will be discussed in the subsections below. Each methodology will be described in detail, and its principle of operation explained. The advantages and disadvantages of each will also be noted so that a clear decision can be made as to which technique may be most suitable for implementation with existing networks.

### **1.2.2 Four-Wave Mixing in Semi-Conductor Optical Amplifiers**

The method described in this technique is particularly unique in comparison to others that will be discussed. The majority of the technologies being investigated by researchers, as well as those presented here, do not demultiplex all OTDM channels in parallel[5]. The use of four wave mixing (FWM) in a semi-conductor optical amplifier (SOA) lends itself to an integrated approach when used with planar light-wave circuit (PLC) technology. This in turn keeps the device size small and provides more functionality than other techniques that may only demultiplex one OTDM channel. Figure 1.2 shows the physical representation of this topology. Dashed lines are used to clearly distinguish the various paths traversed by the OTDM signal.

The demultiplexing apparatus utilizes two input ports, one is used as the optical input for the 160 Gbit/s OTDM data ( $\lambda = 1554$  nm), and the other for an optical

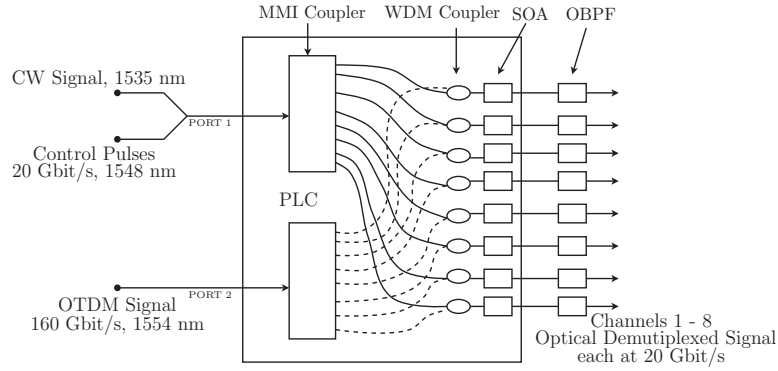


Figure 1.2: Schematic of PLC used to perform demultiplexing by utilizing FWM in SOAs.

control pulse train operating at a frequency of 20 GHz ( $\lambda = 1548$  nm), and a continuous waveform (CW) source ( $\lambda = 1535$  nm)[5]. The duty cycle of the control pulses were chosen such that the width of each bit was equal to the width of the OTDM signal's bit period. Both input ports lead to individual multi-mode-interface (MMI) couplers where they are separated with a 1:8 ratio. Each waveguide exiting a MMI coupler is traversed along a path of different length to inflict the correct amount of delay on the corresponding signal. These delays are then matched to the specific control pulses which have also experience their own delay for use in channel selection. The PLC then uses 8 WDM couplers to effectively combine the signal and control pulse, followed by 8 SOAs in which the FWM process would occur. When FWM occurs, a new signal is created alongside the existing data and control pulses. More specifically, FWM generates a new signal at a frequency[2],

$$\omega_{ijk} = \omega_i + \omega_j - \omega_k, \quad (1.1)$$

when waves at frequencies  $\omega_i$ ,  $\omega_j$ , and  $\omega_k$  co-propagate in an optical medium. In this

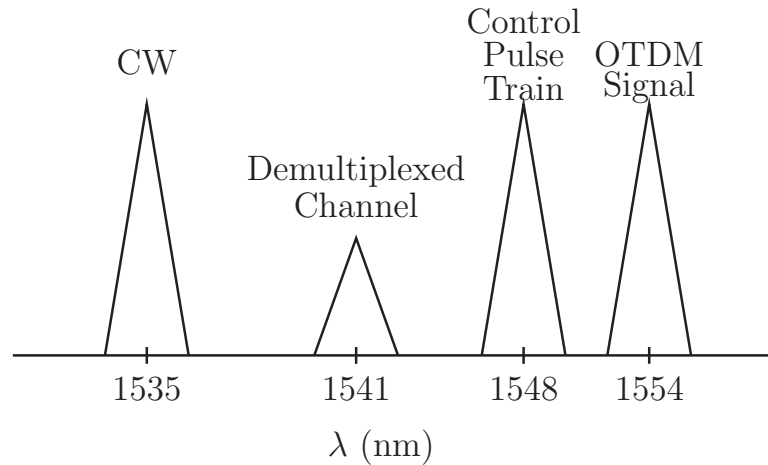


Figure 1.3: Spectrum resulting after FWM product is generated (before OBPF).

case,  $\omega_i = \omega_{OTDM}$ ,  $\omega_j = \omega_{CW}$ , and  $\omega_k = \omega_{control}$ , resulting in the FWM product at  $\lambda = 1541$  nm. This result is shown graphically in Figure 1.3. SOAs were used to generate this response because their fast response to nonlinear effects, and ability to produce gain, result in a high conversion efficiency. The demultiplexed data was filtered out of each channel by means of an optical bandpass filter (OBPF)[5].

A clear advantage to this technique is not only the reduced size of the device (135mm x 40mm), but also that several OTDM channels are demultiplexed in parallel. Even more impressive however, is that this technique operates all optically without the use of any high speed microwave components. This is advantageous because microwave components may generate crosstalk during signal extraction as well as limit the overall speed of the demultiplexer[5].

There are several drawbacks associated with this technique as well. Firstly, the integrated PLC demultiplexer only separates the 160 Gbit/s into 8 20 Gbit/s optical signals. To fully demultiplex the data to the tributary rate of 10 Gbit/s, an

external lithium niobate demultiplexer is used on each of the 8 channels. This adds additional complexity as 8 recovered clock signals are also necessary. The 20 Gbit/s control pulses must also be matched to the repetition rate of the OTDM modulation frequency. Secondly, a power penalty of 2 to 4.5 dB is observed among fully demultiplexed channels (10 Gbit/s each) mainly due to thermal crosstalk between the 8 SOAs[5]. SOAs provide an extra source of penalty due to their generation of amplified spontaneous emission (ASE) noise, and waveform distortions on account of their slow carrier recovery. Lastly, received power differences of approximately 2.5 dB are observed between the 16 tributary signals, and are believed to be caused by the FWM efficiency difference of the SOAs, as well as peak power differences in the OTDM signal[5]. Differences in these efficiencies may be brought about by slightly different values of gain and coupling losses between neighbouring SOAs.

### 1.2.3 Semi-Conductor Optical Amplifier based Symmetric Mach-Zehnder Switch

The configuration presented in this subsection demonstrates simultaneous demultiplexing and clock recovery from a 160 Gbit/s OTDM signal to a 10 Gbit/s signal, using a single symmetric Mach-Zehnder (SMZ) switch and a mode-locked laser diode (MLLD) in an electro-optic loop oscillator configuration[6].

The apparatus consists of the following components: a SMZ, two OBPFs, a polarization controller (PC), two optical delay lines  $\phi_1$  and  $\phi_2$ , a MLLD, two attenuators, an electrical delay line  $E\phi$ , and an electrical high-Q filter and amplifier. The MLLD acts as a local oscillator emitting a 10 GHz signal and enabled the demultiplexing operation by generating synchronous control pulses[6]. The electrical spectrum of

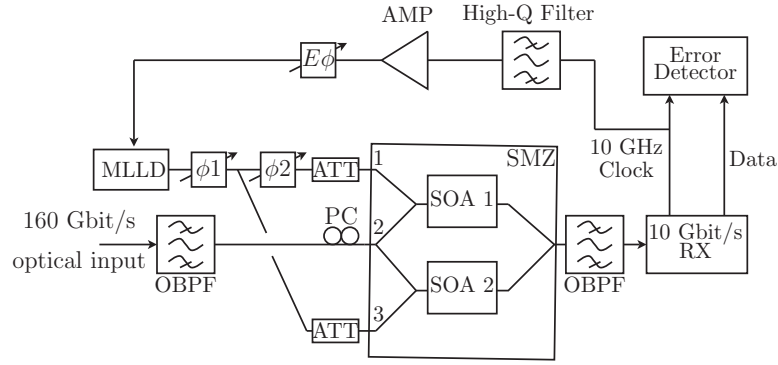


Figure 1.4: Schematic representing the utilization of a SMZ for use in demultiplexing OTDM signals.

the MLLD was monitored, and by adjusting  $E\phi$ , mode-locking was established and the noise level minimized[6]. Further adjustment to  $E\phi$  was performed by observing the bit-error rate (BER) at the receiver. The 160 Gbit/s signal enters port 2 of the device. Ports 1 and 3 contain control signals generated via the MLLD. The input control pulses directed to port 3 are only affected by an attenuator and  $\phi_1$ , which was used to select the correct channel for demultiplexing[6]. The input to port 1, however, is affected by both  $\phi_1$  and  $\phi_2$ , which was noted to adjust the width of the gate used during switching[6]. Upon exiting the SMZ, the 10 Gbit/s signal enters the receiver, which is followed by clock extraction via a phase-locked loop (PLL) and BER analysis.

The most dominant advantage to this technique is that there is no need for ultra-fast optical gate switches or high-speed electronic components. This is possible because the SMZ performed as a phase comparator as well as a demultiplexing unit[6].

A discussion of some numeric results reveals various disadvantages. The OTDM signal entering the demultiplexing unit was chosen to have a pseudo-random bit

sequence (PRBS) of  $2^{15} - 1$  as to avoid a pattern-length dependency of the SMZ[6]. This may result in an unrealistic data stream as the demultiplexed data will not hold a similar pattern[7]. Furthermore, the use of a SMZ in itself gave way to a 1-dB power penalty because of its polarization dependent loss (PDL) characteristics[6].

#### 1.2.4 Gain Transparent Nonlinear Optical Interferometer

With the majority of experiments testing the feasibility of OTDM taking place in a laboratory, the following researched method is more realistic and has been tested over 116 km of field-installed SMF[1]. The information presented pertaining to the setup is quite detailed and informative in comparison to other experiments. Care was also taken with the shape of the input pulse, the maintenance of a PRBS, and optimization of the switching window. As this method has been documented in greater detail when comparing other techniques, it has also been more widely adopted by researchers investigating OTDM relevant technologies. Such technologies independent of the demultiplexing action can include: tunable dispersion compensators and clock recovery methods.

The optical demultiplexer described was a gain transparent ultrafast-nonlinear interferometer (GT-UNI), and demultiplexes the input pulses from 160 Gbit/s to 40 Gbit/s. It consists of an erbium-doped fiber amplifier (EDFA), a polarization beam splitter (PBS), a highly birefringent (hibi) fiber, a circulator, and a SOA. After the data is amplified by the EDFA, it was injected into a PBS and exits via port 3. The state of polarization of the input OTDM signal was controlled during its construction. Each channel was adjusted such that the final OTDM signal was in a single state of polarization. At launch, the optical signal was split into orthogonally

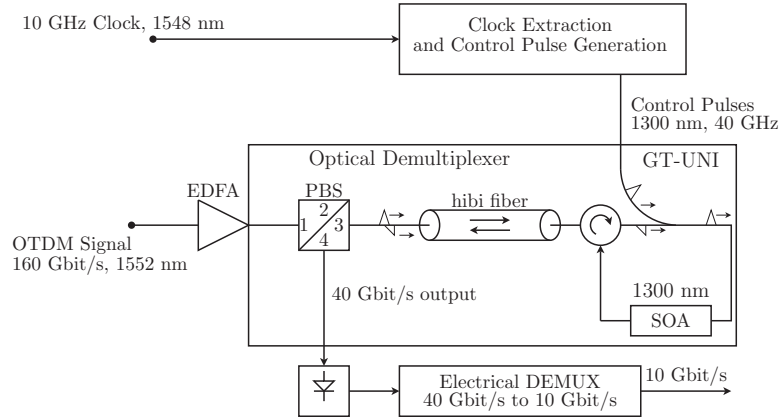


Figure 1.5: GT-UNI used in demultiplexing 160 Gbit/s OTDM signals.

polarized components of equal amplitude[1]. This was done by launching the signal with the appropriate polarization with respect to the principle axis of the hibi fiber[1]. Upon exiting the hibi fiber, the polarization components were delayed in time with respect to one another. This delay is determined by the PMD characteristics and length of the hibi fiber. After passing through the circulator, a 40 GHz control pulse was combined with the signal for channel selection, and both were launched into a polarization insensitive multiple quantum well (MQW) SOA, which is chosen for its nonlinear properties. The pulses were then sent in a backward direction through the same hibi fiber via the circulator. The polarization of the data being sent backward was chosen such that the delay between the two pulses is now reversed and they recombine after the length of the fiber.

The authors of the paper improved the performance of the ultrafast-nonlinear interferometer (UNI) by making two changes to the setup first proposed in [8, 9]. Their first change was to implement a folded geometry, as opposed to a linear setup, to increase the device stability. The second improvement was the addition of a gain

transparent scheme, which improved the linearity of the switch and also reduced noise during transmission. Gain transparency occurs because the control pulses propagate inside the SOAs gain region and result in a refractive index change outside the gain region at the data wavelength[10]. They note that the gain transparent scheme also guarantees that ISI is negligible. As with most OTDM demultiplexers, this methodology extracts only one tributary channel of the OTDM signal. To demultiplex all 16 channels simultaneously, 4 instances of the apparatus shown in Figure 1.5 must be used. Channel selection was achieved by changing the relative delay between the control pulses and the data signal.

The method in which the selected channel leaves the demultiplexer is effective yet not intuitive. The polarization of the recombined pulse (after travelling backwards through the hibi fiber), depends on the phase shift that trailing pulse is subjected to in the loop containing the MQW-SOA. If the pulses encountered an equal shift, then their polarization is the same as the input pulse, and data passes through to port 1 of the PBS, leaving no data to exit the demultiplexer. However, when the control pulse is injected between the polarization separated pulses, the trailing component will be subjected to an additional non-linear phase shift in the SOA loop. This will result in the pulse, after recombination, having a different polarization, and in turn, that pulse will exit via port 4 of the PBS.

In the optimization of their switching window, a 20 dB extinction ratio was achieved. However, they achieved this when demultiplexing to an optical base rate of 40 Gbit/s. When attempting to demultiplex to a tributary rate of 10 Gbit/s a 6 dB penalty incurred in the extinction ratio attributed to smaller nonlinear phase changes at a higher repetition rate of control pulses. A 14 dB degradation of the extinction

ratio would be detrimental to system performance as described in [11]. To avoid such penalties, an electrical demultiplexer was implemented to bring the 40 Gbit/s signal to a final rate of 10 Gbit/s.

To achieve synchronization of the data, a 10 GHz sinusoid was transmitted at a wavelength of 1548 nm, and was extracted by a series of bandpass filters (BPFs). The extracted clock was then used to synchronize a MLLD which generated the 40 GHz control pulses at 1300 nm.

Upon measurement of the 160 Gbit/s signal, receiver sensitivities were -22.4 dBm and -20.7 dBm for tributary rates of 10 Gbit/s and 40 Gbit/s at a BER of  $10^{-9}$ . The authors attributed this loss to the fact that their ETDM receiver was not optimized for RZ signals. Furthermore, they state the importance of the compensation of both chromatic dispersion (CD) and dispersion slope (S) for high single channel data rates and achieved tolerances of  $\pm 50$  m for SMF fiber lengths, and  $\pm 9$  m in dispersion compensating fiber (DCF) lengths (as used in a dispersion compensating scheme). Also made clear was that PMD is to be considered a limiting factor in OTDM transmission.

While adequate performance was achieved with this technique, there are drawbacks that can be noted through the above discussion. Of them, the complexity of such an implementation can be noted as the use of hibi fiber, two electrical multiplexing/demultiplexing units, PBSs, and amplifiers per channel, make this a highly involved solution for practical real world implementation. Another consequence of this technique is the great amount of polarization control needed to achieve the noted performance, especially at a data rate of 160 Gbit/s. As stated above, the poor extinction ratio will also result in unwanted penalties.

### 1.2.5 Travelling-Wave Electro-Absorption Modulator

The proposed method of using a travelling wave electro-absorption modulator (TW-EAM) has come about relatively recently in comparison to other available technologies. It does, however, provide another alternative to existing methods used for demultiplexing OTDM signals with competitive results. A reduced system cost and simultaneous operation of clock recovery and demultiplexing was achieved by taking special care to reduce the number of components needed during operation[4]. Like many techniques, the use of a PLL was implemented for clock recovery as it has been thoroughly investigated in both electronic and optoelectronic applications[4]. TW-EAMs may also be implemented in WDM systems, performing both wavelength conversion, and regeneration[12].

The experimental setup to demultiplex 40 Gbit/s to a base rate of 10 Gbit/s consists of one TW-EAM, an amplifier, an OBPF, and a PLL for clock extraction. Shown in Figure 1.6, the TW-EAM has two optical ports, and two electrical ports. The top and right side ports were designated for outputs, and the bottom and left side port were used as inputs. A 40 Gbit/s signal at  $\lambda_1$  was injected into the left side input port along with a CW signal at a separate wavelength  $\lambda_2$ . Exiting the upper port is a 40 GHz tone from the photocurrent, as well as the 10 GHz clock which is applied to the bottom input port. The 10 GHz clock was removed at the input of the clock recovery unit by a BPF. The 40 GHz tone was needed by the clock recovery unit to generate a 10 GHz sinusoid used for the demultiplexing operation. The 3-dB bandwidth of the TW-EAM is 12 GHz, which results in a 10 Gbit/s signal exiting via the right side output port at a wavelength of  $\lambda_1$ . At the wavelength designated by  $\lambda_2$ , an optical clock also exits and was separated via OBPFs. This optical clock

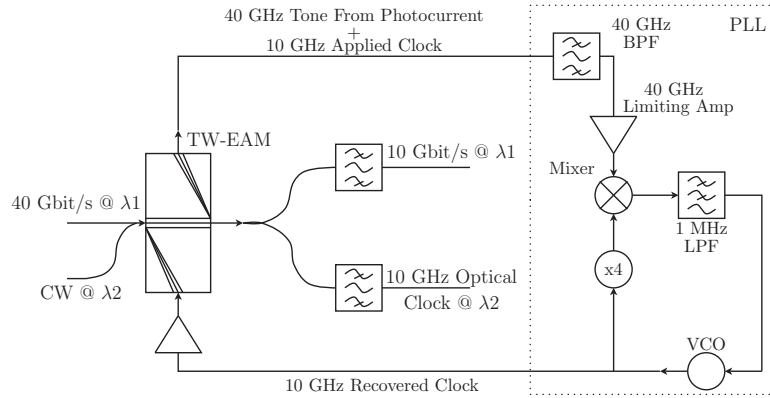


Figure 1.6: Schematic representation of demultiplexing from 40 Gbit/s to 10 Gbit/s using a TW-EAM.

was generated by the injected CW signal on the left input port. The recovered clock exiting the PLL is directed back into the lower port of the TW-EAM, with a proper phase delay, to achieve demultiplexing of a desired channel. Good performance was achieved with this technique as it shows a root-mean-square (RMS) timing jitter on the clock of only 223 fs (typical of PLL based clock recovery units), and a receiver sensitivity of approximately -36.5 dBm for a BER of  $10^{-9}$ .

To extend this method to 160 Gbit/s the addition of a second TW-EAM was implemented with a special standing-wave enhanced design. The setup is similar to that described above, except that the upper output port of the second additional TW-EAM (TW-EAM2) was terminated and extended to optimize the 40 GHz electro-optic (E-O) response. The only other additional components necessary are another amplifier and a multiplier to generate a 40 GHz clock, which was to be applied to TW-EAM2 as shown in Figure 1.7. The addition of an EDFA and optical filter between TW-EAM1 and TW-EAM2 was utilized to compensate for the added losses

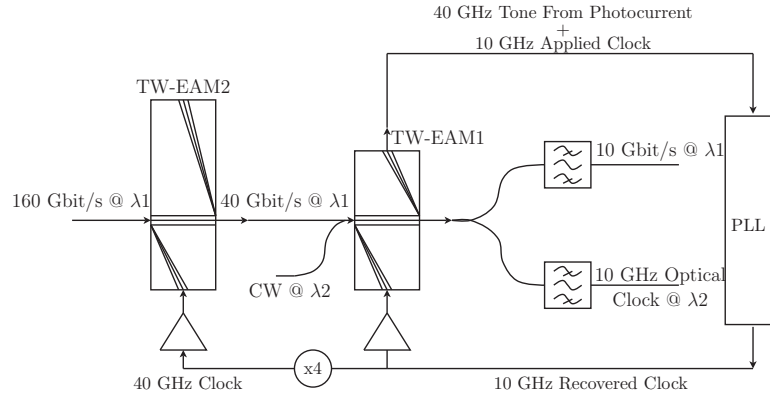


Figure 1.7: Schematic representation of demultiplexing from 160 Gbit/s to 10 Gbit/s using two TW-EAMs.

that incurred.

Disadvantages of this technology, in demultiplexing 160 Gbit/s OTDM signals, comes with the addition of TW-EAM2. Firstly, a standing-wave enhanced design is required to optimize the 40 GHz E-O response at the upper port. TW-EAM2 gives rise to additional penalty by the addition of a polarization dependence of approximately 10 dB. The authors note that this can be reduced by properly compensating the strain in the quantum wells. The tails of the pulses exiting the ring laser (used in pulse generation) are compressed nonlinearly and result in a longer tail to the pulses exiting this type of demultiplexer as well. Due to the resulting ISI, the 160 Gbit/s signal was multiplexed using opposite states of polarization; a process in which adjacent channels carry opposite states of polarization. This was done to accommodate the higher loss of TM polarized channels, which in turn reduces the effects of the incurring ISI. However, the complexity of the system will be increased at both the transmitter and receiver to accomplish this task. TW-EAM2 was also determined to be sensitive

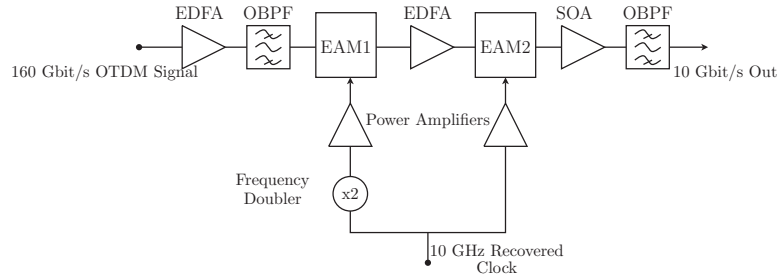


Figure 1.8: Configuration of a concatenated EAM scheme to demultiplex 160 Gbit/s OTDM Signals.

to input power, therefore further restricting performance. While achievable, it seems clear that demultiplexing the data rate of interest (160 Gbit/s) by the addition of TW-EAM2, results in many sources of additional system penalty.

### 1.2.6 Electro-Absorption Modulator and Phase Lock Loop

The use of electro-absorption modulators (EAMs) has become a widely accepted method of performing both demultiplexing and clock recovery of high speed OTDM signals. Advantages of using these devices include their stability, compactness, low driving voltages and good switching window characteristics[13, 14]. Due to their availability and the scalability of the technique, much research has gone into developing this method as a viable solution to high speed demultiplexing and clock recovery with the aid of a PLL.

There have been several variations to the experimental setup proposed in Figure 1.8, however, the use of two concatenated devices seems to dominate the currently published literature. The driving waveform and number of EAMs used have been altered in other attempts, such as in [14], [15], and [16]. The methods outlined

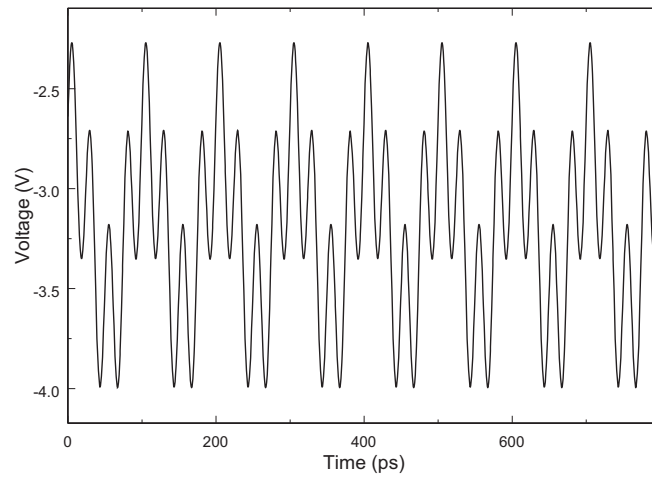


Figure 1.9: Driving waveform showing a strong 10 GHz component on a 40 GHz sinusoid.

in [14] and [15] exhibit techniques in which a 40 GHz sinusoid causes the EAM to gate the OTDM signal in 100 ps intervals (resulting in a 10 Gbit/s tributary signal). Using Figure 1.9 as an example, the OTDM signal entering an EAM driven by this sinusoid will be passed through the gate every 100 ps as the reverse bias approaches -2 V. In [16], a self-cascaded EAM scheme is implemented, however, the duration of the switching window is not suitable for 160 Gbit/s demultiplexing (15.2 ps). In a standard concatenated EAM scheme, a 160 Gbit/s signal enters the first EAM which is driven by a 20 GHz sinusoid (limited by the EAM). Upon exit, the data is now at 20 Gbit/s as bits not selected by the EAM gate have been absorbed by the EAM itself. Similarly, the 20 Gbit/s signal exits the second EAM at a bit rate of 10 Gbit/s due to the 10 GHz driving waveform (the tributary rate). The data can then be used to keep the clock and data synchronized via a PLL, or passed to a receiver for the purpose of signal detection.

To demultiplex all 16 channels of a 160 Gbit/s OTDM signal, the aforementioned topology must appear in a receiver 16 times. This is similar to the other methods investigated, except that of the PLC topology presented in Section 1.2.2. The switching window produced a suppression ratio of 23 dB over a 4 ps duration[13]. Timing jitter on the recovered clock is said to be below 230 ps which decreases with an increase in input power[13]. An example of the data rate scalability of this technique is shown in [17]. By simply driving the first EAM at 40 GHz as opposed to 20 GHz, researchers were able to successfully demultiplex and recover a clock from a 320 Gbit/s signal using a nearly identical technique based on EAMs. A scheme using 40 GHz and 10 GHz to drive the first and second EAMs may also be used to demultiplex a 160 Gbit/s

OTDM signal. In this case, the neighbouring bits are far more suppressed. This results in a 40 Gbit/s optical signal exiting the first EAM as opposed to the 20 Gbit/s mentioned above. To avoid waveform distortions, a 40 GHz EAM must be used.

One might argue that due to the use of microwave components, the choice of EAMs may not be favourable. Despite any opinion, EAMs hold much promise in the future of ultra high speed optical signal processing providing good performance with minimal complexity, and relatively simple control.

### 1.3 EAMs for Practical Implementation

Of all the technologies discussed above, the use of EAMs to demultiplex a high bit rate OTDM signal has been the most widely accepted and studied. Reasons for acceptance of EAMs for demultiplexing include system complexity considerations, and ability to be easily integrated into existing networks. Furthermore, the implementation of this technique requires only the use of commercially available components, producing an immediate and effective solution to performing OTDM[14]. EAMs can also be monolithically integrated with SOAs, resulting in the potential to decrease cost. They also exhibit low driving voltages, a high modulation efficiency, and a low polarization dependence[18].

In a real world implementation, the tandem EAM topology also fairs well compared to other techniques mainly due to the insensitivity EAMs exhibit towards changes of the input signal state of polarization. While other methods greatly depend on fine adjustment of polarization controllers or specialized proprietary component designs, the use of EAMs with a PLL will guarantee that the electrical clock signal tracks the data signal over the designed loop bandwidth. Channel selection is then

performed by changing the driving waveforms' relative phase by an amount equivalent to  $N$  bit periods to select the  $N^{\text{th}}$  channel.

Due to all the benefits that are present with the use of EAMs in high speed optical demultiplexing and clock recovery, it was decided that the research presented in this thesis investigate the performance trade-offs associated with their use. In Chapter 2 a description of the system performance measures will be presented. They will be used to characterize this technique in a way that would be consistent with resulting eye-diagrams. Also presented in Chapter 2 is a blueprint of the topology used during mathematical system simulation. In Chapter 3, the major sources of system penalty in performing OTDM transmission will be described. The method in which these impairments are simulated will also be outlined. Chapter 4 will provide numerical and graphical results that represent the limitations posed by each of the aforementioned impairments. Resulting trade-offs will be evaluated and discussed. Finally, Chapter 5 will provide a comprehensive summary of the findings presented in this research, as well as any future considerations that may be foreseen due to these findings, such as the importance of OTDM in pushing to even higher bandwidths through the use of WDM[5].

This thesis presents contributions in both the knowledge of implementing such an OTDM system, as well as understanding the system performance trade-offs incurred by various sources of penalty. The necessary implementation procedures of mathematically simulating an EAM based OTDM system are given and explained (including pulse shape importance and maintenance of a PRBS signal). Clear system performance concerns in regards to dispersion, dispersion slope, timing jitter, PMD, and non-linearities are explained and quantified. The tolerances calculated in this

thesis are of value when attempting to assemble and/or simulate such an OTDM system; in the laboratory, or in the field.

# Chapter 2

## Simulated System Architecture

### 2.1 Introduction

To evaluate the use of electro-absorption modulators (EAMs) as a suitable choice for demultiplexing optical time division multiplexing (OTDM) signals, a mathematical simulation capability was developed using MatLab. The following sections will first describe how the system performance is specified through the simulation. It will also show, for purposes of accuracy, that the three measures defined can actually be used interchangeably showing good agreement that the results to be presented in Chapter 4 are accurate. Finally, the system itself will be described, outlining both the physical components that are illustrated mathematically, as well as the various tasks that were necessary to provide an accurate representation of a real world implementation. MatLab was also used to verify that optimal conditions were met while performing these simulations. Details of the optimization are presented with respect to driving conditions of the EAMs.

## 2.2 Measures of System Performance

### 2.2.1 Introduction

In order to discuss how changes in various transmission impairments affect the overall system performance, it is important to define how these changes will be measured, as well as the system they are acting on. To perform these measurements, the electrical eye-diagram that results at the receiver was analyzed using three different methods: eye-opening factor penalty (EOFP), eye-opening penalty (EOP), and power penalty (PP).

In order to examine the amount of penalty incurred during simulation, a back-to-back (B2B) scenario was first realized to provide a basis for comparison. A B2B simulation represents a transmitted signal that has not undergone any signal distortions and is essentially error free. The penalty may be calculated by using a power ratio,

$$P(dB) = 10\log_{10} \left( \frac{M_{B2B}}{M_D} \right) \quad (2.1)$$

or a voltage ratio,

$$P(dB) = 20\log_{10} \left( \frac{M_{V,B2B}}{M_{V,D}} \right) \quad (2.2)$$

and is then represented in units of decibels (dB). In Eq. (2.1)  $M_{B2B}$  and  $M_D$  represent the B2B and distorted power measurements of the eye-diagram. Similarly in Eq. (2.2),  $M_{V,B2B}$  and  $M_{V,D}$  represent the B2B and distorted voltage measurements.

### 2.2.2 Eye-Opening Factor Penalty

The figure of merit known as eye-opening factor (EOF) is recognized in a technical brief by Tektronix as an accurate way to determine system performance based on

the measurements of an optical eye-diagram. The origin of the measurement came about as many optical systems were migrating to the return-to-zero (RZ) format and new techniques and tools were needed to provide a more accurate performance evaluation[19]. The RZ format was adopted as bandwidth demands continued to increase and it became more cost effective to change existing systems, rather than try to compensate for the limitations that non-return-to-zero (NRZ) bit patterns were inflicting[19]. Advantages of the RZ signal format compared to that of the NRZ format are predominant when implementing high bit rate, long-haul systems. Due to the shorter duration of the pulses, the data traverses the optical fiber with less distortion due to nonlinear effects (such as self phase modulation (SPM)) while transmitting at a lower average power[19]. However, this results in a larger bandwidth making RZ signals less tolerant to dispersive effects. Good dispersion compensating techniques can, and have been proven to help mitigate these effects. The result is a longer transmission distance containing more channels, thereby more effectively meeting the demands of increasing bit rates.

The measurement of EOF relies on the mean value of the marks and spaces ( $\mu_1$ ,  $\mu_0$ ), as well as their respective standard deviations ( $\sigma_1$ ,  $\sigma_0$ ). For these vertical measurements, 5% of the opening of the eye-diagram, centered at the maximum, was used to give the same statistical significance as an NRZ measurement[19]. The smaller time interval (NRZ requires 20% of the eye opening), is reflective of the smaller pulse width possessed by the RZ modulation format[19]. However, Tektronix was quick to note that because of this, four times the amount of data is also needed during data collection; thereby, taking four times as long in a physical experiment[19].

The EOF is defined as the ratio of the height of the eye-diagram opening, within

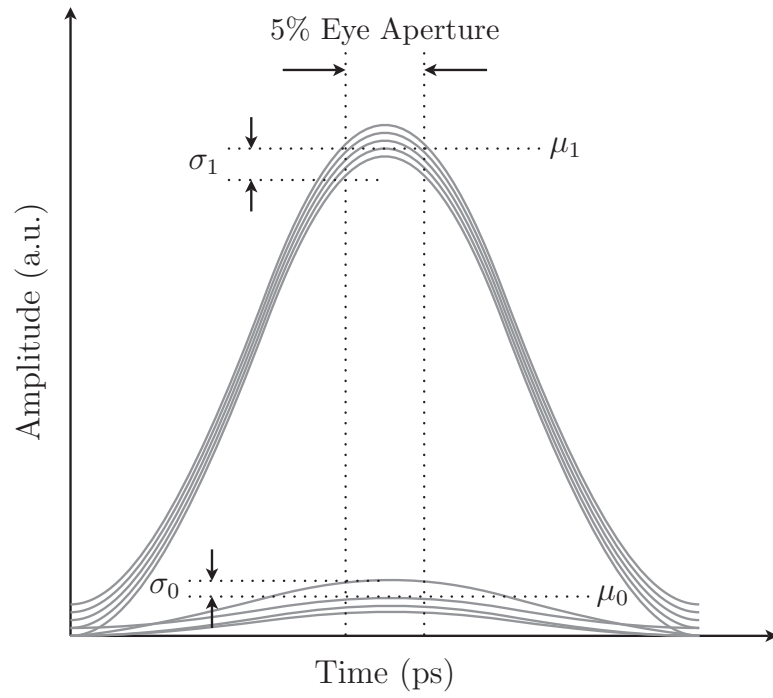


Figure 2.1: Visual depiction of how the EOF is determined.

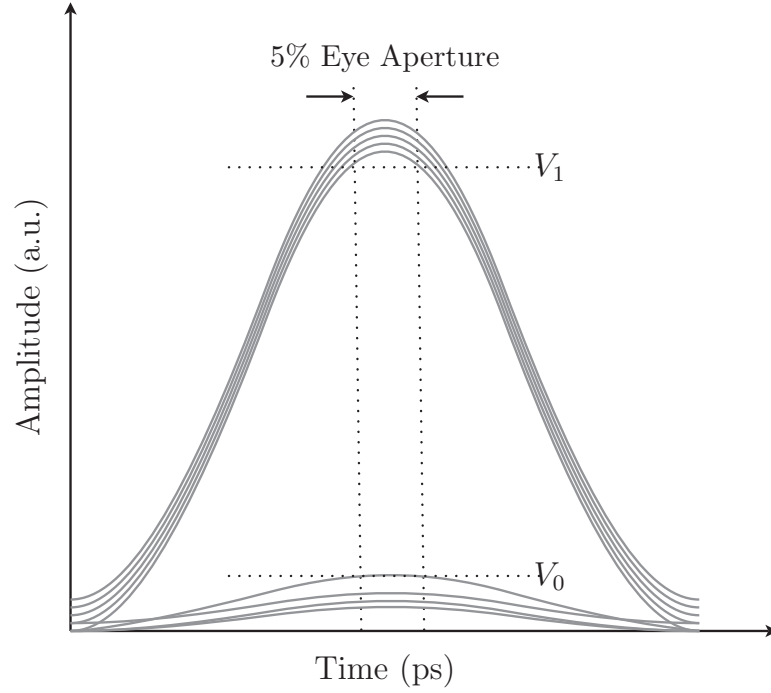


Figure 2.2: Visual depiction of how the EOP is determined.

one standard deviation of the amplitude[19]. Therefore, the equation defining EOF becomes,

$$EOF = \frac{(\mu_1 - \sigma_1) - (\mu_0 + \sigma_0)}{\mu_1 - \mu_0}. \quad (2.3)$$

The EOF parameters are related to an eye-diagram by Figure 2.1. The resulting measurement will give a fraction as to how open the eye-diagram is at the receiver. A completely open eye-diagram would be defined by an EOF of 1. Eq. (2.1) can then be used to produce a measurement of EOF.

### 2.2.3 Eye-Opening Penalty

The definition of EOP extends from that of the eye-opening (EO) which is synonymous with eye-closure (EC). Figure 2.2 and Eq. (2.4) show that the EO for an eye-diagram is simply  $V_1 - V_0$ [20]. During simulation, the values of  $V_1$  and  $V_0$  were taken as the minimum of the marks and the maximum of the spaces in the 5% window discussed above. The EOP is then defined as the ratio of an undistorted measurement of EO, to that of one containing distortions[20]. The critical aspect of this measurement is that both the distorted and undistorted signals must be under the same average power[20]. This was done in simulation by normalizing the signals to the same average power before conducting any further calculations. It should also be noted that because the noise is subtracted in the numerator for EOF, the result is a ratio less than 1. Alternatively with EOP, the noise in the denominator causes the ratio to be larger than 1.

$$EO = V_1 - V_0 \quad (2.4)$$

$$EOP = \frac{V_{1,u} - V_{0,u}}{V_{1,d} - V_{0,d}} \quad (2.5)$$

An explicit definition of EOP is shown in Eq. (2.5) where the subscript  $u$  and  $d$  signify the undistorted and distorted signals. As with the EOF, Eq. (2.1) is used where the B2B case is the same as the undistorted case. Therefore, EOP can be expressed in a dB value by Eq. (2.6).

$$EOP(dB) = 10\log_{10}(EOP) \quad (2.6)$$

As Eq. (2.5) is an electrical quantity, and given the relationship of optical power  $P$  and electrical field  $E$  ( $P \propto |E|^2$ ), Eq. (2.6) may also be calculated by means displayed

in Eq. (2.7) using a voltage ratio (as described in Eq. (2.2)).

$$\begin{aligned} EOP(dB) &= 10\log_{10}\left(\frac{|E_{B2B}|^2}{|E_M|^2}\right) \\ &= 20\log_{10}\left(\frac{|E_{B2B}|}{|E_M|}\right) \end{aligned} \quad (2.7)$$

The subscripts  $B2B$  and  $M$  represent the B2B and measured values of the electric field.

### 2.2.4 Power Penalty

The power penalty, regarding system performance, is governed by both the receiver sensitivity and the bit-error rate (BER). A receiver is considered more sensitive if it can achieve the same performance with less optical power incident upon it[2]. Therefore, the receiver sensitivity is defined in optical communications as the minimum average received power that is required to operate the system at a given BER (for example,  $10^{-9}$ )[2].

To calculate the receiver sensitivity during the MatLab simulation, we must first examine the opening of the received electrical eye-diagram. If the minimum value of the marks is greater than the maximum value of the spaces, the eye-diagram is referred to as open. If the opposite is true, the eye-diagram is closed and cannot be used for evaluation. As we are only interested in obtaining the best performance, the entire eye-diagram need not be examined. Instead, only sample times near the pulse center are considered. This is shown qualitatively in Figure 2.3. The number of sampling times used near the center of the pulse may be adjusted to ensure the simulator does not conclude that an endpoint is optimal. For each instance in time within this window, the values of marks and spaces are separated along with the signal

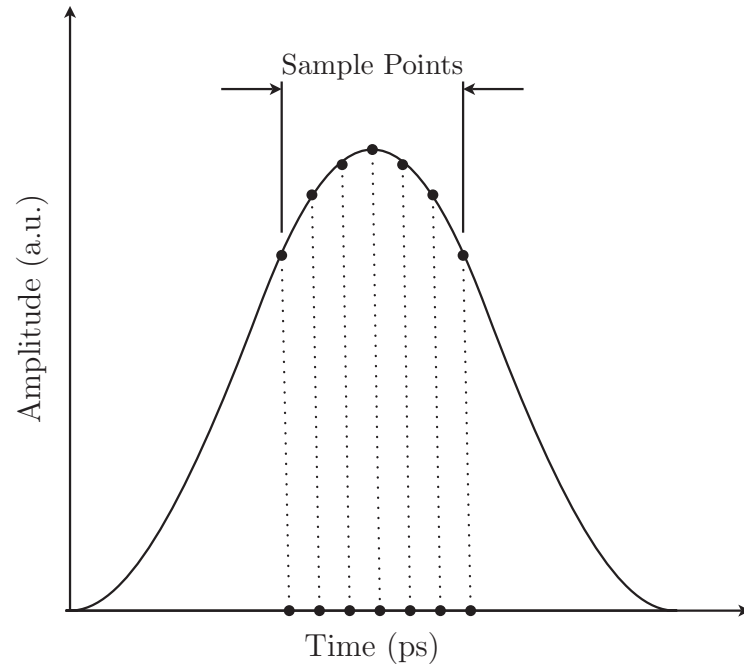


Figure 2.3: Visual aid of how the receiver sensitivity is calculated.

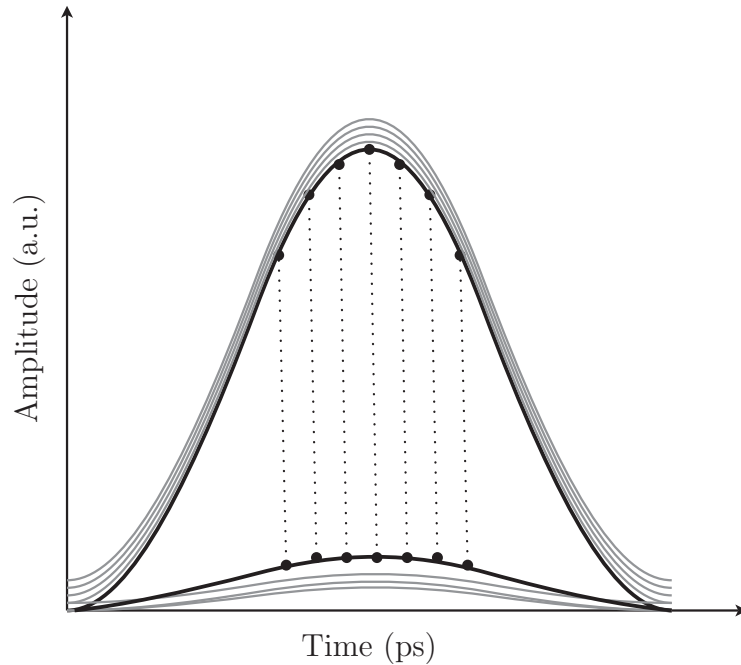


Figure 2.4: Visual depiction of separating the inner sampled data of the eye-diagram.

dependant noise contributions and placed in a vector for subsequent BER calculations. As we are only interested in the inner rails of the eye-diagram in determining possible sampling times, these values are collected when determining if the eye-diagram is to be considered open. Shown in Figure 2.4 is a visual depiction of that described above; the sampled data of interest is highlighted in bold.

The calculation of BER is dependant on the sampling time and the threshold level in the eye-diagram (including all values of marks and spaces, not just the inner rails). For each sampling time,  $\tau$ , the BER is calculated using an optimal threshold level. An approximation as to what optical attenuation is needed to maintain a BER of

$10^{-9}$  is calculated for each sampling time,

$$OA_{\tau,i} = Q \frac{2\sqrt{N_{SI}S_1^2 - 2N_{SI}S_0S_1 + N_{SI}S_0^2 + N_1N_0Q^2 + N_0Q + N_1Q}}{S_0^2 + S_1^2 - 2S_0S_1}, \quad (2.8)$$

where  $N_1$  and  $N_0$  represent the noise value where the 1 is a minimum and the 0 is at a maximum. Similarly,  $S_1$  and  $S_0$  represent the signal value where the 1 is a minimum and the 0 is a maximum. These values are determined when examining all values of marks and spaces near the pulse center. The signal independent noise contribution is denoted by  $N_{SI}$  and Q-factor by  $Q$ . Eq. (2.8) is the expression for  $Q(OA_{\tau,i})$  solved for  $OA_{\tau,i}$ . The actual optical attenuation ( $OA_\tau$ ) needed to obtain the target BER of  $10^{-9}$  is calculated by the optimization routine denoted *fzero* which solves,

$$0 = \log_{10}(BER_a(OA_\tau)) - \log_{10}(BER_t) \quad (2.9)$$

where  $BER_a$  and  $BER_t$  represent the actual and target BERs.  $OA_{\tau,i}$  from Eq. (2.8) is used by *fzero* as an initial guess to reduce computation time.

As *fzero* will vary the optical attenuation about the initial guess,  $OA_{\tau,c}$  will represent the current attenuation being investigated in the minimization. To determine what value of  $OA_\tau$  will solve Eq. (2.9), a second minimization routine denoted *fminbnd* determines the optimal sampling threshold for  $OA_{\tau,c}$ . Defining the optimal sampling threshold as  $I_D$ , *fminbnd* calculates the BER for values of  $I_D$  between the maximum of the spaces and minimum of the marks. The current threshold level being investigated by *fminbnd* is denoted as  $I_{D,c}$ . The BER is calculated for the values of  $OA_{\tau,c}$  and  $I_{D,c}$  using  $\mathbf{S}_{e1}$ ,  $\mathbf{S}_{e0}$ ,  $\mathbf{N}_{e1}$ , and  $\mathbf{N}_{e0}$  which represent all values of marks and spaces (both signal and noise respectively), evaluated to be close to the center of the eye-diagram. The length of the above vectors is  $L$ , and each hold data for an instance of  $\tau$  from  $\tau_1$  to  $\tau_L$ . The BER is defined as one half of the probability of detecting a

zero when a one is received, plus one half of the probability of detecting a one when a zero is received[2]. Defining  $BER_{1,\tau}$  and  $BER_{0,\tau}$  as,

$$BER_{1,\tau} = Q_{gauss} \left( \frac{OA_{\tau,c}(S_{e1,\tau} - I_{D,c})}{\sqrt{(OA_{\tau,c}N_{e1,\tau}) + N_{SI}}} \right) \quad (2.10)$$

$$BER_{0,\tau} = Q_{gauss} \left( \frac{OA_{\tau,c}(I_{D,c} - S_{e0,\tau})}{\sqrt{(OA_{\tau,c}N_{e0,\tau}) + N_{SI}}} \right) \quad (2.11)$$

where[21],

$$\begin{aligned} Q_{gauss}(x) &= \frac{1}{\sqrt{2\pi}} \int_x^\infty \exp\left(-\frac{u}{2}\right) du \\ &= \frac{1}{2} \operatorname{erfc}\left(\frac{x}{\sqrt{2}}\right) \end{aligned} \quad (2.12)$$

the BER may be determined numerically by use of Eq. (2.13).

$$\begin{aligned} BER &= \frac{1}{2} [P(0|1) + P(1|0)] \\ &= \frac{1}{2} \left[ \frac{\sum_{\tau=\tau_1}^{\tau_L} BER_{1,\tau}}{NUM_1} + \frac{\sum_{\tau=\tau_1}^{\tau_L} BER_{0,\tau}}{NUM_0} \right] \end{aligned} \quad (2.13)$$

The values  $NUM_1$  and  $NUM_0$  are the number of samples which represent a 1 and 0 respectively. Values  $I_1$  and  $I_0$  represent the mean values of the ones and zeros respectively, while  $\sigma_1$  and  $\sigma_0$  represent their variance. The function  $Q_{gauss}(x)$  calculates the probability that a normal random variable obtains a value larger than  $x$ . Using this method of determining the BER dictates the underlying assumption that both the signal and noise follow a gaussian distribution.

By the methods described above, a threshold value that minimizes the BER is determined by *fminbnd* for the  $OA_{\tau,c}$  under investigation by *fzero*. Experimentally, the above described method is equivalent to an optical attenuator adjusted in a lab setting to measure a system's performance. The optical attenuation for a particular

sample point ( $\tau$ ) can then be expressed as,

$$OA_{dB}(\tau) = 10\log_{10}OA_{\tau}, \quad (2.14)$$

resulting in a receiver sensitivity ( $RS_{dBm}(\tau)$ ) of,

$$RS_{dBm}(\tau) = 10\log_{10}(ROP) + 30 + OA_{dB}(\tau), \quad (2.15)$$

where  $ROP$  is the received optical power. The value of 30 is used to convert the value of  $ROP_{dB}$  into units of dBm.

This process of calculating  $OA_{dB}(\tau)$  and  $RS_{dBm}(\tau)$  is performed for each sample point in the effective eye-diagram. The sampling time that has yielded the best (or minimum)  $RS_{dBm}(\tau)$  is selected as the optimal sampling time. The optimal sampling threshold ( $I_D$ ) that corresponds to the optimal sampling time,  $OA_{dB}$ , and  $RS_{dBm}$  are then passed back to the simulator as determined values.

The PP associated with this data is calculated in reference to a B2B case. As receiver sensitivity is reported in values of dBm, the resulting PP is simply the difference between these two cases as shown in Eq. (2.16). The value  $RS_D$  represents the receiver sensitivity of the measured, distorted eye-diagram.

$$PP(dB) = RS_D(dBm) - RS_{B2B}(dBm) \quad (2.16)$$

## 2.3 Transmitter Design

### 2.3.1 Introduction

While the research presented here is mostly centered around OTDM receiver performance, there still lies importance in the design of the transmitter, as well as the bit

pattern used in experimentation. The use of a mode-locked laser diode (MLLD) is typically necessary to produce a stream of ultra-narrow pulses, while a Mach Zehnder modulator (MZM) or EAM is used to produce a realistic data stream or pseudo-random bit sequence (PRBS). To interleave several data streams, fiber delay lines or planar lightwave circuits (PLCs) are also needed. Other pulse sources include: mode-locked fiber ring lasers, continuous waveform (CW) lasers modulated by a MZM or EAM, and supercontinuum pulse generators[22]. However, these methods require the addition of complex methods to control the shape of the pulse where the use of a MLLD is a straight forward, stable, and compact solution[22]. For example, externally modulated CW sources generate insufficiently narrow pulse widths and extinction ratio characteristics. As a result, additional pulse compression and regeneration techniques are necessary.

For simulation purposes, it is not necessary to simulate the transmitter exactly as it would appear in a laboratory experiment, but only account for details that would change the pulse shape and bit pattern. Section 2.3.2 will describe the physical components that are modelled at the transmitter, as well as the different details which were granted special attention in an effort to generate an authentic OTDM signal.

### **2.3.2 Simulated Implementation**

The physical representation of the transmitter used during simulations is quite straight forward. Instead of modulating a CW signal via a MZM, a constant stream of marks, in the shape of a hyperbolic secant, was produced at a frequency of 160 GHz. A MZM was implemented to gate this succession of marks into a 128-bit PRBS, which results

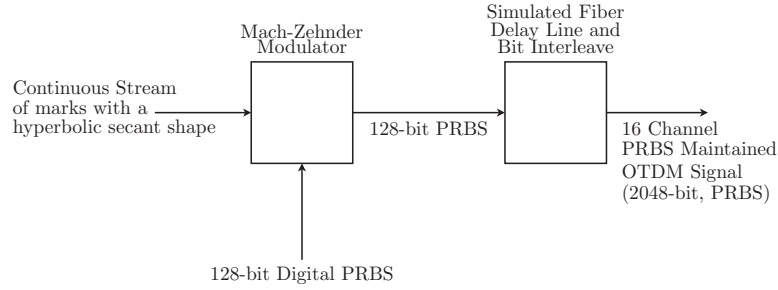


Figure 2.5: Schematic of simulated transmitter design.

in a pulse shape reflecting the output of a MLLD and not the MZM. If CW light was used the pulse shape would have been limited to the extinction characteristics of the modulator.

A schematic of the simulated transmitter is shown in Figure 2.5. The output of the MZM is governed by,

$$S_{out}(t) = [\cos(\theta_d) + jMZ_\delta \sin(\theta_d)]e^{j\theta_s} \sqrt{2S_M} \quad (2.17)$$

where  $\theta_d$  and  $\theta_s$  are the difference and sum of the phase retardations of the optical signal in each arm,  $MZ_\delta$  is the asymmetry parameter, and  $S_M$  is defined as a constant stream of marks. The asymmetry parameter  $MZ_\delta$  is a number larger than zero when the splitting ratio of the couplers is not equal, and/or there is some physical asymmetry between the two arms of the MZM. For the system being described in this research,  $MZ_\delta = 0$ . The effects of temperature change and polarization dependencies are neglected.

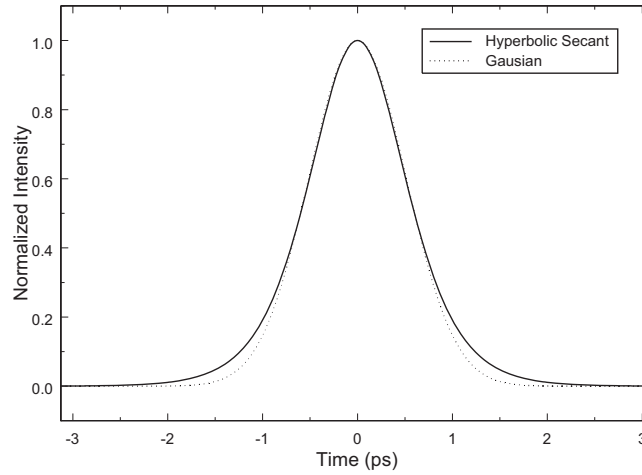


Figure 2.6: Hyperbolic secant and gaussian pulse shape comparison.

### 2.3.3 Generating an OTDM Signal

To generate a realistic signal for the purpose of testing OTDM performance, special care was taken in the pulse shape, as well as the maintenance of the PRBS through the course of multiplexing the 16 channels. Researchers have generated pulses with a full width at half maximum (FWHM) as narrow as 1.2 ps using a MLLD followed by a MZM[1]. To effectively mimic this output, a hyperbolic secant function was chosen as the pulse shape. The hyperbolic secant pulse exhibits a heavier tail to its shape than a gaussian pulse, resulting in the need for a reduced duty cycle[11].

The shape of the pulse is dictated by,

$$S(t) = P \cdot \operatorname{sech}^2 \left( \frac{t - t_0}{T_0} \right) e^{\frac{-iCt^2}{2T_0^2}} \quad (2.18)$$

where  $P$  is the peak intensity,  $t_0$  is the center of the pulse,  $C$  is the chirp parameter

and,

$$T_0 = \frac{FWHM}{2\cosh^{-1}(\sqrt{2})}. \quad (2.19)$$

The FWHM was set to 1.2 ps to imitate the results shown in the literature. The resulting pulse shape is shown in contrast to a gaussian pulse in Figure 2.6, each set with a FWHM of 1.2 ps and a normalized peak intensity of 1. The chirp parameter,  $C$ , and pulse center,  $t_0$ , were set to 0. The chirp parameter was set to 0 as to avoid an additional variable when reporting system performance results. A positive or negative chirp parameter would affect the degree of pulse broadening that occurs during transmission. Therefore, a non-zero chirp parameter would skew the results from the expected. Clearly visible is the heavier tail associated with the hyperbolic secant pulse shape. Eq. (2.18) gives a more accurate representation of the pulse shape that exits a MLLD, rather than assuming a gaussian shape, and therefore gives more accurate results in simulating this OTDM system.

To interleave a  $2^7-1$  bit sequence while maintaining a PRBS data stream, the data is copied and shifted against itself by [1, 23],

$$\frac{2^7 - 1}{n} \text{ bits}, \quad n = 2, 4, 8, 16 \quad (2.20)$$

for each value of  $n$ . The value  $n$  is equal to  $2^N$ , where  $N$  is the number of original sequences being interleaved. The original 128-bit sequence used is a  $2^7 - 1$  PRBS with an extra 0 added into the sequence where there exists 6 zeros in a row. This is also referred to as a de Bruijn sequence. While seemingly trivial, simulating this technique requires more attention than mentioned in literature. The concealed detail is that the MatLab routine must first seek out where there lies 7 successive zeros and remove one of them. After interleaving the bit sequence 4 times, the result is a  $2^7 - 1$  bit sequence repeated 16 times. On completion of the final stage, the extra 16 zeros may

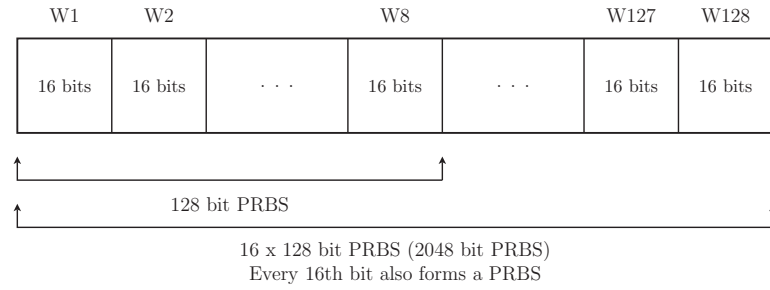


Figure 2.7: Diagram of resulting bit-sequence after interleaving 16 tributary signals.

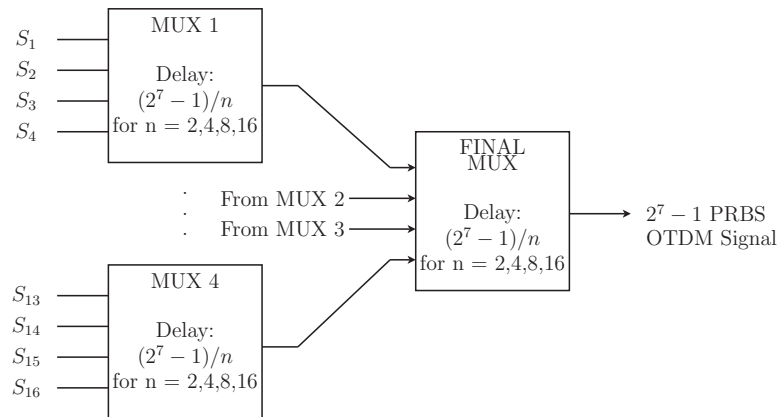


Figure 2.8: Graphical representation of using 4:1 multiplexers to bit-interleave and maintain a PRBS signal.

then be reinserted where there exists 6 zeros in each of these 16,  $2^7 - 1$  bit sequences, resulting in a 2048-bit bit de Bruijn sequence. This was done to maintain an array size which was a power of 2, thereby reducing the complexity and computation time of the simulator. The resulting 2048-bit sequence can be seen in Figure 2.7 where every 16th bit in the sequence forms a PRBS (ie.  $W1(1) + W2(1) + \dots + W128(1)$  where the number in parentheses represents the position of the bit in each 16-bit word).

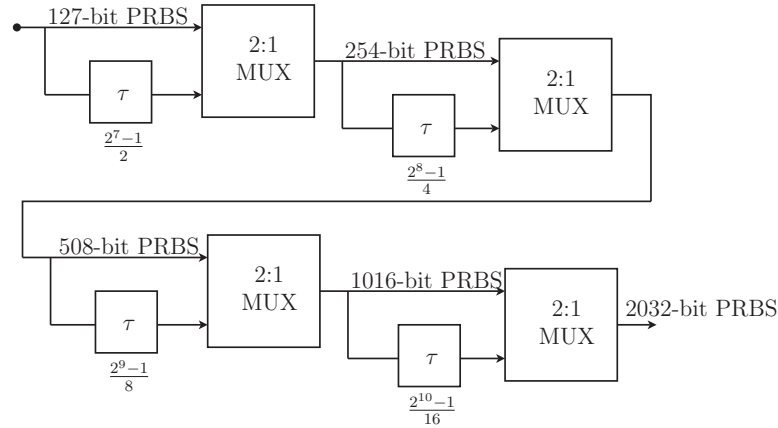


Figure 2.9: Graphically shows how a series of 2:1 multiplexors with appropriate signal delays maintain a PRBS signal.

For readers interested in simulating this technique, there are two methods in which it is possible. A parallel combination of 4:1 multiplexors may be used as in Figure 2.8 with delays defined by Eq. (2.20). Values  $S_1$  through  $S_{16}$  are 16  $2^7-1$  PRBSs which have identical bit patterns. Alternatively, a series of 2:1 multiplexors as shown in Figure 2.9 can also produce a correct PRBS using the delays specified in the diagram by  $\tau$ . In the simulations conducted for this work, the latter of the two methods is used.

## 2.4 Fiber Model

### 2.4.1 Introduction

With the limited amount of funds available to create new networks, emerging technologies should be designed to use existing hardware already set in place. The use and incorporation of OTDM into these networks should use existing fiber spans, along

with various methods of compensation, to effectively transmit error free signals over significant distances. In reality, without compensation, the distance that may be traversed is relatively small in comparison to existing 10 Gbit/s systems. This is due to the increased sensitivity that ultra-narrow pulses have to pulse broadening impairments such as dispersion.

To compensate these distortions, the use of dispersion compensating fiber (DCF) is often used, and will be implemented in the simulations presented in this document. Chapter 3 will discuss these techniques in detail, while the following subsection defines the mathematical model that dictates how the signal is affected while traversing an optical fiber.

## 2.4.2 Simulated Fiber Spans

The equation which represents basic propagation through a single-mode fiber (SMF) is[2],

$$\tilde{\mathbf{E}}(x, y, z, \omega) = \hat{\mathbf{x}}F(x, y)\tilde{B}(0, \omega) \exp(i\beta z) \quad (2.21)$$

where  $\hat{\mathbf{x}}$  is the polarization unit vector,  $F(x, y)$  is the field distribution of the fundamental fiber mode,  $\tilde{B}(0, \omega)$  is the Fourier transform of the initial amplitude  $B(0, t)$ , and  $\beta$  is the propagation constant. Eq. (2.21) only applies if non-linear effects are neglected. Furthermore, Eq. (2.21) does not account for fiber losses as the attenuation coefficient is not included.

The pulse broadening that occurs during fiber transmission is associated with the frequency dependance of  $\beta$ [2]. As an approximation  $\beta$  may be written as[2],

$$\beta(\omega) \approx \beta_0 + \beta_1(\Delta\omega) + \frac{\beta_2}{2}(\Delta\omega)^2 + \frac{\beta_3}{6}(\Delta\omega)^3 \quad (2.22)$$

where  $\beta_m = (d^m \beta / d\omega^m)_{\omega=\omega_0}$ , and  $\Delta\omega = \omega - \omega_0$  where  $\omega_0$  is the carrier frequency. The value of  $\beta_0$  may be neglected as it does not change with respect to  $\omega$ . The  $\beta_1$  term may also be omitted as the pulse does not change shape in the absence of  $\beta_2$  and  $\beta_3$ . The resulting transfer function reflecting the changes in pulse shape due to broadening can be expressed as,

$$H(z, \omega)_\beta = \exp\left(-\frac{i\beta_2}{2}z(\Delta\omega)^2 - \frac{i\beta_3}{6}z(\Delta\omega)^3\right). \quad (2.23)$$

The attenuation coefficient,  $\alpha$ , is used to describe the amount of power lost through an optical fiber.

$$P_{out} = P_{in} \exp[-\alpha z] \quad (2.24)$$

Eq. (2.24) can be used while taking into account,

$$P = |\mathbf{I}|^2 \quad (2.25)$$

to form the attenuation transfer function,

$$H(z)_\alpha = \exp\left(-\frac{\alpha}{2}z\right). \quad (2.26)$$

The total transfer function through an optical fiber, neglecting nonlinearities, consists of the above loss due to attenuation, and the pulse broadening effects due to first and second order dispersion effects.

$$\begin{aligned} H_L(z, \omega) &= H(z)_\alpha \cdot H(z, \omega)_\beta \\ &= \left[\exp\left(-\frac{\alpha}{2}z\right)\right] \cdot \left[\exp\left(-\frac{i\beta_2}{2}z(\Delta\omega)^2 - \frac{i\beta_3}{6}z(\Delta\omega)^3\right)\right] \end{aligned} \quad (2.27)$$

Eq. (2.21) may be re-written combining  $\hat{\mathbf{x}}$ ,  $F(x, y)$ , and  $\tilde{B}(0, \omega)$  as the input optical field  $\tilde{\mathbf{E}}_{in}(x, y, z, \omega)$ . The resulting field exiting the optical fiber may then be calculated

by,

$$\begin{aligned}
\tilde{\mathbf{E}}_{out}(x, y, z, \omega) &= \hat{\mathbf{x}}F(x, y)\tilde{B}(0, \omega) \cdot H_L(z, \omega) \\
&= \tilde{\mathbf{E}}_{in}(x, y, z, \omega) \cdot H_L(z, \omega) \\
&= \tilde{\mathbf{E}}_{in}(x, y, z, \omega) \exp \left[ z \left( -\frac{\alpha}{2} - i\frac{\beta_2}{2}(\Delta\omega)^2 - i\frac{\beta_3}{6}(\Delta\omega)^3 \right) \right] \quad (2.28)
\end{aligned}$$

where  $\tilde{\mathbf{E}}_{out}(x, y, z, \omega)$  and  $\tilde{\mathbf{E}}_{in}(x, y, z, \omega)$  are the Fourier transforms (FTs) of the time domain fiber output and input signals, respectively.

The values of  $\alpha$ ,  $\beta_2$  and  $\beta_3$  are calculated by supplying the fiber variables of attenuation per meter ( $\alpha_L$ ), zero dispersion wavelength ( $\lambda_{ZD}$ ), and values of reference dispersion ( $D_{ref}$ ), dispersion slope ( $S_{ref}$ ) at a specific wavelength ( $\lambda_{ref}$ ). During simulation, the values of  $D_{ref}$  and  $S_{ref}$  vary according to the amount of residual dispersion, and residual dispersion slope present at  $\lambda_{ref}$ . The value  $\lambda$  is the wavelength of the OTDM signal, and  $\lambda_{ref}$  is the wavelength at which  $D_{ref}$  and  $S_{ref}$  are known (typically 1550 nm).

$$\alpha = \alpha_L \frac{\ln 10}{10} \quad (2.29)$$

$$\beta_2 = \frac{-D\lambda^2}{2\pi c} \quad (2.30)$$

$$D = D_{ref} \left( \frac{\frac{1/\lambda}{\lambda_{ZD}}}{\frac{1/\lambda_{ref}}{\lambda_{ZD}}} \right) \quad (2.31)$$

$$\beta_3 = \frac{(2D + \lambda S_{ref})\lambda^3}{(2\pi c)^2} \quad (2.32)$$

A common technique used to calculate non-linear effects occurring in optical transmission links is the split-step Fourier method[2, 20, 24]. Figure 2.10 shows the optical fiber being split into  $N$  sections of equal length. This is more commonly referred as the *Fixed-Step-Size* split-step Fourier method. The optical field first propagates the distance  $h/2$  with only dispersion and fiber loss acting upon it. At  $z + h/2$  (the

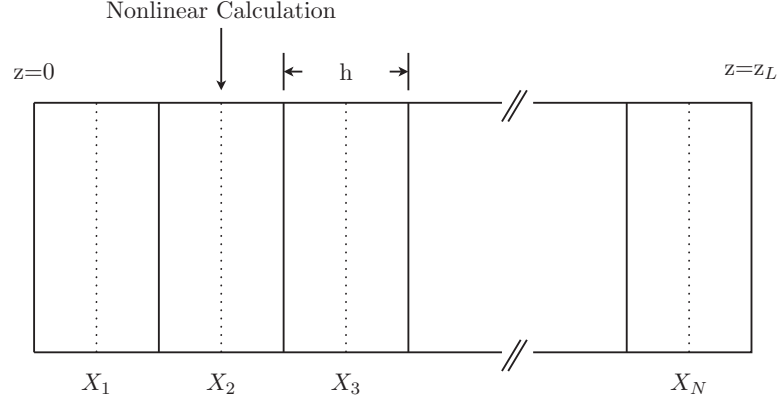


Figure 2.10: Visual aid in describing the split-step Fourier method.

section midpoint), the effect of non-linearities over the whole section length  $h$  are calculated by multiplying the field by a non-linear term. For the remaining distance  $h/2$ , only the linear impairments are considered. During calculation of the split-step Fourier method, the nonlinear effects are assumed lumped at the midpoint of each section[25]. The accuracy of a *Fixed-Step-Size* approach is improved upon by increasing the number of sections in the fiber[26].

During MatLab simulation, the number of sections is defined as  $n_l$ , and the length of each section is  $h = z_L/n_l$  (where  $z_L$  represents the total length of fiber). For each section, the linear propagation effects are calculated in the frequency domain, as shown in Eq. (2.28) and the non-linear effects in the time domain. The non-linear effect ( $NL$ ) is calculated for each section and is defined as,

$$NL(z, t) = \gamma h |S_{in}(z, t)|^2 \quad (2.33)$$

$$\gamma = \frac{2n_2\pi}{\lambda A_{eff}} \quad (2.34)$$

where  $A_{eff}$  is the effective area of the transmission fiber,  $n_2$  is the non-linear coefficient,  $h$  is the length of each section, and  $S_{in}(z, t)$  is the input signal represented in

the time-domain. Defining the non-linear transfer function as  $H_{NL}(z, t)$ ,

$$\begin{aligned} H_{NL}(z, t) &= \exp[-iNL(z, t)] \\ &= \exp[-i\gamma h |S_{in}(z, t)|^2] \end{aligned} \quad (2.35)$$

the output to each section of fiber with length  $h$  may be calculated in three steps. For values of  $z$ , from  $z_N$  to  $h/2$  (where  $z_N$  represents the the position along the fiber at the input to section  $X_N$  in Figure 2.10),

$$\tilde{\mathbf{E}}_{out}(x, y, z, \omega)_1 = \tilde{\mathbf{E}}_{in}(x, y, z, \omega) \exp \left[ z \left( -\frac{\alpha}{2} - i\frac{\beta_2}{2}(\Delta\omega)^2 - i\frac{\beta_3}{6}(\Delta\omega)^3 \right) \right]. \quad (2.36)$$

At  $z = h/2$ , the non-linear effects are calculated assuming their effect over the total section length  $h$ ,

$$\tilde{\mathbf{E}}_{out}(x, y, z, \omega)_2 = \mathcal{F} \left\{ S_{in}(z, t)_1 \exp \left[ -i\gamma h |S_{in}(z, t)_1|^2 \right] \right\} \quad (2.37)$$

where  $S_{in}(z, t)_1$  is the inverse Fourier transform of  $\tilde{\mathbf{E}}_{out}(x, y, z, \omega)_1$  from Eq. (2.36). Finally, for values of  $z$  from  $z_N + h/2$  to  $z_N + h$ ,

$$\tilde{\mathbf{E}}_{out}(x, y, z, \omega)_3 = \tilde{\mathbf{E}}_{out}(x, y, z, \omega)_2 \exp \left[ z \left( -\frac{\alpha}{2} - i\frac{\beta_2}{2}(\Delta\omega)^2 - i\frac{\beta_3}{6}(\Delta\omega)^3 \right) \right]. \quad (2.38)$$

The addition of non-linearities to fiber transmission results in self phase modulation (SPM) of the OTDM signal. The performance of the system will then be further limited as the signal is subjected to additional pulse broadening[2]. The effect of SPM and other non-linearities will be discussed further in Chapters 3 and 4. The effect of this non-linearity is best subsided by reducing the average power of the transmitted signal which would sufficiently reduce the effect of  $\gamma$  on the propagation constant[2]

$$\beta' = \beta + \gamma P_{avg}. \quad (2.39)$$

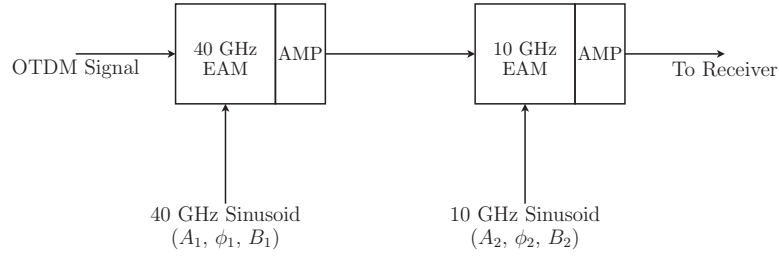


Figure 2.11: Schematic for driving EAMs with different frequencies.

As the average power ( $P_{avg}$ ) increases, the effect  $\gamma$  has on pulse broadening also increases. In Eq. (2.39),  $\beta'$  is the change in phase the signal experiences caused by the signal power (ie. SPM);  $\gamma$  is the proportionality constant.

## 2.5 Demultiplexer Design

### 2.5.1 Introduction

The demultiplexer used during simulation is based on the concatenated EAM scheme suggested for clock recovery and demultiplexing in [13]. Two methods of driving the EAMs were initially tested. The first being the use of two sinusoidal signals with different frequencies (40 GHz and 10 GHz), and the second, a combination of the two. The latter method is similar to that presented in [15]. Recall Figure 1.9 from Section 1.2.6.

Figure 2.11 and Figure 2.12 show these two methods schematically. While both techniques demultiplex the incoming bit sequence, the advantage to using two separate frequencies becomes apparent when optimizing the variables and observing the amount of power exiting the last EAM. When using the apparatus described by

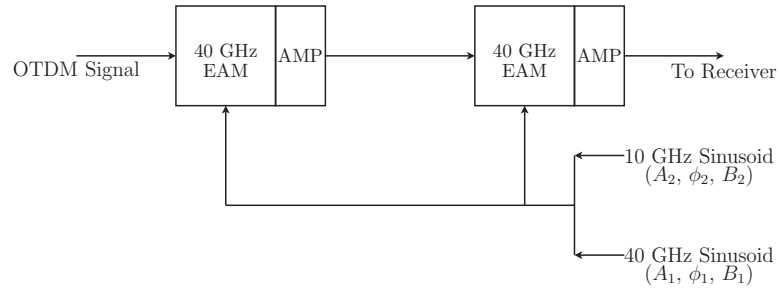


Figure 2.12: Schematic for driving EAMs with a sum of frequencies.

Figure 2.12 to demultiplex the OTDM signal, the shape of the driving waveform as well as the need for effective absorption of neighbouring bits, left the target channel 26.14 dB more absorbed, than when driving the EAMs with separate frequencies. It was then discarded as an effective solution to demultiplex OTDM signals as additional amplifiers may be necessary, further increasing the cost and complexity of the system while lowering the signal-to-noise ratio (SNR).

## 2.5.2 EAM Gate Model

The selection of EAMs for use in OTDM is dependant on both their frequency response as well as extinction ratio characteristics. Generally, multiple quantum well (MQW) devices are chosen as they exhibit larger extinction characteristics than bulk devices[27]. The frequency response of EAMs is limited by the device capacitance and inductance[27]. These values are determined by the device fabrication and design which may be represented by a lumped element circuit model outlining their state of origin[27]. Recent advances in microwave technology have made high frequency EAMs, such as that from OKI Electronics, available that show insertion losses of 9 dB for a 40 GHz device. The insertion loss of a lower frequency 10 GHz EAM may

be made to be as low as 4 dB[28]. Being commercially available, the use of a 40 GHz EAM is presented in this research as opposed to the 20 GHz EAM implemented in [13].

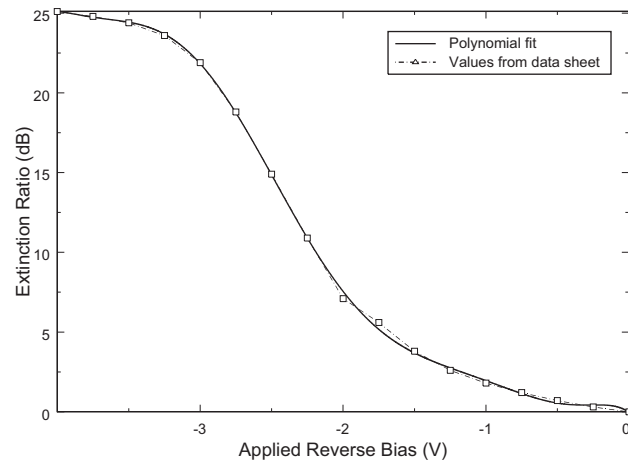
To observe the characteristics of the EAMs, and how effectively they would perform the task of demultiplexing OTDM signals, their absorption curves were first entered into MatLab at various points via a data sheet. A polynomial fit was then applied for subsequent calculations. The data sheets were provided by OKI Electric Industry Co., a leading manufacturer of high bit rate EAMs. Using this technique, various values of extinction along the curve could be used to effectively transmit or absorb the simulated OTDM signal passing through the EAMs.

Figure 2.13(a) and Figure 2.13(b) show the absorption curve for both the 40 GHz and 10 GHz EAMs respectively. As the tandem EAMs are intended to gate the OTDM signal, and pass only one channel, the waveforms driving them should be operating in the right side of these curves when the target channel bits are passing through them. Alternatively, the combination of the EAMs should be driven on the left side of the curves to absorb neighbouring channels. It can be shown that various sinusoids will provide different amounts of absorption and different switching window characteristics based on their driving amplitude, phase and bias. These waveforms are characterized as,

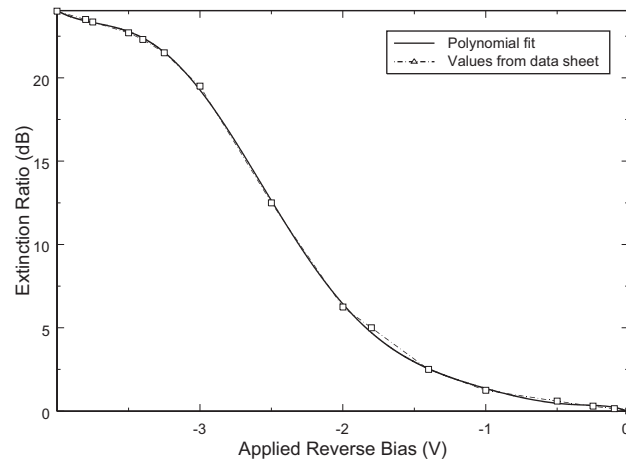
$$D_1(t) = A_1 \sin(2\pi f_1 t + \phi_1) - B_1 \quad (2.40)$$

$$D_2(t) = A_2 \sin(2\pi f_2 t + \phi_2) - B_2 \quad (2.41)$$

where  $f_1$  is 40 GHz and  $f_2$  is 10 GHz,  $A_1$ ,  $A_2$ ,  $\phi_1$ ,  $\phi_2$ ,  $B_1$ , and  $B_2$  are the respective amplitude, phase and bias for each driving sinusoid. The intensity of the light exiting the modulators is dependant upon the interaction of these driving waveforms on their



(a)



(b)

Figure 2.13: Absorption characteristics for: (a) 40 GHz EAM (b) 10 GHz EAM.

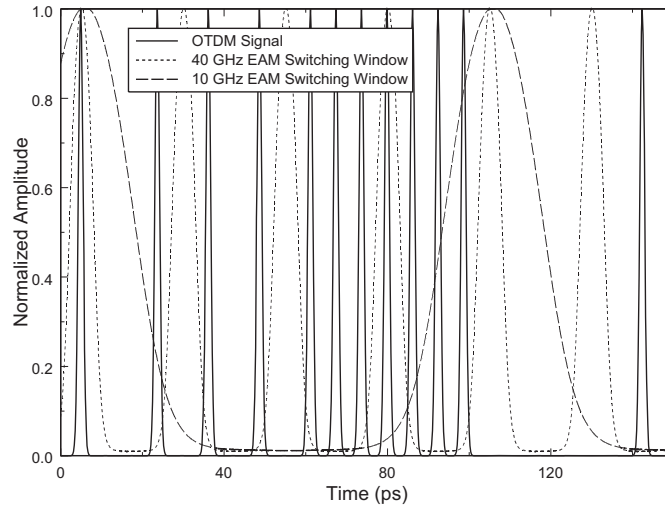


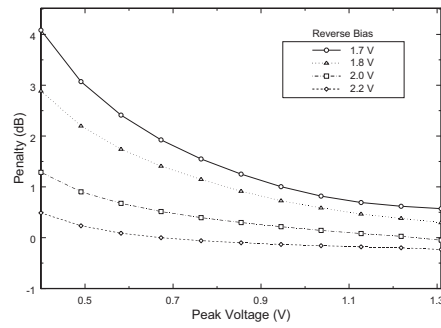
Figure 2.14: Back-to-back OTDM Signal, 40 GHz and 10 GHz EAM optimal switching windows.

respective absorption curves. Taking into account the gain ( $G$ ) of the amplifiers from Figure 2.11, the intensity transfer function can be defined as

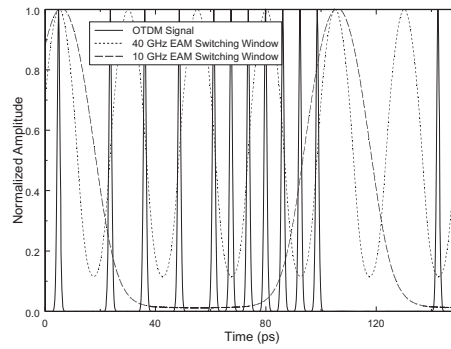
$$I_{out}(t) = I_{in}(t) \cdot 10^{\frac{G-\alpha(t)}{10}} \quad (2.42)$$

where  $\alpha(t)$  represents the value of extinction that occurs when  $D_1(t)$  or  $D_2(t)$  are applied to the appropriate EAM absorption curve.

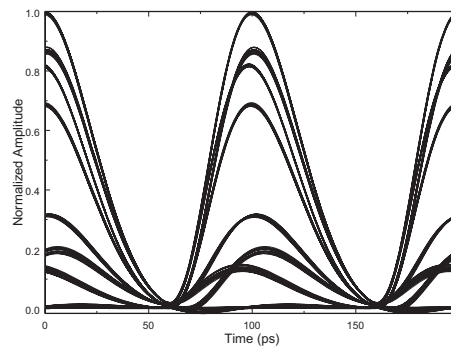
To illustrate the effect Eq. (2.40) and (2.41) have on the resulting performance, a simulation was constructed which allowed  $A_1$ ,  $A_2$ ,  $B_1$ , and  $B_2$  to vary while their respective phases  $\phi_1$  and  $\phi_2$  were kept at their optimum values of 0.2806 and 1.1984 radians. Section 2.5.3 goes into further detail concerning the calculations and methods used to obtain these optimal values. A time-domain plot of the OTDM signal, and switching windows is shown in Figure 2.14 in a B2B case. Note how several bits are



(a)

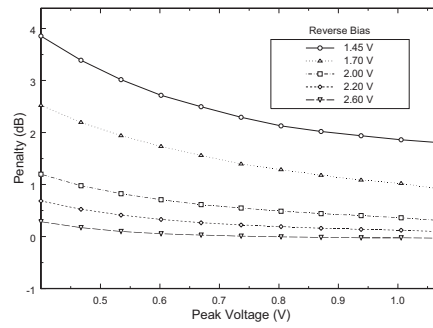


(b)

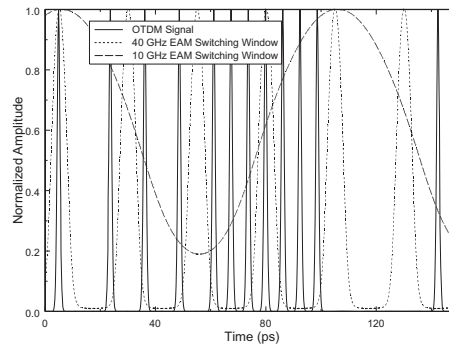


(c)

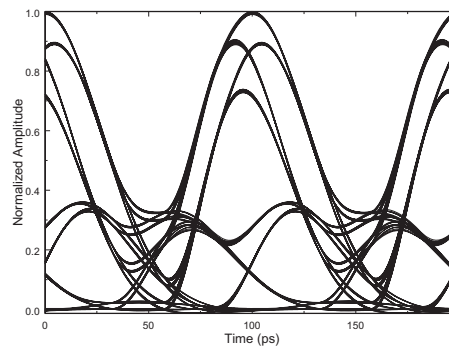
Figure 2.15: (a) Penalty (EOFP) that arises from varying  $A_1$  and  $B_1$  with  $D_2(t)$  set with optimal values. (b) Example of change in 40 GHz EAM switching window (Peak Voltage = 0.6 V, Reverse Bias = 1.7 V). (c) Electrical eye-diagram.



(a)



(b)



(c)

Figure 2.16: (a) Penalty (EOFP) that arises from varying  $A_2$  and  $B_2$  with  $D_1(t)$  set with optimal values. (b) Example of change in 10 GHz EAM switching window (Peak Voltage = 0.7 V, Reverse Bias = 1.45 V). (c) Electrical eye-diagram.

passed by the 40 GHz EAM only to be absorbed by the 10 GHz EAM.

When characterizing the 40 GHz EAM,  $A_1$  was varied between 0.4 V and 1.35 V, and  $B_1$  from 1.7 V to 2.2 V. The values of  $A_2$  and  $B_2$  remained optimally fixed at 1.1052 V and 2.8948 V. The system performance was measured for each combination of  $A_1$  and  $B_1$  and their penalties recorded in terms of EOF. The simulation results are shown in Figure 2.15(a), and show improved performance as  $A_1$  and  $B_1$  become larger. Measures were taken during simulation to avoid combinations of  $A_1$  and  $B_1$  that result in a  $D_1(t)$  which lies outside the constraints of Figure 2.13(a). Figure 2.15(b) shows a time-domain representation of the OTDM signal and the resulting switching windows acting upon it. The peak voltage was set to 0.6 V and the reverse bias to 1.7 V in this example. The received electrical eye-diagram is shown in Figure 2.15(c) to more clearly show the effects a non-optimal 40 GHz switching window can have on the demultiplexed signal.

Similarly for the 10 GHz EAM,  $A_2$  and  $B_2$  are varied while  $D_1(t)$  remains optimally fixed. The values of  $A_2$  vary from 0.4 V to 1.1 V, and  $B_2$  from 1.45 V to 2.6 V. As with the 40 GHz EAM, the values of  $A_2$  and  $B_2$  are varied, and the resulting penalty is recorded in terms of EOF. The results are shown in Figure 2.16. It is clear that as the switching window characteristics change, unwanted bits will become partially passed by the tandem EAM gates, resulting in inter-symbol interference (ISI). Note that to exclude other sources of system penalty, these simulations were performed in a B2B manner over 10 m of optical fiber, artificially set to have negligible dispersion and dispersion slope contributions. All penalties above are relative to the optimal B2B eye-diagram as defined by the EAM driving waveforms outlined in Section 2.5.3.

### 2.5.3 Optimization of Gates

In an effort to make certain that the selection of amplitude, phase, and bias of each driving waveform is correct, an optimization routine was written for the demultiplexing setup described in Figures 2.11 and 2.12. The routine uses code which describes the transmission system along with the function *fmincon* supplied by MatLab, to find a minimum of a scalar multi-variable function. The EOF of the received electrical signal was selected as the function to minimize, and was simply negated to achieve proper execution. In supplying an initial estimate with an upper and lower bound for all 6 variables in question, the optimization function performs a linear search for those that generate the best performance.

To test validity of the optimization, a separate routine was created to generate contour plots in an effort to visualize a maximum. Due to the nature of the plot, two sets of variables from the driving waveforms must remain fixed and are set to the global optimized values, while the variable pair in question is swung about the calculated optimum value. The result is a two dimensional contour revealing that the optimization in fact did produce an accurate result. The resulting plots are shown in Figures 2.17, 2.18, and 2.19 where the optimal values found in the optimization routine are  $A_1 = 1.1307$  V,  $A_2 = 1.1052$  V,  $\phi_1 = 0.2806$  radians,  $\phi_2 = 1.1984$  radians,  $B_1 = 2.8633$  V, and  $B_2 = 2.8948$  V (as designated on the plots by the black dot). The EOF recorded with this optimal set of variables is 0.9943 (or 99.43%) and is indicated by a black dot on each of the contour plots. To increase clarity, the number of contours shown in each plot was reduced as the optimal EOF was rounded to a value of 1.0. Note that it is numerically impossible to achieve an EOF greater than 1.0. This total loss through the EAM gates of 0.02 dB. From the resulting plots it

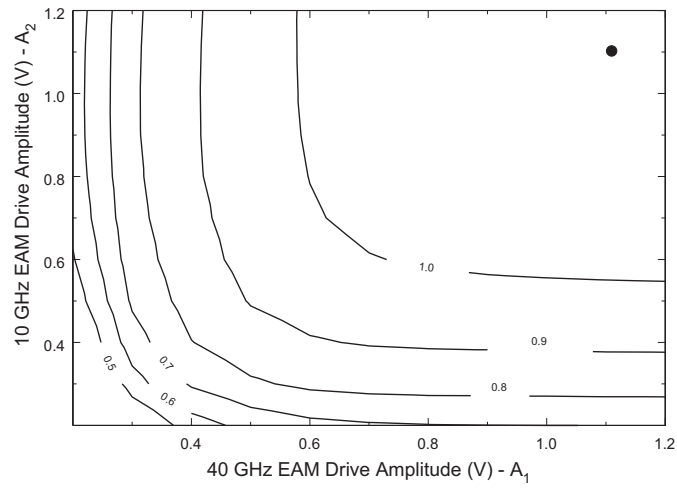


Figure 2.17: Effect on EOF by varying driving waveform amplitude.

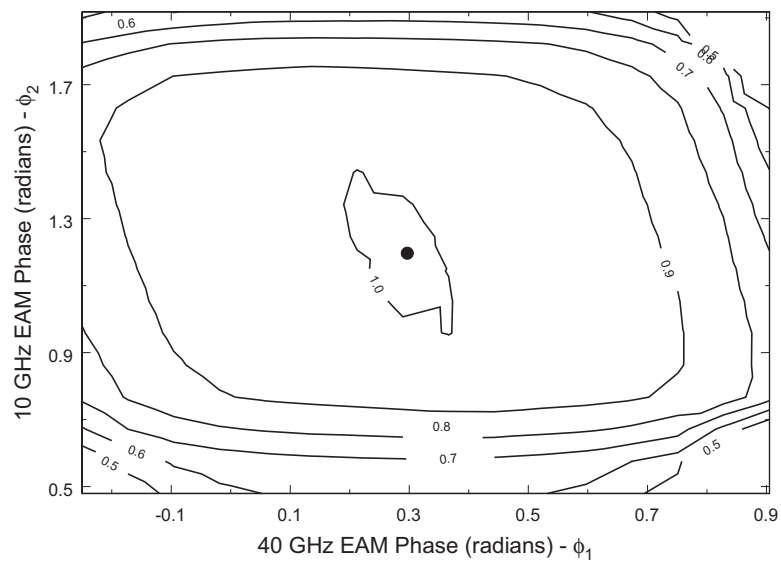


Figure 2.18: Effect on EOF by varying driving waveform phase.

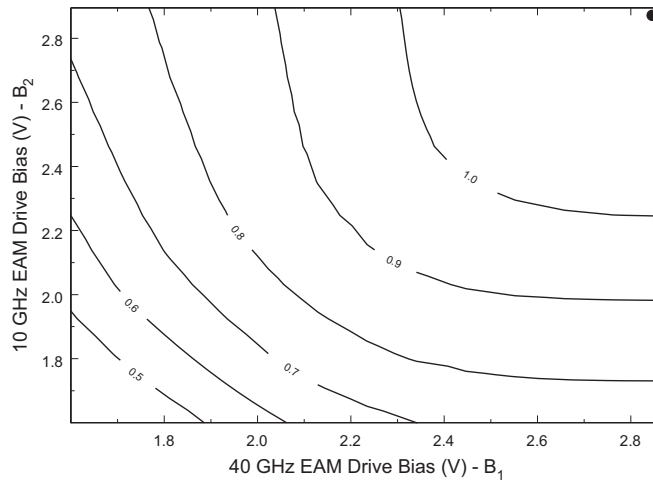


Figure 2.19: Effect on EOF by varying driving waveform bias.

is evident that the phase of the driving waveforms is most sensitive and would result in the largest amount of penalty if altered from its optimum value. In contrast, the amplitude of the waveforms is the least sensitive, followed closely by the bias.

## 2.6 Receiver Design

### 2.6.1 Introduction

The design of the receiver is of great importance when determining the performance a system can attain. A widely used method to increase the performance of such a receiver is to optically pre-amplify the data stream using an erbium-doped fiber amplifier (EDFA) placed before the photodetector. In performing a large preamplification, the amplified spontaneous emission (ASE) noise generated by the EDFA can

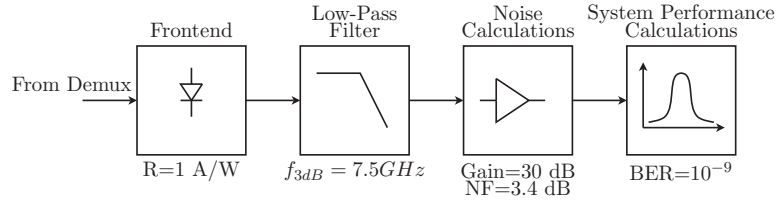


Figure 2.20: Schematic of simulated receiver design.

be made to dominate the thermal noise and the sensitivity may be improved by up to 20 dB[2]. Due to the large increase available in system performance, the preamplified approach was used during the work presented in this thesis. This section will describe in detail how such a receiver is simulated in MatLab, and what tradeoffs may be associated with changes in the topology presented.

## 2.6.2 System Implementation

The MatLab routine that simulates the receiver is described in Figure 2.20 and shows clearly how the system simulation takes place. After demultiplexing the OTDM signal, the channel in question becomes incident on a photodiode with a responsivity ( $R$ ) of 1 A/W. The detected signal is quantified as,

$$S_{eRX}(t) = R|S_{oDEMUX}(t)|^2 \quad (2.43)$$

where the subscripts of  $e$  and  $o$  signify electrical and optical signals. The received electrical data is then passed through a filtering algorithm specifying a 4th order Bessel filter with a 3-dB bandwidth of 7.5 GHz. This low bandwidth filter will increase the pulse width of the low duty-cycle 10 Gbit/s signal available after the demultiplexer.

The use of the EDFA will cause not only signal amplification but also the addition of ASE noise. The EDFA calculations are done after the signal passes through the

photodiode and filter. The spectrum of the ASE noise is adjusted to account for the ASE noise from the in-line amplifier. Calculated at this point are: the received signal, now affected by the gain of the EDFA, as well as the signal-dependent and signal-independent noise associated with the gain. The signal-dependent noise is defined as the sum of the signal-spontaneous beat noise and shot noise due to the signal,

$$\begin{aligned}
 S_{D,n}(t) &= S_{SpB,n}(t) + S_{SHOT,n}(t) \\
 &= \left[ 2RG_{EDFA} \cdot CL_{in} \cdot CL_{out}^2 \cdot NO \cdot S_n(t) \right] \\
 &\quad + \left[ G_{EDFA} \cdot q \cdot CL_{in} \cdot CL_{out} \cdot S_n(t) \right] \quad (2.44)
 \end{aligned}$$

where  $R$  is the responsivity,  $G_{EDFA}$  is the gain of the EDFA,  $CL_{in}$  and  $CL_{out}$  are the input and output coupling losses of the preamplifier,  $NO$  is the noise power over the ASE noise bandwidth,  $S_n(t)$  is a time sampled noise signal, and  $q$  is the value of electron charge. The signal-independent noise consists of the sum of the thermal noise, shot noise due to the ASE, the spontaneous-spontaneous beat noise, and the dark current,

$$\begin{aligned}
 S_{I,n} &= S_{THERM,n} + S_{SHOT,ASE} + S_{Sp-Sp,n} + S_{DARK,n} \\
 &= [PSD \cdot BW_n] + [4RqCL_{out}NO \cdot BW_{OF} \cdot BW_n] \\
 &\quad + \left[ 4(R \cdot CL_{out}NO)^2 \cdot 2BW_{OF}BW_{n,i} \right] + [2qI_{DARK}BW_n] \quad (2.45)
 \end{aligned}$$

where  $PSD$  is the power spectral density of the input noise current,  $BW_n$  is the equivalent noise bandwidth of the receiver filter,  $BW_{OF}$  is the optical filter bandwidth,  $BW_{n,i}$  is the noise bandwidth integral, and  $I_{DARK}$  is the photodiode dark current. Finally, the electrical signal output is calculated by,

$$S_{e,out}(t) = G_{EDFA}CL_{in}CL_{out}S_{e,in}(t) \quad (2.46)$$

| Parameter                 | Value       | Units              |
|---------------------------|-------------|--------------------|
| Fiber length              | 50          | km                 |
| Residual Dispersion       | -2.5 – +2.5 | ps/nm              |
| Residual Dispersion slope | 0.05        | ps/nm <sup>2</sup> |

Table 2.1: Simulation configuration in measuring penalty due to dispersion for EOP, EOFP, and PP.

where the electrical signal present after the photodiode and low-pass filter is denoted by  $S_{e,in}(t)$ . The signal-dependent and signal-independent noise calculations are then passed to the receiver sensitivity calculation routine which consists of the measurements and calculations described in Section 2.2.4.

## 2.7 Defining System Performance

Due to the fact that there are different measures that may be used for system performance evaluation, it is important to see how closely each represents the effects of changes that might be associated with different sources of penalty. Even though the definition of each of the measures described above differ, they should accurately give some representation as to what penalties may be incurred, and show agreement with their results.

To test these results, artificial amounts of dispersion and dispersion slope were applied to the optimized system. Table 2.1 and 2.2 outline the operating conditions in simulating dispersion and dispersion slope as sources of penalty. All non-linear effects

| Parameter                 | Value       | Units              |
|---------------------------|-------------|--------------------|
| Fiber length              | 50          | km                 |
| Residual Dispersion       | 0.005       | ps/nm              |
| Residual Dispersion slope | -5.5 – +5.5 | ps/nm <sup>2</sup> |

Table 2.2: Simulation configuration in measuring penalty due to dispersion slope for EOP, EOF, and PP.

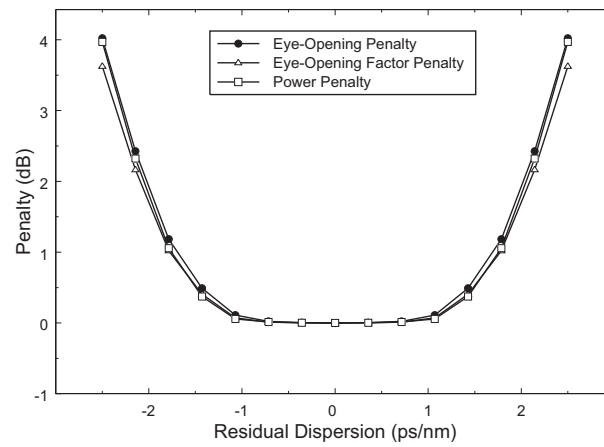


Figure 2.21: Penalty agreement when measuring residual dispersion.

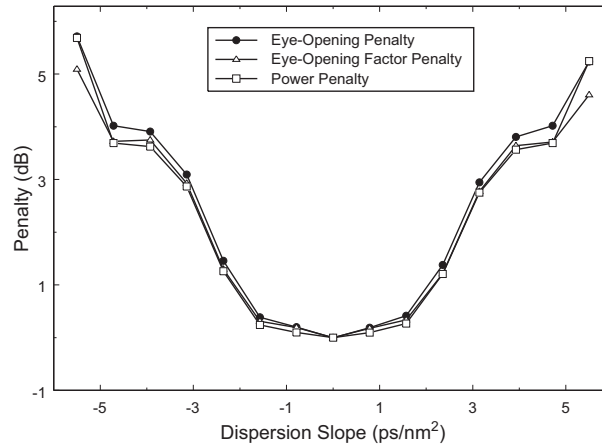


Figure 2.22: Penalty agreement when measuring dispersion slope.

are neglected in performing these simulations. Tables 4.1 - 4.4 of Chapter 4 show all other system variables used in generating these results. In Figure 2.21, the residual dispersion was varied from -2.5 to 2.5 ps/nm over a 50 km span while neglecting dispersion slope. Similarly in Figure 2.22, the residual dispersion is neglected while the dispersion slope is varied from -5.5 to 5.51 ps/nm<sup>2</sup> over 50 km of optical fiber. The result is that these three measures of system performance closely track one another, especially below the 3 dB penalty point. Generally, values of penalty that exceed 3-dB are of little interest as systems are not designed to operate within those conditions. Furthermore, the agreement between these measures of system penalty may not have been obvious as EOFP and EOP do not include noise considerations, where the calculation of PP does. The similar results shown may be explained as the penalty becomes dominated by the pulse broadening effects of dispersion and dispersion slope.

Such an effect is expected in performing transmission at 160 Gbit/s.

As these measurements are performed on the electrical eye-diagram that results at a 10 Gbit/s receiver, they should also show good agreement when measuring the system performance that results by various other system performance impairments. From the discussion above, it is clear that no single measurement of system performance gives an advantage over the other, and that since their differences are insignificant, any one of them may be used. The remainder of this document will refer to measured impacts of system performance as penalty, and will be reported in units of decibels, as a result of the above findings. EOP will be used throughout Chapter 4 in reporting results related to various sources of system penalty.

# Chapter 3

## Transmission Impairments

### 3.1 Introduction

In this chapter we examine the effects of the various system impairments which are of greatest consequence during the transmission of optical time division multiplexing (OTDM) signals. For each impairment, an introduction to the cause and background theory will first be explained, along with the method of compensation and/or simulation structure. The impairments included are: attenuation, chromatic dispersion, dispersion slope, timing jitter, polarization mode dispersion (PMD), and nonlinearities[22].

## 3.2 Dispersion

### 3.2.1 Background

As a pulse traverses an optical fiber, the group velocities that each spectral component experiences differ by small amounts. The effect of these differing group velocities is known as dispersion, and is comprised of two influences, material dispersion and waveguide dispersion[2],

$$D = D_M + D_W. \quad (3.1)$$

Material dispersion is associated with the dependency of silica's refractive index on optical frequency[2]. The waveguide dispersion however is greatly dependent upon fiber parameters such as core radius and refractive index profile, making it possible to alter the design of the fiber and control its contribution[2].

Fiber dispersion impacts the system performance by causing optical pulses to broaden. This effect is attributed to different spectral components of an optical pulse arriving at the receiver at different times, as a consequence of their individual group velocities[2]. The group velocity is defined as[2],

$$v_g = (d\beta/d\omega)^{-1} \quad (3.2)$$

where  $\beta$  is the propagation constant. The relationship between the group velocity and the dispersion parameter  $D$  is[2],

$$D = \frac{d}{d\lambda} \left( \frac{1}{v_g} \right) = -\frac{2\pi c}{\lambda^2} \beta_2 \quad (3.3)$$

where  $\beta_2$  is the second derivative of the propagation constant with respect to optical frequency. The amount of pulse broadening that will occur during propagation is determined by the value of  $\beta_2$ [2].

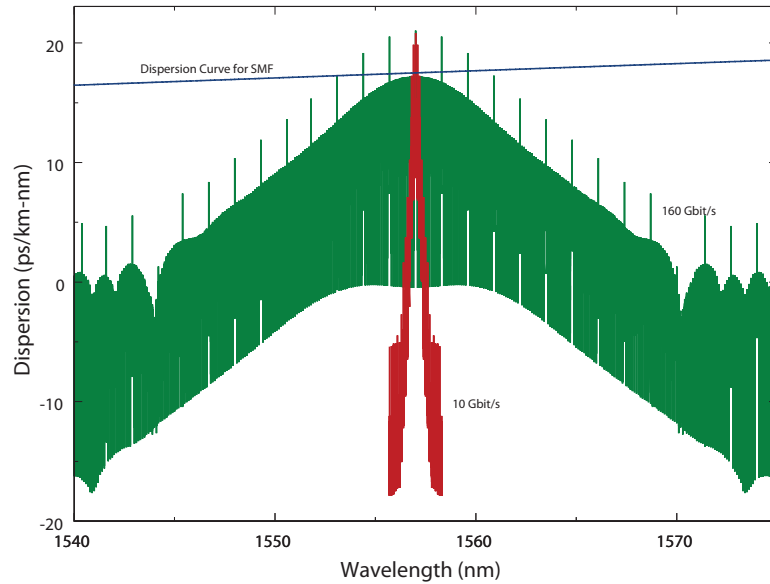


Figure 3.1: The effect of SMF dispersion slope on the optical signal spectrum of 160 Gbit/s and 10 Gbit/s bit rates.

While the discussion above has been limited to the effects of  $\beta_2$ , it is important to discuss the effects of  $\beta_3$ , and dispersion slope  $S$ [29]. Due to the high bit rate, and hence, large bandwidth of typical OTDM signals the dispersion slope can play a pivotal role. While launching a 10 Gbit/s signal near the zero dispersion wavelength  $\lambda_{ZD}$ , the effect of the dispersion slope may be considered negligible. Figure 3.1 is a representation of the effect dispersion slope has over larger bit rate optical signals. Clearly the dispersion at various frequencies of 160 Gbit/s signal spectrum will differ, regardless of whether or not the signal was launched near  $\lambda_{ZD}$ . As a result, additional pulse broadening will occur for various values of dispersion slope. There has also been suggestion that tunable dispersion slope compensation may be necessary as the bit rate of systems continues to increase[29].

Additional pulse broadening may also be brought about by non-linear effects such as self phase modulation (SPM). Even more troubling is that the effects of SPM are more prominent inside dispersion compensating fibers (DCFs) where the effective area is close to  $20 \mu m^2$ [2]. The impact of non-linearities, brought on by an increased launch power, will be investigated more thoroughly in Chapter 4.

The effect of the mechanisms described above requires that compensation techniques be implemented to subside them. If inadequately compensated, the pulse broadening brought about by the dispersive properties of the fiber will lead to channel crosstalk (in the form of inter-symbol interference (ISI)) as neighbouring bits begin to overlap their designated bit periods[11]. A large amount of research has gone into quantifying these impairments as OTDM signals are considered dispersion limited if improperly compensated.

### 3.2.2 Compensation Methodology

As mentioned above, the total effective dispersion acting on a transmitted signal is dependant on both material and waveguide dispersion, the latter of which may be controlled through fiber design. More specifically, the waveguide dispersion of a fiber may be designed to be largely negative, thereby negating the effects of the material dispersion. This technique is realized in the design of DCFs, where the waveguide dispersion is designed such that the overall dispersion of the DCF is sufficiently negative. DCFs provide an all optical technique that can provide complete compensation with both dispersion and dispersion slope matched. This is possible only when non-linear factors brought about by large optical peak powers remain negligible[2].

In order to understand how this compensation occurs, it is important to observe

how an optical pulse will travel through a combination of single-mode fiber (SMF) and DCF. We know from Chapter 2 that the first order dispersion parameter is,

$$\beta_2 = \frac{-D\lambda^2}{2\pi c} \quad (3.4)$$

and the second order dispersion parameter is,

$$\beta_3 = \frac{\lambda^3}{(2\pi c)^2} \left[ \lambda \frac{dD}{d\lambda} + 2D \right] \quad (3.5)$$

by solving for  $\beta_3$  in the equation defining dispersion slope[2],

$$S = \left( \frac{2\pi c}{\lambda^2} \right)^2 \beta_3 + \left( \frac{4\pi c}{\lambda^3} \right) \beta_2. \quad (3.6)$$

The transfer function of an optical fiber can then be written from the basic propagation equation,

$$\begin{aligned} H(\Delta f) &= \exp [j\beta L] \\ &= \exp \left[ j \left( \frac{\beta_2}{2} \Delta\omega^2 + \frac{\beta_3}{6} \Delta\omega^3 \right) L \right] \\ &= \exp \left[ j \left( \frac{\pi\lambda^2 DL}{c} \Delta f^2 \left( 1 - \frac{\lambda}{3c} \left( 2 + \frac{\lambda S}{D} \right) \Delta f \right) \right) \right] \\ &= \exp [j(a\Delta f^2 + b\Delta f^3)] \end{aligned} \quad (3.7)$$

neglecting loss and non-linear effects ( $\Delta\omega = 2\pi\Delta f$ ). In order to compensate the accumulated dispersion along the fiber link, a DCF may be used at the end of a transmission length. When combining the effects of both fibers (SMF and DCF) the transfer function becomes,

$$H_1(\Delta f)H_2(\Delta f) = \exp [j((a_1 + a_2)\Delta f^2 + (b_1 + b_2)\Delta f^3)] \quad (3.8)$$

where,

$$a_1 + a_2 = \frac{\pi\lambda^2}{c} [D_1L_1 + D_2L_2] \Delta f^2 \quad (3.9)$$

and,

$$b_1 + b_2 = \frac{\pi\lambda^3}{3c^2} [2(D_1L_1 + D_2L_2) + \lambda(S_1L_1 + S_2L_2)] \Delta f^3. \quad (3.10)$$

In order for the dispersive effects to be negated and the originally launched signal to exit the DCF, the terms  $a_1 + a_2$  and  $b_1 + b_2$  must equal zero. From the above explanation it is clear that for this to occur Eq. (3.11) and Eq. (3.12) must be satisfied [2, 24].

$$D_1L_1 + D_2L_2 = 0 \quad (3.11)$$

$$S_1L_1 + S_2L_2 = 0 \quad (3.12)$$

To achieve both dispersion and dispersion slope compensation, typically the length of the SMF is fixed and known, while the length of the DCF may be altered according to its own parameters to achieve compensation. SMF (G.655) has a dispersion parameter of 17.5 ps/(km-nm) at a wavelength of 1550 nm, and a dispersion slope of 0.09 ps/(km-nm<sup>2</sup>). The DCF used during simulation was modelled by observing the parameters of the OFS RightWave EHSDK-C Dispersion Compensating Module. From the OFS data sheet we can conclude that the dispersion parameter of the DCF is -60 ps/(km-nm) resulting in a 14.583 km length needed to achieve perfect compensation after 50 km of SMF. To achieve perfect dispersion slope compensation Eq. (3.12) is similarly used resulting in a DCF dispersion slope of -0.308 ps/(km-nm<sup>2</sup>).

$$RDS_{DCF} = \frac{S_{DCF}}{D_{DCF}} = \frac{S_{SMF}}{D_{SMF}}. \quad (3.13)$$

Combining these results and therefore perfectly compensating both first and second order dispersion results in a relative dispersion slope (RDS) of 0.0051 nm<sup>-1</sup> which is similar to that of the dispersion compensating modules (DCMs) available commercially. The OFS DCF shows a RDS of 0.01 nm<sup>-1</sup>. Figure 3.2 shows schematically

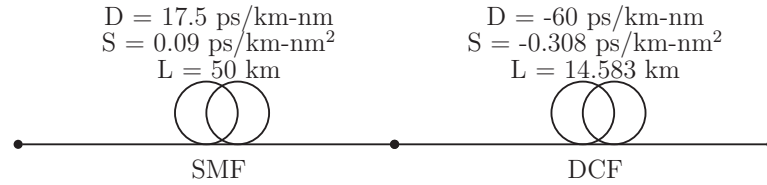


Figure 3.2: Visual representation and values for perfect dispersion and dispersion slope compensation.

the transmission link, outlining the parameters discovered above. For Eq. (3.11) and (3.12) to be simultaneously satisfied, the SMF and DCF must have the same RDS.

## 3.3 Jitter

### 3.3.1 Background

Recalling the discussion in Chapter 2 regarding the calculation of receiver sensitivity, and therefore system penalty, an optimal sampling time was chosen that resulted in the best performance. In practical systems the sampling time is often not optimal as a result of a fluctuations in the received signal. These fluctuations are known as timing jitter and are an additional source of penalty in OTDM systems[2].

It becomes further important to quantify jitter in an OTDM system as its effect increases proportionally with bit rate[30]. Furthermore, it has been shown that the tolerance an optical system can withstand decreases with a decreasing return-to-zero (RZ) pulse duty cycle[31]. With OTDM signals possessing both large bit rates and narrow pulse widths, fluctuations in a recovered clock will undoubtedly be a significant source of penalty.

The source of jitter may result from various components within a transmission link. The total effect of the resulting jitter can be divided into two contributions: random jitter (RJ) and deterministic jitter (DJ)[30, 31]. The accumulation of RJ results from random processes such as thermal and shot noise, and is assumed to follow a gaussian distribution[30]. The penalties associated with DJ can arise from asymmetries in the recovered clock, periodic electromagnetic effects from power supplies, and ISI from data dependant effects and dispersion[30]. The total jitter acting on a recovered clock ( $C(t)$ ) is represented as a fluctuating phase noise ( $\phi_T(t)$ ) and its impact is shown mathematically in Eq. (3.14).

$$C(t) = \sin(2\pi ft + \phi_T(t)) \quad (3.14)$$

This resulting phase noise not only affects the optimal sampling time of the receiver, but also the switching window used to demultiplex a specific OTDM channel. The impacted driving waveforms for the electro-absorption modulators (EAMs) can now be expressed as,

$$D_x(t) = A_x \cdot \sin(2\pi f_x t + \phi_x + \phi_T(t)) - B_x, \quad (3.15)$$

where  $A_x$ ,  $\phi_x$ , and  $B_x$  are the amplitude, phase, and bias for EAM driving waveform  $D_x(t)$  (where  $x=1,2$ ). The total phase noise is expressed as the sum of both the random and deterministic contributions[31]:

$$\phi_T(t) = \phi_R(t) + \phi_D(t). \quad (3.16)$$

As timing jitter is often measured as units of time shifted away from an optimal value, the total jitter may be expressed as[31],

$$t_j(t) = t_{jR}(t) + t_{jD}(t) \quad (3.17)$$

where,

$$t_j(t) = \frac{\phi_T(t)}{2\pi f_x}. \quad (3.18)$$

This may be expressed in terms of a root mean squared value as[31],

$$t_{jRMS} = \sqrt{E[t_j(t)^2]} \quad (3.19)$$

where  $E[t_j(t)^2]$  is the expectation of  $t_j(t)^2$ . As the total jitter is assumed to be a random process following a gaussian distribution, Eq. (3.19) may be described as[31],

$$t_{jRMS}^2 = \mu_j^2 + \sigma_j^2 \quad (3.20)$$

where  $\mu_j$  and  $\sigma_j$  represent the mean and standard deviation. Furthermore, as a non-zero mean corresponds to a fixed delay in time, the total RMS timing jitter may be simplified to,

$$t_{jRMS} = \sigma_j. \quad (3.21)$$

$t_{jRMS}$  most accurately describes jitter, as it is quantified in terms of the gaussian probability density function and is expressed in units of time[31].

For the purposes of quantifying system performance degradation due to jitter, it becomes less important as to its causes or origin and more dependant on how its presence affects the bit-error rate (BER). The use of a phase-locked loop (PLL) as a clock recovery unit is well documented, as is its analysis of contributors to timing jitter which may be explored in [32]. In Chapter 4, a method of adjusting the sampling time will be presented and simulated to document the effect of timing jitter on OTDM signal transmission.

## 3.4 Polarization Mode Dispersion

### 3.4.1 Background

The importance of studying polarization effects on OTDM signals is caused by the extremely narrow pulses transmitted. Both an increase in signal bit rate and fiber transmission lengths have brought about its thorough characterization[33]. Random perturbations that occur in the fiber will have an effect on the travelling mode and gives way to additional pulse broadening. Due to its dispersive qualities acting on the pulse/mode, PMD is an additional source of system penalty.

As an optical signal traverses an imperfect, or field installed, optical fiber it will encounter random perturbations which give way to birefringence. Birefringence can thereafter lead to periodic power exchanges between the two principle states of polarization[2]. The birefringence is defined by[33],

$$\Delta n_{eff} = n_s - n_f \quad (3.22)$$

where  $n_s$  and  $n_f$  represent the effective indices of refractive index of the slow and fast moving  $HE_{11}$  modes.

The perturbations that lend to additional birefringence are characterized as either intrinsic or extrinsic. Intrinsic perturbations include noncircular core and nonsymmetrical stress fields in the glass surrounding the core region[33]. Extrinsic perturbations typically result as the fiber is subjected to external forces during the handling and installation processes[33]. Such stresses that may occur included lateral stresses, bending of the cable, or twisting[33]. Variations of 1% from a circular core due to these stresses can lead to noticeable performance degradation in optical systems[33].

The method in which PMD should be treated is dependant upon the length of

transmission being pursued. When using short optical fibers, it is assumed that any perturbations acting on the fiber are constant over its length[33]. During transmission the two orthogonally polarized modes will experience a phase slippage resulting in a cyclic evolution from linear to various elliptical states. After a distance denoted by  $L_B$ , the beat length, the modes will return to their original linear states of polarization. The beat length is inversely proportional to the birefringence by[33],

$$L_B = \frac{\lambda}{\Delta n_{eff}}. \quad (3.23)$$

The beat length is defined as the period in which the two orthogonally polarized modes will exchange power[2]. Typically  $\Delta n_{eff} \approx 10^{-7}$ , therefore at  $\lambda = 1557$  nm, the beat length is approximately 15.57 m. In short fibers, the PMD is typically reported in units of picoseconds per kilometer. This is attributed to the assumption that for short fibers, the birefringence is assumed to be uniform[33]. This assumption would lead to very large penalties as the fiber length increases.

For large fiber lengths, the effects of PMD do not accumulate linearly through transmission[33]. One may consider a long fiber as several instances of short fibers, each providing a different effect on the optical field due to their own set of perturbations. This leads to a random and statistical approach to PMD and a square root length dependence[33]. For this reason, PMD research is typically performed using mathematical simulations of stochastic processes in an attempt to accurately characterize its effects. In general, the PMD inflicted upon a transmitted signal is link and application dependant.

To determine whether a specific span of fiber should be treated as short or long, the parameter  $l_c$ , the correlation length, must be considered. It is defined as the length of fiber at which the average power in the orthogonally polarization mode,

$P_{\perp}$ , is within  $1/e^2$  of that in the starting mode,  $P_{\parallel}$ [33]. The explicit mathematical definition is given in Eq. (3.24).

$$\frac{\langle P_{\parallel}(l_c) \rangle - \langle P_{\perp}(l_c) \rangle}{P_{total}} = \frac{1}{e^2} \quad (3.24)$$

## 3.5 Non-Linear Effects

### 3.5.1 Background

Non-linear transmission effects occur in optical fibers simply because silica is a dielectric. It is well known that dielectrics respond in a non-linear fashion when exposed to intense electromagnetic fields of light[2]. The phenomena associated with losses due to non-linear behaviour include: stimulated Raman scattering (SRS), four wave mixing (FWM), stimulated Brillouin scattering (SBS), and non-linear phase modulation. In SRS, large input powers cause the lightwave to be scattered by the silica molecules; SBS occurs due to the compression of silica in the presence of a large electromagnetic field[2]. Non-linear phase modulation in OTDM signals results from SPM and intra-channel cross-phase modulation (XPM). SPM occurs when the optical signal beats against itself causing non-linear frequency chirping. In contrast, XPM results when two or more optical channels are transmitted within close spectral proximity of one another[2]. These phase modulations lead to further signal degradation through the effect of dispersion, resulting in further pulse broadening.

Non-linear phase modulation results as the refractive index of silica is dependant upon the non-linear coefficient. The resulting refractive index may be expressed as[2],

$$n'_j = n_j + n_2 \left( \frac{P}{A_{eff}} \right). \quad (3.25)$$

As shown in Eq. (3.25), both the optical power and effective area of the transmission fiber will vary the amount of non-linearity associated with transmission. It should be clear to the reader that as the effective area of the fiber becomes smaller, such as in DCFs, the effect of a large optical power on the non-linear coefficient will increase.

The onset of SPM brings about additional pulse broadening as the propagation constant becomes power dependant and may now be expressed as[2],

$$\beta' = \beta + \gamma P \quad (3.26)$$

where  $\gamma$  was defined earlier in Eq. (2.34), and is related to both the non-linear coefficient, and effective area. As the optical phase increases linearly during transmission, a non-linear phase shift is then generated by  $\gamma$ . This phase shift can be quantified as[2],

$$\Phi_{NL} = \gamma P_{in} L_{eff} \quad (3.27)$$

where  $L_{eff}$  is the effective interaction length and is given by[2],

$$L_{eff} = \frac{1 - e^{-\alpha L}}{\alpha}. \quad (3.28)$$

The system performance degradation associated with SPM is the most dominant non-linear effect associated with single wavelength transmission[2].

Secondary non-linear effects on OTDM pulse propagation are that of FWM and XPM. While all pulses transmitted in an OTDM system share the same wavelength, new and unwanted pulses (referred to as ghost pulses) may be generated in the time domain. The term intra-channel FWM is used as an analogy to FWM which creates new waves in the spectral domain[2]. Alternatively, intra-channel XPM affects only the phase of the pulses. However, as phase is time dependant, the resulting frequency chirp leads to timing jitter through dispersion[2]. While these effects are possible

sources of additional system performance degradation, for single channel optical systems, the dominant non-linear effect that limits system performance is SPM[2]. As a result, intra-channel effects on system performance was not accounted for during MatLab simulations.

The additional pulse broadening brought about by non-linearities is further amplified in the presence of residual dispersion and dispersion slope. As OTDM systems are considered dispersion limited, it becomes extremely important to quantify this combinations of effects. Chapter 4 will provide more detail on how the system performance is altered in the presence of both non-linearities and the dispersive properties of SMF.

# Chapter 4

## Simulation Results & Discussion

### 4.1 Introduction

Utilizing the system outlined in Chapter 2 to simulate the impairments described in Chapter 3, this chapter aims to give a clear assessment of the system tolerance. In performing these simulations, we are able to quantify the system sensitivity in relation to dispersion, dispersion slope, timing jitter, polarization mode dispersion (PMD), and nonlinear effects. System sensitivity to these transmission impairments must be quantified if such a system were to be implemented in the field. For each simulation, a complete disclosure of the operating conditions will be given, followed by graphical and numerical results, and discussion of the findings.

### 4.2 Global Operating Conditions

Within all simulations performed, there exists several variables that remain fixed. The simulations are broken down into systems/functions of: transmitter (TX), fiber,

demultiplexer, and receiver (RX). These values are presented in Tables 4.1 to 4.4. The demultiplexer used is that which was presented in Figure 2.11.

Back-to-back (B2B) simulations are performed over 10 m of single-mode fiber (SMF) with an average power of 10 dBm. Measurements of penalty relative to the B2B performance, are calculated in terms eye-opening penalty (EOP).

## 4.3 Dispersion

### 4.3.1 Introduction

The tolerances a 160 Gbit/s optical time division multiplexing (OTDM) system exhibits towards both first and second order dispersion are less than that of lower bit rate systems. The ultra-narrow pulses of a 160 Gbit/s OTDM signal are far more sensitive to changes in group delay, limiting the system performance considerably. To thoroughly investigate the system response to group delay, several different scenarios were constructed in MatLab and their results presented graphically in terms of system penalty.

### 4.3.2 System Tolerance

In the first set of simulations performed, the optical signal was launched into an equivalent fiber given by Eq. (3.8) in which the residual dispersion was altered through each pass of the fiber. This equivalent fiber is effective in simulating the combination of SMF and dispersion compensating fiber (DCF) given that the optical power is kept sufficiently low, such that non-linear effects may be neglected. The dispersion was set to a maximum of  $\pm 0.06$  ps/(km-nm). This was done to avoid large amounts of

| Device      | Parameter                          | Value  | Units  |
|-------------|------------------------------------|--------|--------|
| Transmitter | Bit rate                           | 160    | Gbit/s |
|             | Samples per bit (160 Gbit/s)       | 32     |        |
|             | Samples per bit (10 Gbit/s)        | 512    |        |
|             | PRBS                               | 128    | bits   |
|             | Transmission wavelength            | 1557   | nm     |
|             | Electrical signal rise-time        | 0.25   | ps     |
|             | Electrical signal fall-time        | 0.25   | ps     |
|             | Duty cycle                         | 25     | %      |
| MZM         | Bias Voltage                       | 0.5    | V      |
|             | Relative modulation voltage, arm 1 | -0.5   | V      |
|             | Relative modulation voltage, arm 2 | 0.5    | V      |
| TX Filter   | Filter type                        | Bessel |        |
|             | 3-dB bandwidth                     | 130    | GHz    |
|             | Filter order                       | 8      |        |

Table 4.1: Globally defined TX operating conditions.

| Device | Parameter                                     | Value                  | Units                 |
|--------|---|------------------------|-----------------------|
| SMF    | Attenuation                                   | 0.22                   | dB/km                 |
|        | Non-linear coefficient                        | $2.31 \times 10^{-20}$ | $\text{m}^2/\text{W}$ |
|        | Effective area                                | 80                     | $\mu\text{m}^2$       |
|        | Zero dispersion wavelength ( $\lambda_{ZD}$ ) | 1312                   | nm                    |
| DCF    | Attenuation                                   | 0.33                   | dB/km                 |
|        | Non-linear coefficient                        | $2.31 \times 10^{-20}$ | $\text{m}^2/\text{W}$ |
|        | Effective area                                | 20                     | $\mu\text{m}^2$       |
|        | Zero dispersion wavelength ( $\lambda_{ZD}$ ) | 1312                   | nm                    |

Table 4.2: Globally defined fiber operating conditions.

| Device                | Parameter           | Value  | Units   |
|-----------------------|---------------------|--------|---------|
| EAM Drive 1           | Amplitude ( $A_1$ ) | 1.1307 | V       |
|                       | Phase ( $\phi_1$ )  | 0.2806 | radians |
|                       | Bias ( $B_1$ )      | 2.8633 | V       |
|                       | Frequency ( $f_1$ ) | 40     | GHz     |
| EAM Drive 2           | Amplitude ( $A_2$ ) | 1.1052 | V       |
|                       | Phase ( $\phi_2$ )  | 1.1984 | radians |
|                       | Bias ( $B_2$ )      | 2.8948 | V       |
|                       | Frequency ( $f_2$ ) | 10     | GHz     |
| Integrated Amplifiers | Gain                | 10     | dB      |

Table 4.3: Globally defined demultiplexer operating conditions.

| Device     | Parameter                   | Value                 | Units |
|------------|-----------------------------|-----------------------|-------|
| EDFA       | Gain                        | 30                    | dB    |
|            | Noise figure                | 3.4                   | dB    |
|            | 3-dB saturation power       | 15                    | dBm   |
|            | Optical filter bandwidth    | 400                   | GHz   |
|            | Input coupling loss         | 0                     | dB    |
|            | Output coupling loss        | 0                     | dB    |
| Photodiode | Responsivity                | 1                     | A/W   |
|            | Dark current                | 10                    | nA    |
|            | Input noise current density | $3.4 \times 10^{-22}$ | W/Hz  |
| RX Filter  | Filter type                 | Bessel                |       |
|            | 3-dB bandwidth              | 7.5                   | GHz   |
|            | Filter order                | 4                     |       |

Table 4.4: Globally defined RX operating conditions.

| Parameter                 | Value       | Units              |
|---------------------------|-------------|--------------------|
| Fiber length              | 50          | km                 |
| Residual Dispersion       | -3.0 – +3.0 | ps/nm              |
| Residual Dispersion slope | 0.05        | ps/nm <sup>2</sup> |

Table 4.5: Simulation configuration in measuring penalty due to dispersion over an equivalent fiber.

eye-opening penalty ( $>3$  dB). The non-linear term of the fiber propagation equation was also neglected to isolate linear transmission performance.

The B2B electrical eye-diagram can be seen in Figure 4.1. A circle is used to designate where the eye-opening lies as its location may become questionable due to the large amount of pulse broadening resulting from residual dispersion. The resulting eye-opening penalties are shown in Figure 4.2. The evolution of the electrical eye-diagram is shown in Figure 4.3 for the varying values of dispersion outlined in Table 4.5. The dispersion tolerance of a system is defined as the residual dispersion range ( $\Delta D$ ) that will cause less than 1 dB of penalty[34]. Using this definition and the data collected from Figure 4.2, it can be concluded that a change of smaller than  $\pm 1.7$  ps/nm in residual dispersion defines the system tolerance.

The varying amplitudes seen in Figure 4.3 can be explained by examining the optical eye-diagrams before and after the demultiplexer, and their respective electrically received eye-diagrams. Figure 4.4 shows this evolution for Figures 4.3(a), 4.3(b), and 4.3(c). For reference, a B2B case is plotted in Figure 4.5. As the residual dispersion increases, and the optical pulse broadens, neighbouring pulses will begin to

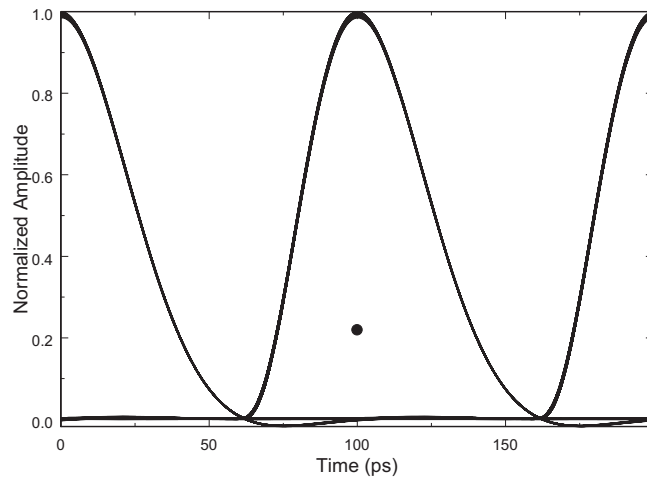


Figure 4.1: Back-to-back eye-diagram.

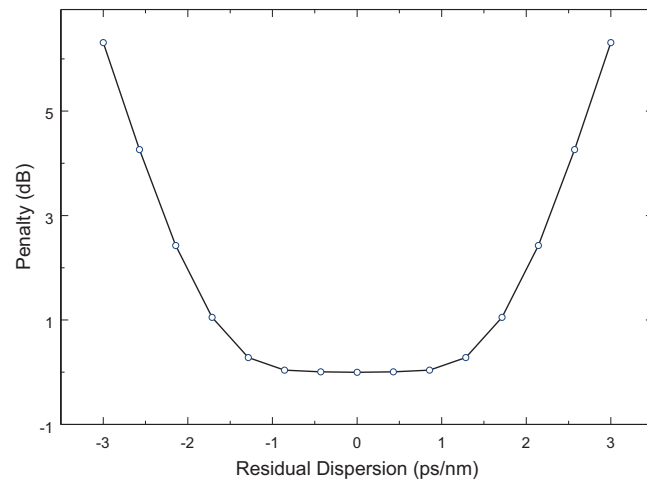


Figure 4.2: Penalty (EOP) due to changes of residual dispersion.

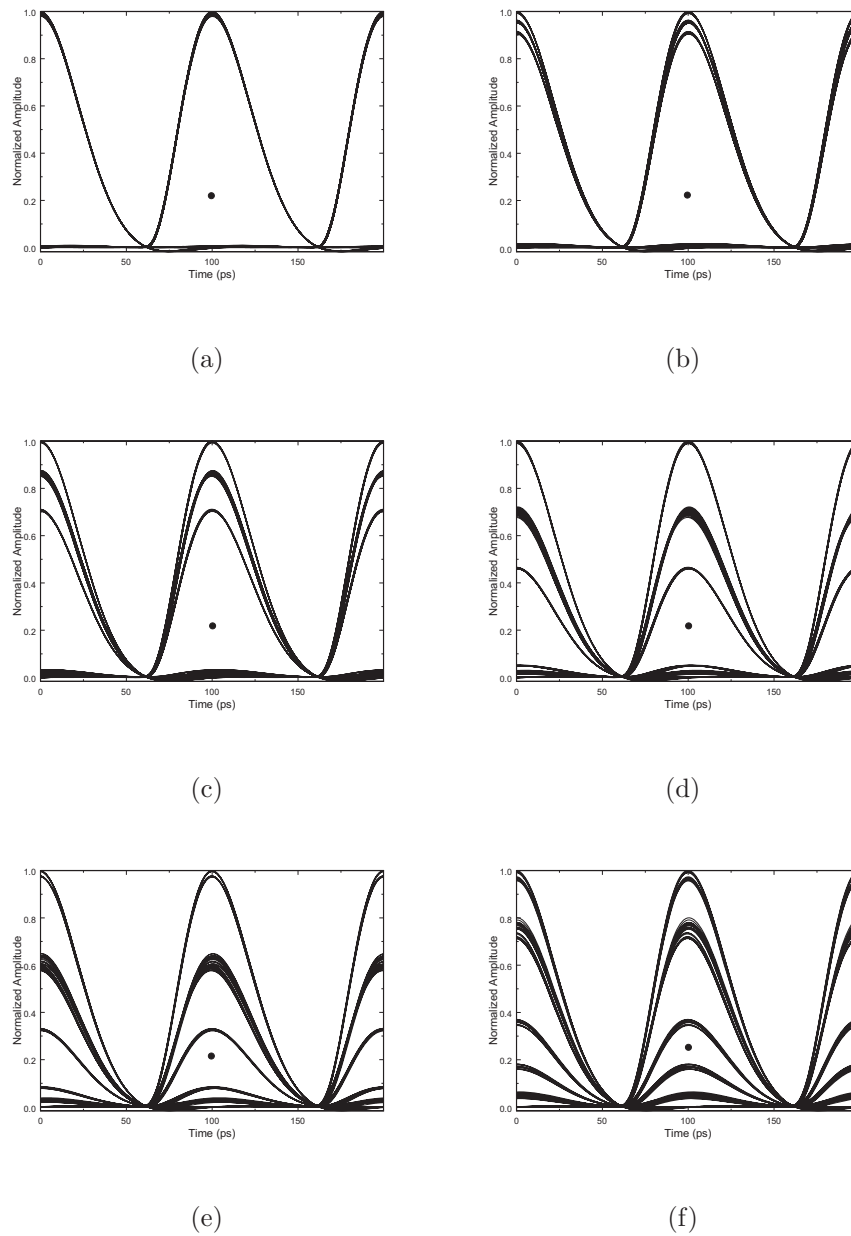


Figure 4.3: Electrical eye-diagram evolution with an equivalent residual dispersion of: (a) 0.86 ps/nm, (b) 1.29 ps/nm, (c) 1.71 ps/nm, (d) 2.14 ps/nm, (e) 2.57 ps/nm, and (f) 3.0 ps/nm.

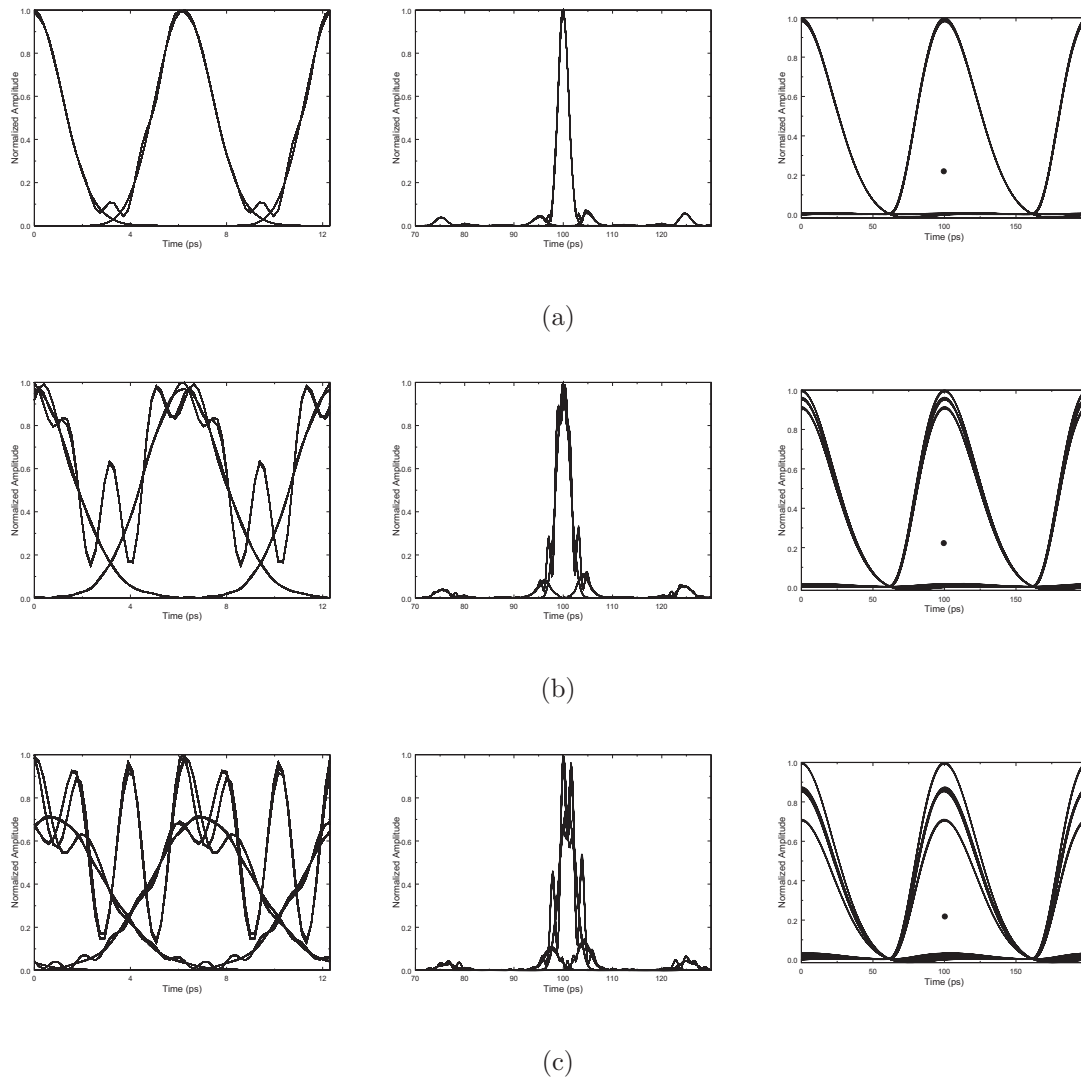


Figure 4.4: From left to right: optical eye-diagrams taken before the demultiplexer, after the demultiplexer, followed by the electrical eye-diagram, for a residual dispersion of: (a) 0.86 ps/nm , (b) 1.29 ps/nm, and (c) 1.71 ps/nm.

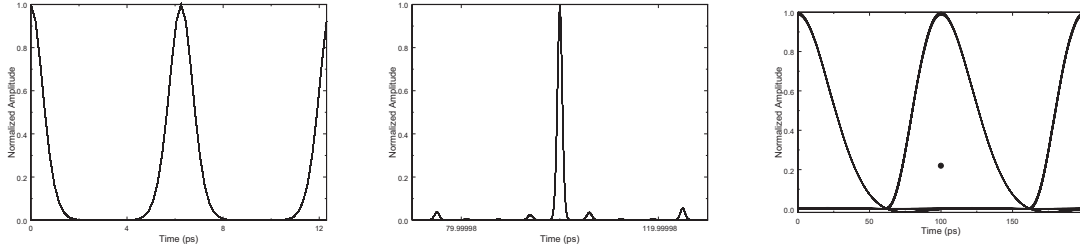
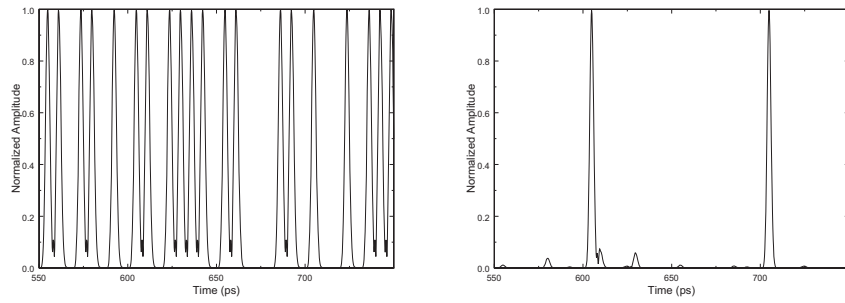


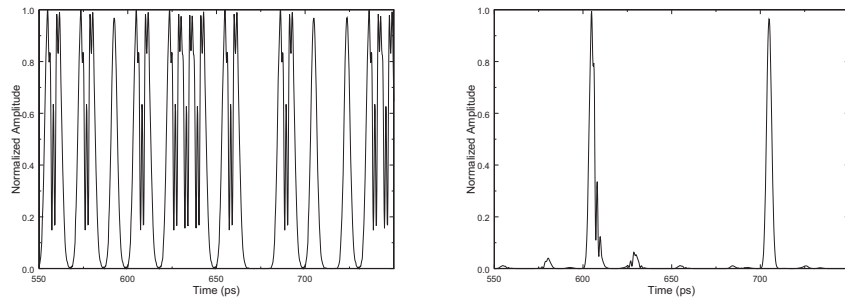
Figure 4.5: From left to right: B2B optical eye-diagrams taken before the demultiplexer, after the demultiplexer, followed by the electrical B2B eye-diagram.

overlap, resulting in inter-symbol interference (ISI). The onset of this effect is seen in Figure 4.4(a). With the additional rise of residual dispersion in Figure 4.4(b), the cause of the distinct amplitude variations at the receiver becomes evident. The increased amount of pulse broadening has spread the neighbouring optical bits within the switching window of the electro-absorption modulator (EAM) gates. Figure 4.4(c) shows a more dramatic example of the above effect. The electrically received eye-diagrams have been filtered at 7.5 GHz, thereby broadening the pulses, while removing unwanted spectral components. The varying amplitudes in the optical domain are therefore translated into the electrical domain. Figure 4.6 shows the varying amplitudes in the time domain.

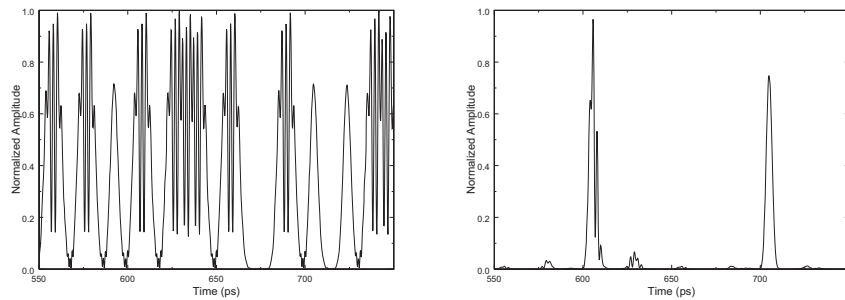
The optical eye-diagrams taken after the demultiplexer also show a distortion in the zeros. This can be explained by recalling that the optimization of the gating variables, in Section 2.5.3, is performed on the electrical eye-diagram. While the channel to be demultiplexed may be completely passed by the first EAM gate, it may be absorbed (fully or partially) by the second EAM gate. These partially absorbed unwanted bits come through the demultiplexer as distortion in the spaces. Figure 4.7



(a)



(b)



(c)

Figure 4.6: From left to right: optical time-domain OTDM signal taken before and after the demultiplexer, for a residual dispersion of: (a)  $0.86 \text{ ps/nm}$ , (b)  $1.29 \text{ ps/nm}$ , and (c)  $1.71 \text{ ps/nm}$ .

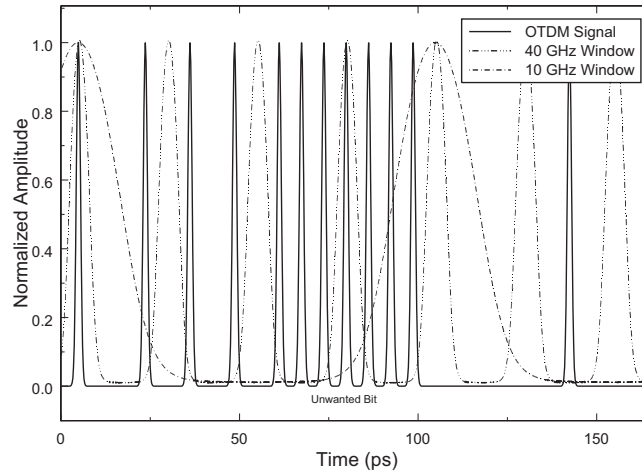


Figure 4.7: Time domain 160 Gbit/s OTDM signal, and both EAM switching windows.

shows a time domain representation of a 160 Gbit/s signal, as well as the switching windows acting upon it due to the EAM gates. As this effect is related to the gates, it will appear in all eye-diagrams which are taken after the demultiplexer. The variation in the amplitude of both marks and spaces can be clearly seen to be due to both ISI and the EAM gates.

The system dispersion slope tolerance can be similarly defined by simulating for various values of slope. The operating conditions of this simulation are found in Table 4.6. The evolution of the electrical eye-diagram is shown in Figure 4.8.

In performing these calculations, we find that the system can withstand a residual dispersion slope of approximately  $\pm 2.2$  ps/nm<sup>2</sup> to produce under 1 dB of penalty.

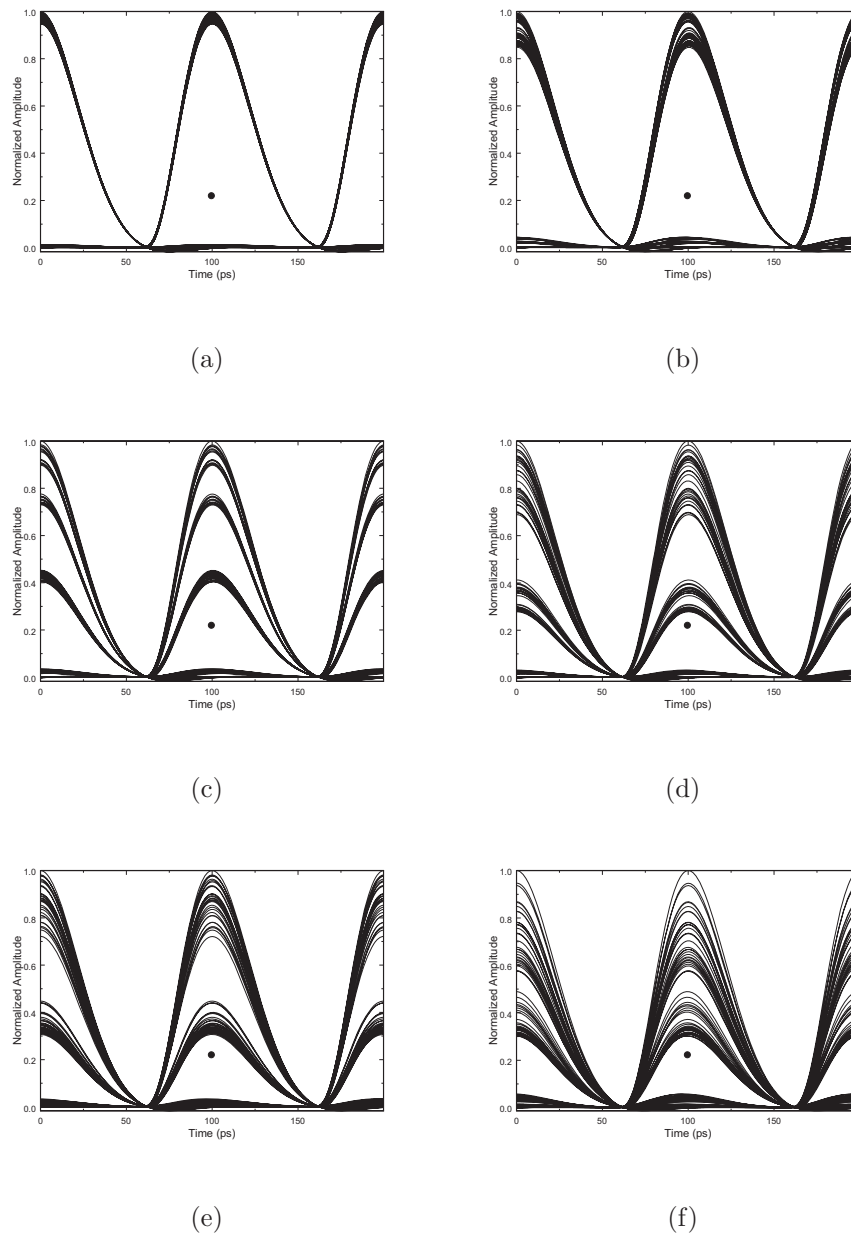


Figure 4.8: Electrical eye-diagram evolution with an equivalent dispersion slope length product of: (a)  $1.43 \text{ ps/nm}^2$ , (b)  $2.14 \text{ ps/nm}^2$ , (c)  $2.86 \text{ ps/nm}^2$ , (d)  $3.57 \text{ ps/nm}^2$ , (e)  $4.29 \text{ ps/nm}^2$ , and (f)  $5.00 \text{ ps/nm}^2$ .

| Parameter                 | Value       | Units              |
|---------------------------|-------------|--------------------|
| Fiber length              | 50          | km                 |
| Average power             | 10          | dBm                |
| Residual Dispersion       | 0.005       | ps/nm              |
| Residual Dispersion slope | -5.0 – +5.0 | ps/nm <sup>2</sup> |

Table 4.6: Simulation configuration in measuring penalty due to dispersion slope over an equivalent fiber.

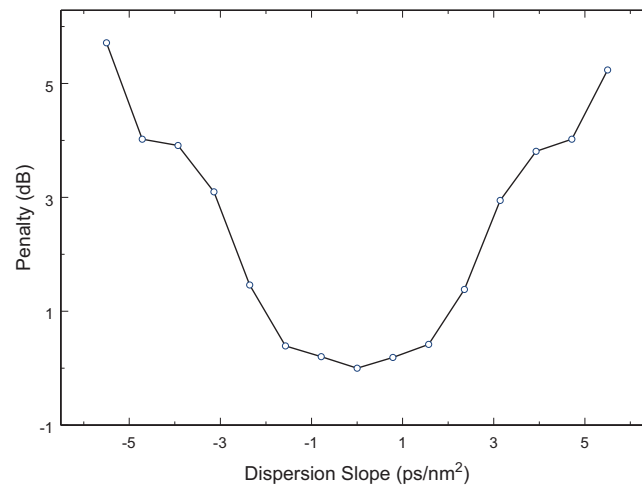


Figure 4.9: Penalty (EOP) due to increased residual dispersion slope.

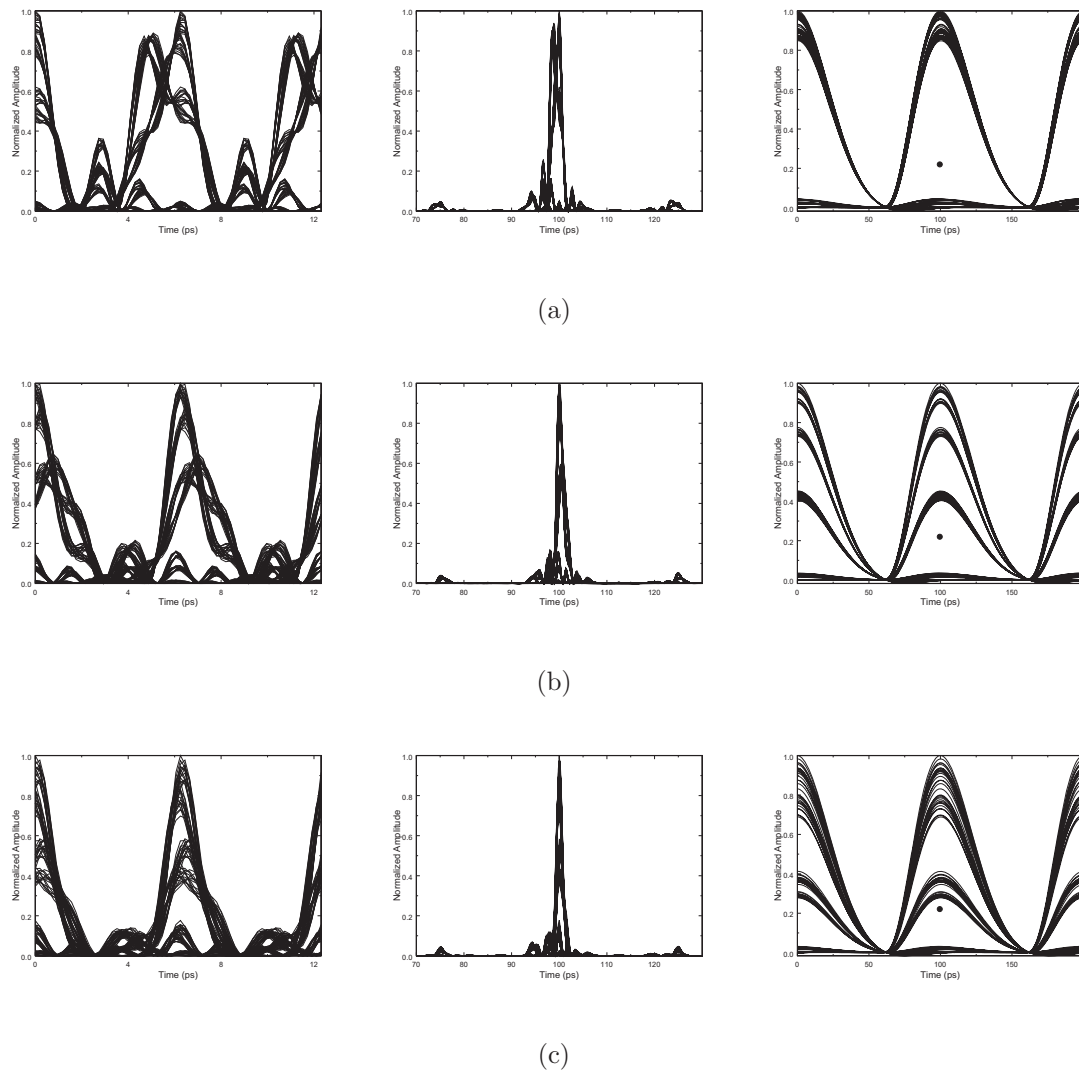
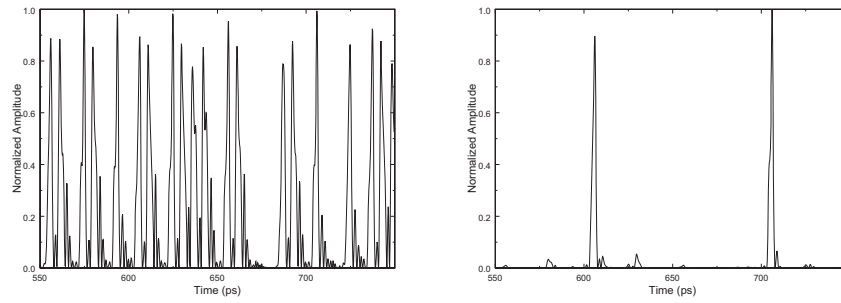
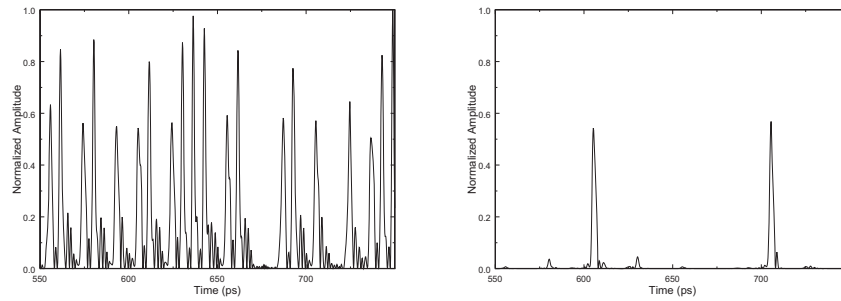


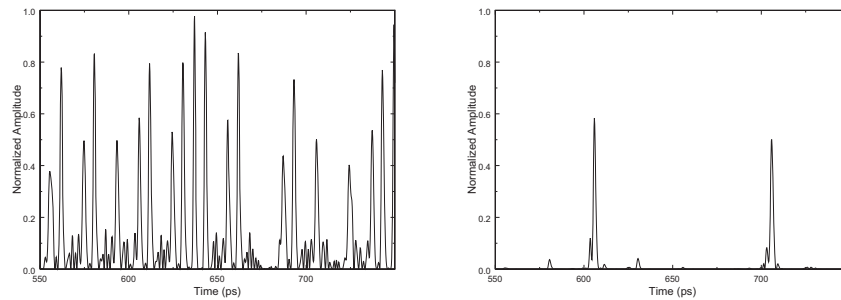
Figure 4.10: From left to right: optical eye-diagrams taken before the demultiplexer, after the demultiplexer, followed by the electrical eye-diagram, for a dispersion slope length product of: (a) 2.14 ps/nm<sup>2</sup>, (b) 2.86 ps/nm<sup>2</sup>, (c) 3.57 ps/nm<sup>2</sup>.



(a)



(b)



(c)

Figure 4.11: From left to right: optical time-domain OTDM signal taken before and after the demultiplexer, for a dispersion slope length product of: (a)  $2.14 \text{ ps/nm}^2$ , (b)  $2.86 \text{ ps/nm}^2$ , (c)  $3.57 \text{ ps/nm}^2$ .

The results, in terms of system penalty measured by EOP, are presented in Figure 4.9. The optical eye-diagrams in relation to Figures 4.8(b), 4.8(c), and 4.8(d), are presented in Figure 4.10, to aid in the explanation of the greater variance associated with the marks when analyzing the effects of dispersion slope. In applying varying amounts of dispersion slope, the optical waveform has become highly distorted before the demultiplexer. This can be seen clearly by examining the differences between Figure 4.4 and Figure 4.10. When passing through the receiver, the optical signal gets shaped by the filter. Similarly to the residual dispersion case, Figure 4.11 shows the time domain representation of the optical signal before and after the demultiplexer. A greater amplitude variance in the electrical domain can be attributed to the shaping of the amplitude distortions in the optical domain. The amplitude variations are due mostly to the distortions caused by an increased dispersion slope, and less so due to the EAM gating function.

When concerned with the design of a system and how adequately it would compensate for dispersive effects, a more practical approach must be investigated. To accomplish this, a length of standard SMF was simulated followed by a length of DCF. In such a system, the length of the SMF is typically fixed as the fiber may already be installed. For this reason, varying the length of the DCF and noting the penalty that arises is a more sensible method to determine the system tolerance. The DCF used during these simulations is that which was discussed and calculated in Section 3.2.2, outlining the compensation methodology.

To verify the calculations performed to achieve compensation, the resulting dispersion coefficients were multiplied by the respective fiber lengths, and plotted in

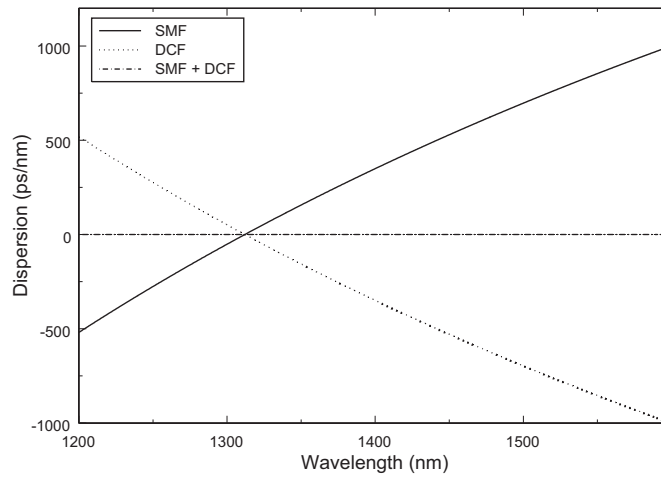


Figure 4.12: Visual representation of perfectly compensated dispersion curve. Lengths of SMF and DCF are 50 km and 14.583 km respectively.

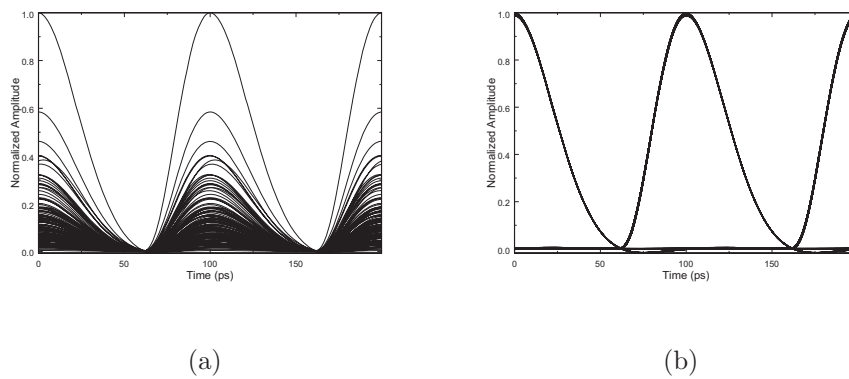


Figure 4.13: Electrical eye-diagrams for: (a) uncompensated signal after 50 km of SMF, and (b) fully dispersion compensated received electrical signal.

| Parameter            | Value         | Units                    |
|----------------------|---------------|--------------------------|
| SMF fiber length     | 50            | km                       |
| SMF dispersion       | 17.5          | ps/(km-nm)               |
| SMF dispersion slope | 0.09          | ps/(km-nm <sup>2</sup> ) |
| DCF fiber length     | 14.54 – 14.63 | km                       |
| DCF dispersion       | -60.0         | ps/(km-nm)               |
| DCF dispersion slope | -0.308        | ps/(km-nm <sup>2</sup> ) |
| Average power        | 10            | dBm                      |

Table 4.7: Simulation configuration in measuring penalty due to a variation in the optimum DCF length for perfect dispersion and dispersion slope compensation

Figure 4.12. The SMF and DCF are designated by the positive and negative sloping curves respectively, while the horizontal line is their resulting sum. The representation of the received electrical eye-diagrams are shown in Figure 4.13 for both uncompensated and full compensation. Figure 4.13(a) has the appearance of a return-to-zero (RZ) eye-diagram due to the gating function performed by the EAMs.

When varying the length of the DCF away from the optimal value, increasing amounts of penalty will incur as Eq. (3.11) and Eq. (3.12) are no longer satisfied. This way we effectively introduce a mismatch in both dispersion and dispersion slope compensation. This can also arise in wavelength division multiplexing (WDM) systems as perfect slope matching between the fiber span and DCF does not occur across all channels. The operating conditions used in varying the DCF length are presented in Table 4.7 and the setup is described in Figure 3.2. The values of penalty associated

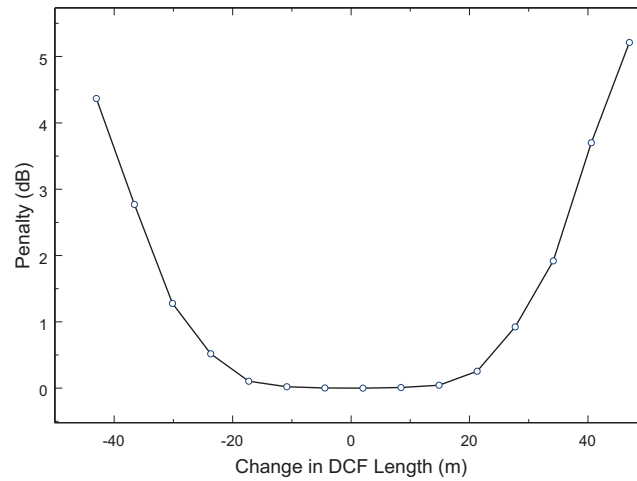


Figure 4.14: Penalty (EOP) due to change in length of DCF.

with varying the length of DCF are displayed in Figure 4.14 and show that to obtain less than 1 dB of penalty there is a 28 meter constraint. Therefore, if compensation is to be performed using commercially available DCF on previously installed SMF spans, the length of the DCF must be cut to within 28 m of the optimal calculated value for this system. The requirement may then be quantified by noting that the length of DCF used to compensate for accumulated dispersion along a SMF, must be within 0.2% of the perfect compensation length.

Inspecting Figures 4.2 and 4.14 reveals that the results stated above are in good agreement. When multiplying the dispersion of the DCF by the length calculated to obtain 1 dB of penalty, the result is a dispersion tolerance of -1.68 (ps/nm)

$$\begin{aligned}
 D(ps/nm) &= L(km) \cdot D\left(\frac{ps}{km - nm}\right) \\
 &= -1.68(ps/nm)
 \end{aligned}$$

$$\approx -1.7(\text{ps/nm}). \quad (4.1)$$

This result is in good agreement with the dispersion tolerance of  $\pm 1.7$  (ps/nm) from Figure 4.2.

## 4.4 Jitter

### 4.4.1 Introduction

The combined timing jitter in this OTDM system may be expressed as a combination of its effects at both the receiver and the demultiplexing unit. At the receiver, shifting the sampling time away from the optimal condition can effectively mimic the effects of the signal itself shifting. In fact, doing so is analogous to keeping the sampling time stationary while the signal experiences timing jitter.

The penalty incurred on account of timing jitter acting on the OTDM demultiplexing unit is due to the impact jitter of the recovered clock signal has on the alignment of the gating window with the input signal. This may occur with or without the evidence of timing jitter on the received electrical signal. For this reason, both effects should be simulated separately. While jitter of the received signal may occur in any system, the impact of jitter in this system is that which occurs at the demultiplexer.

The aim of this section is to quantify these combined effects and clearly state which causes the largest system performance degradation.

### 4.4.2 System Tolerance

The effect of a shifting waveform was characterized in MatLab by noting changes in system performance that are associated with an imperfect sampling time. Figure 4.15 shows graphically how the sampling time was shifted at the receiver. As the system collects data at a rate of 512 samples per bit (using the 10 Gbit/s electrical signal), the resulting time per sample ( $T_s$ ) is 0.195 ps, as per the 100 ps bit period of the received electrical 10 Gbit/s signal. The value of  $T_s$  remains at 0.195 ps in the optical domain as well. This is possible as there are only 32 samples per bit in the 6.25 ps, 160 Gbit/s OTDM bit period. Eq. (4.2) shows how the sampling time is changed during simulation where  $s_{t,new}$  is the new adjusted sampling time,  $s_t$  is the optimal sampling time, and  $mT_s$  is an integer multiple of  $T_s$ . Figure 4.16, shows the EOP due to sampling the received electrical eye-diagram at several instances of time away from the optimal sampling time. Table 4.8 outlines the operating conditions in performing the above simulation. As the received electrical eye-diagram is not altered during each shift of the sampling time, it remains quantitatively the same as a B2B eye-diagram.

$$s_{t,new} = s_t - mT_s \quad (4.2)$$

Characterizing the effect of timing jitter on the EAM gates requires an applied phase offset to their driving waveforms. The phase offset (given by increments of  $T_s$ ) was added to each EAM driving waveform. This effectively mimics the effects of the jitter on the recovered clock. Eq. (4.3) shows how each driving waveform is altered by increments of  $T_s$ . Table 4.9 outlines the operating conditions for subsequent simulations. Figure 4.17 shows the evolution of the received electrical eye-diagram as

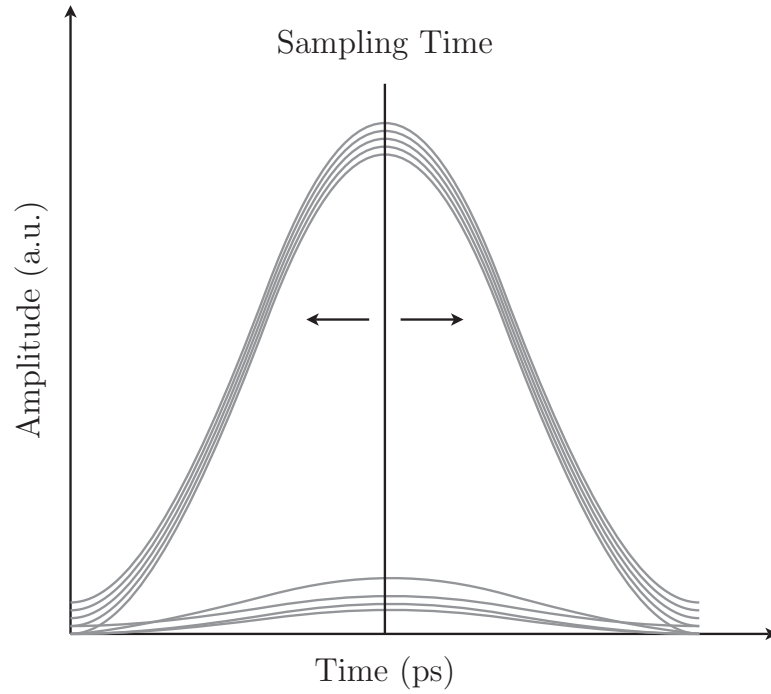


Figure 4.15: Jitter is simulated by altering the sampling time of the decision threshold.

| Parameter        | Value       | Units                    |
|------------------|-------------|--------------------------|
| Fiber length     | 10          | m                        |
| Average power    | 10          | dBm                      |
| Dispersion       | 17.5        | ps/(km-nm)               |
| Dispersion slope | 0.09        | ps/(km-nm <sup>2</sup> ) |
| Jitter           | -25 – 18.75 | ps                       |

Table 4.8: Simulation configuration in measuring penalty due to timing jitter of the received electrical signal.

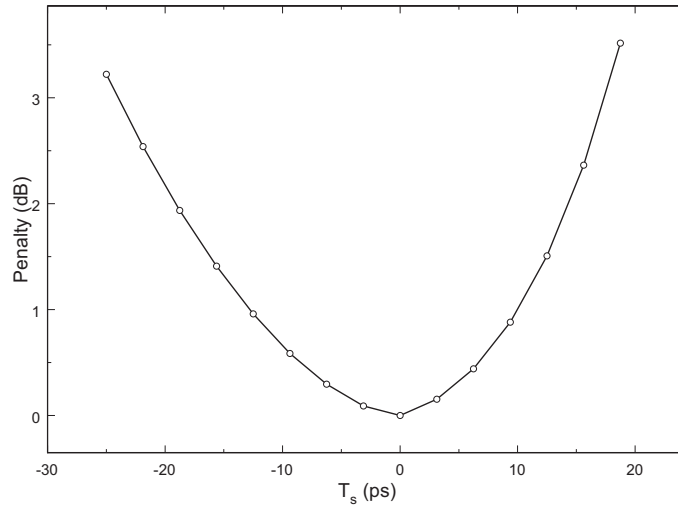


Figure 4.16: Penalty (EOP) due to sampling the eye-diagram at various times.

the demultiplexed optical signal changes due to imperfect channel selection.

$$D_x(t - T_s) = A_x \cdot \sin(2\pi f_x(t - T_s) + \phi_x) - B_x \quad (4.3)$$

To more clearly illustrate how these changes take place, several instances of the optical eye-diagram are plotted along with the corresponding electrical eye-diagrams in Figure 4.18. As the switching window becomes increasingly displaced from the target channel, there is a two fold effect. Firstly, the marks of the target OTDM channel will be clipped by the gates, which will in turn, decrease the pulse amplitude. Secondly, the neighbouring OTDM channels will begin to appear in the eye-diagrams as they become partially passed by the EAM gates. This can be seen clearly in the optical eye-diagrams taken after the demultiplexer of Figure 4.18. Asymmetry in the eye-diagram will increase as the EAM gates fail to fully absorb unwanted bits.

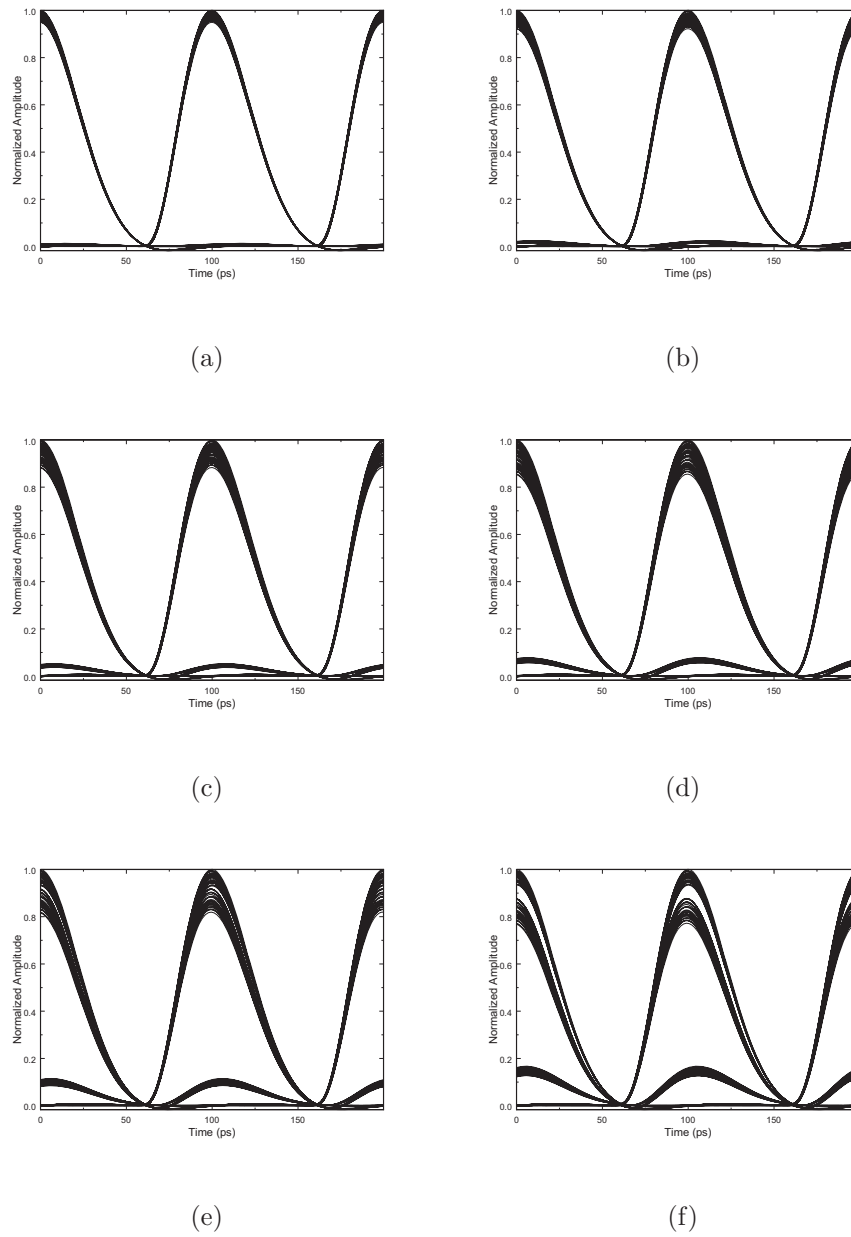


Figure 4.17: Electrical eye-diagram evolution with  $T_s$  in the amount of: (a) 0.781 ps, (b) 1.172 ps, (c) 1.562 ps, (d) 1.758 ps, (e) 1.953 ps, and (f) 2.148 ps.

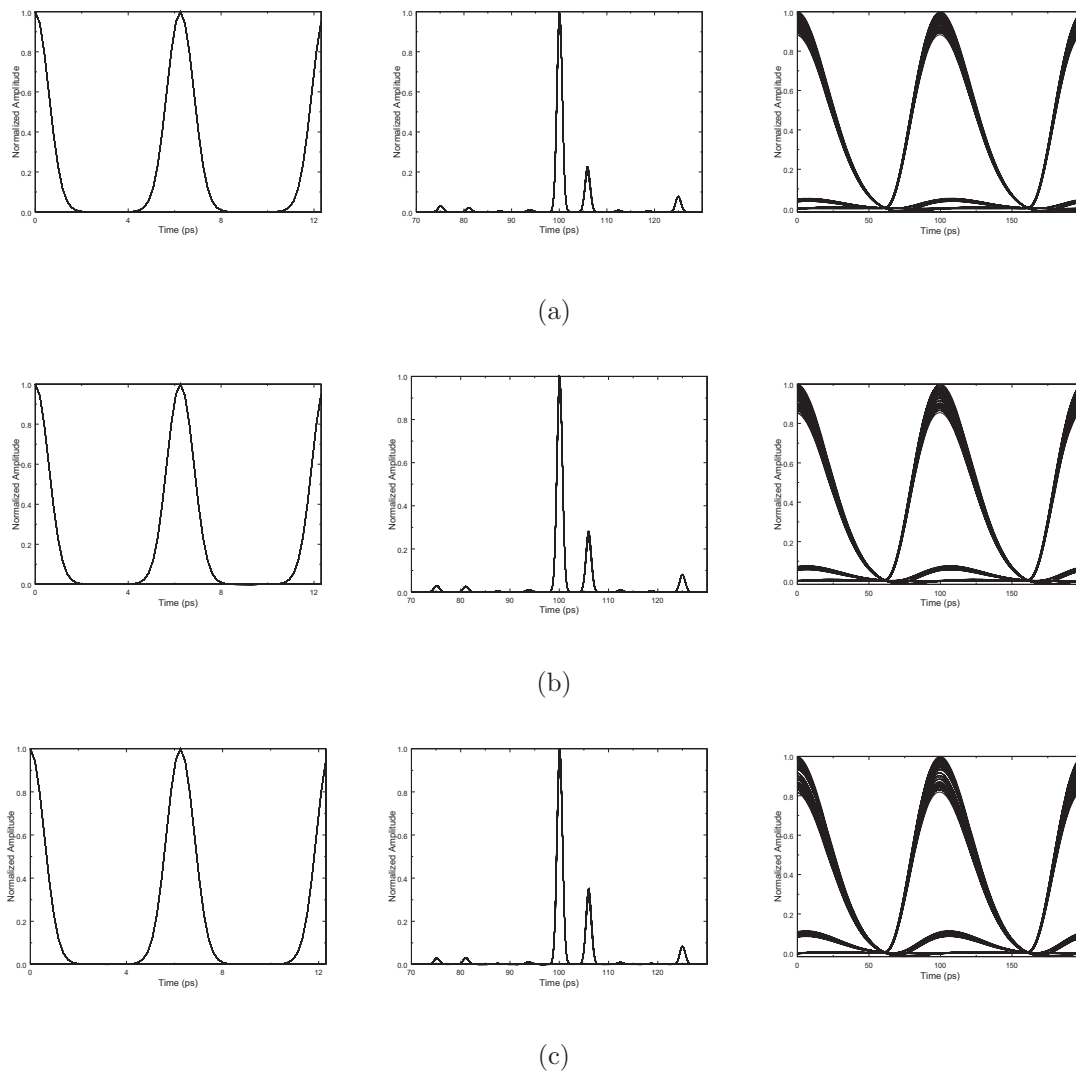
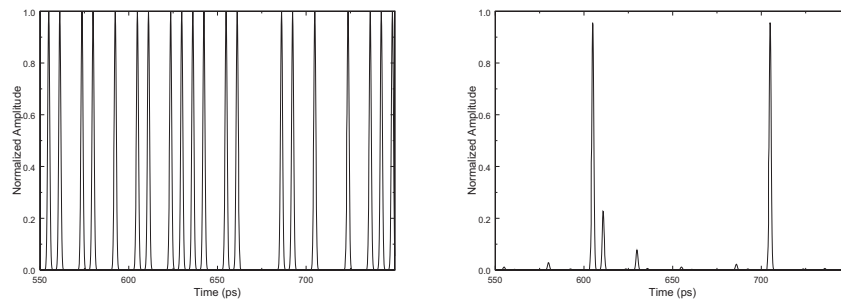
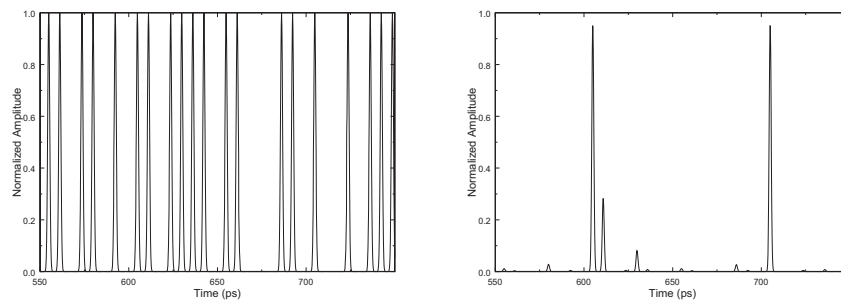


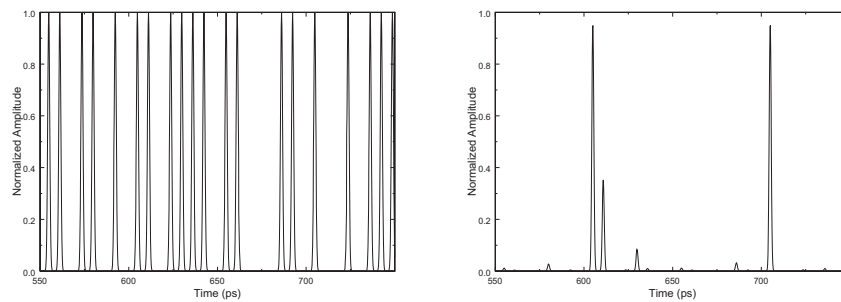
Figure 4.18: From left to right: optical eye-diagrams taken before the demultiplexer, after the demultiplexer, followed by the electrical eye-diagram, for  $T_s$  equal to: (a) 1.562 ps, (b) 1.758 ps, (c) 1.953 ps.



(a)



(b)



(c)

Figure 4.19: From left to right: optical time-domain OTDM signal taken before and after the demultiplexer, for  $T_s$  equal to: (a) 1.562 ps, (b) 1.758 ps, (c) 1.953 ps.

| Parameter        | Value          | Units                    |
|------------------|----------------|--------------------------|
| Fiber length     | 10             | m                        |
| Average power    | 10             | dBm                      |
| Dispersion       | 17.5           | ps/(km-nm)               |
| Dispersion slope | 0.09           | ps/(km-nm <sup>2</sup> ) |
| Jitter           | -2.539 – 2.148 | ps                       |

Table 4.9: Simulation configuration in measuring penalty due to timing jitter of the recovered clock signal.

After filtering is performed at the receiver, the unwanted bits appearing in the optical eye-diagrams are translated to amplitude distortions in the electrical eye-diagram, as the target and adjacent pulses overlap in the time domain. As the peaks of these two pulses are separated by 6.25 ps in the optical eye-diagrams, evidence of the same separation can be seen in the electrical eye-diagrams. As the pulses are broadened by the filter in the receiver, the placement in time of their peaks will remain unchanged. Both of the above effects lead to a decrease in system performance. Figure 4.19 shows the time-domain representation of the values simulated in Figure 4.18, and shows graphically the effects explained above.

The jitter tolerance (JT) is defined as the amount of jitter that can be withstood by the clock-and-data recovery (CDR) circuit, while achieving a specified amount of penalty[35]. Keeping with the other definitions of performance presented in this work, it was decided that a 1 dB penalty may be allotted as a maximum. The results of these simulations are displayed in Figure 4.20 according to Table 4.9. The results show that

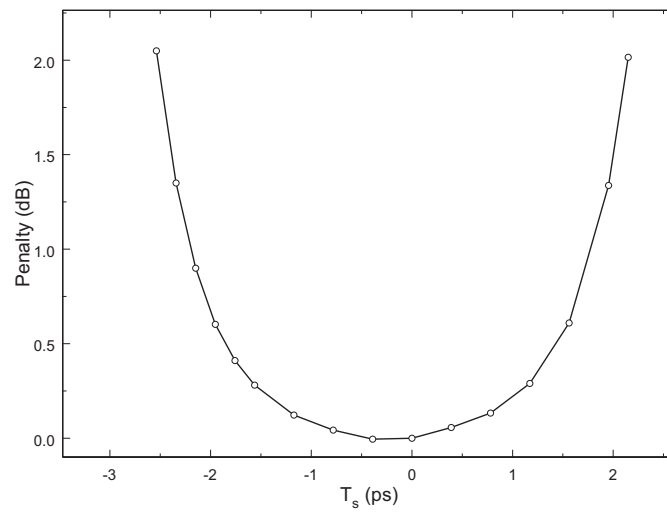


Figure 4.20: Penalty (EOP) due to change in  $T_s$  on the demultiplexing EAM gates.

in order to operate below 1-dB of system penalty, the effects of timing jitter on the demultiplexer must result in  $mT_s$  between -2.192 ps to 1.772 ps. The differences in these reported values are due to the shape the pulse takes, as well as the location of the optimal sampling time. The value of  $s_{t,new}$  will be unique to each amount of penalty seen at the receiver as the optimal sampling time  $s_t$  will also change. In comparing Figures 4.16 and 4.20, it can be concluded that the sensitivity the EAM gates exhibit, clearly dominate the system performance concerns with respect to timing jitter.

## 4.5 Polarization Mode Dispersion

### 4.5.1 Introduction

To effectively model the effects on OTDM system performance brought about by PMD, the principle states model was adopted. The optical pulse is split into two pulses, each arriving at the output of the fiber at different times[33]. This results in the optical energy of the pulse at the input becoming dispersed in time as it arrives at the output[33]. The model assumes that the differential group delay (DGD) caused by PMD is small in comparison to the bit period[33].

### 4.5.2 System Tolerance

To recreate the effect of pulse broadening due to PMD in MatLab, two signals were propagated through an optical fiber, representing both the perpendicular and parallel polarized modes. To mimic the delay associated with the fast and slow moving components, an artificial amount of delay between the two was inserted by shifting the array that defines the OTDM signal in the perpendicular mode. In combining

| Parameter            | Value    | Units                    |
|----------------------|----------|--------------------------|
| Fiber length         | 10       | m                        |
| Average power        | 10       | dBm                      |
| Dispersion           | 17.5     | ps/(km-nm)               |
| Dispersion slope     | 0.09     | ps/(km-nm <sup>2</sup> ) |
| Delay in $E_{\perp}$ | 0 – 3.52 | ps                       |

Table 4.10: Simulation configuration in measuring penalty due to PMD.

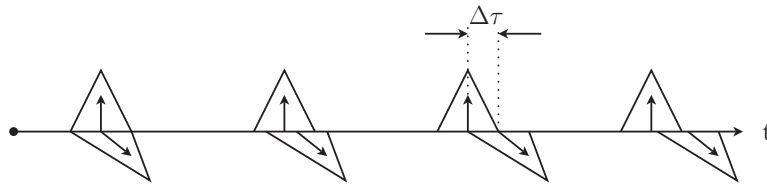


Figure 4.21: Illustration showing the delay in arrival time associated with PMD.

the two modes at the output of the fiber by,

$$E_{out} = \hat{x}E_{\parallel} + \hat{y}E_{\perp} \quad (4.4)$$

it is assumed that over the course of transmission the periodic exchange of power has rendered the average power in both states equal[33]. As Eq. (4.4) will intuitively lead to pulse broadening brought about by this artificial PMD (shown in Figure 4.21), the resulting bit stream was passed on to the error detection and penalty measurement routine. Table 4.10 outlines the operating conditions for the following MatLab simulations. Performing this simulation over 10 m of SMF renders the results effectively free of distortions due to dispersion and/or dispersion slope.

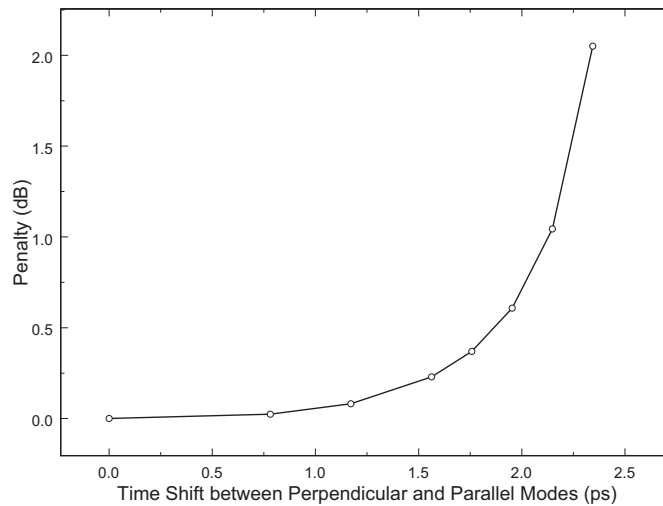


Figure 4.22: Penalty (EOP) due to increased amount of PMD.

To relate the amount of penalty associated with a shift in orthogonally polarized modes, we must first define a benchmark which would be tolerable by the system. The maximum amount of penalty allowable is defined as 1 dB for a fraction of time of 30 minutes per year[33]. As the time domain optical signal is represented by 32 samples per bit, a shift of one sample corresponds to a 0.195 ps shift within the bit period (6.25 ps). To achieve less than 1 dB of penalty a maximum shift of approximately 2.15 ps is permitted. The results of this simulation may be observed in Figure 4.22. Figure 4.23 shows the electrical eye-diagram evolution in performing the above simulation.

The eye-diagrams taken before and after the demultiplexer show an interesting result. Figure 4.24 shows that upon exiting the fiber, the two modes have recombined to create what appears to be two pulses within the same bit period. This can also be seen when observing the time-domain plots of Figure 4.25. This effect is translated

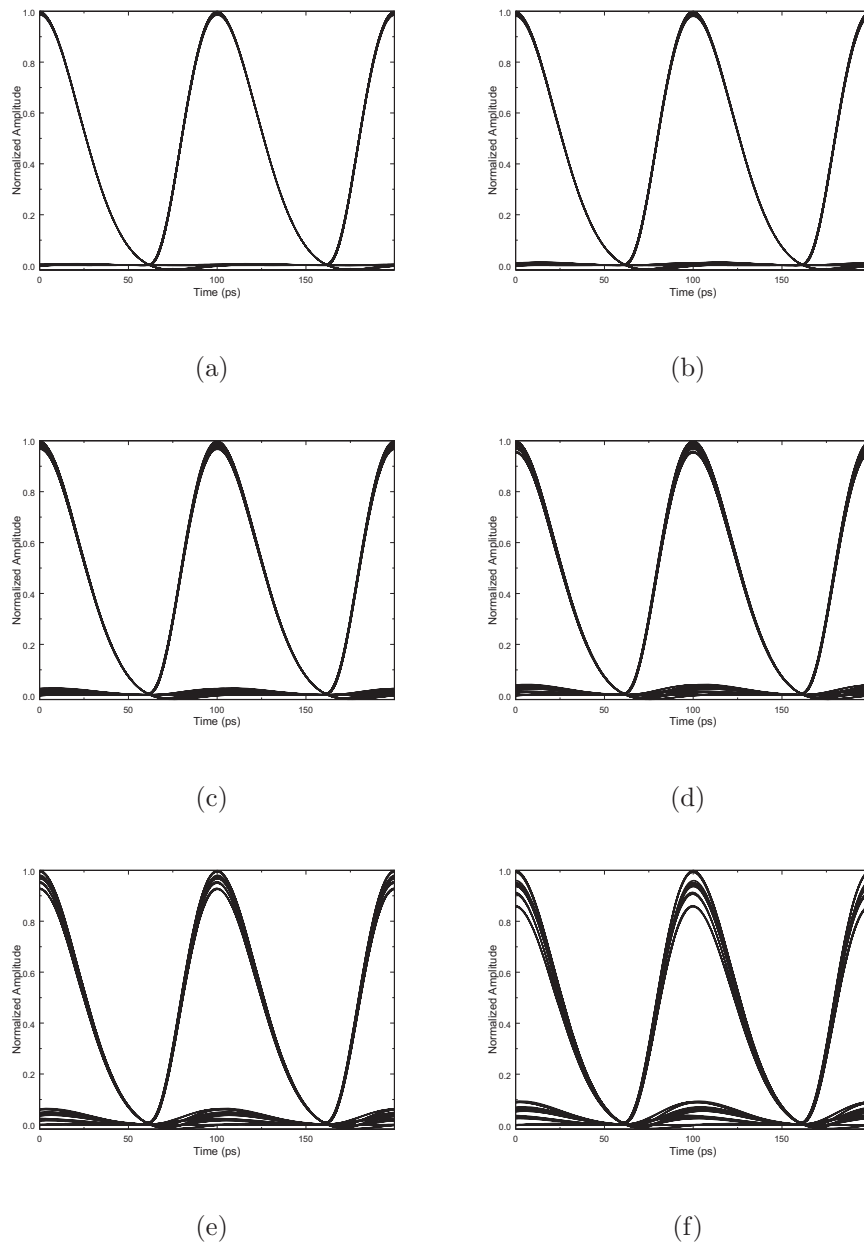


Figure 4.23: Electrical eye-diagrams, taken after the receiver, for a shift of the perpendicular travelling mode by: (a) 0.39 ps, (b) 0.78 ps, (c) 1.17 ps, (d) 1.56 ps, (e) 1.95 ps, and (f) 2.73 ps.

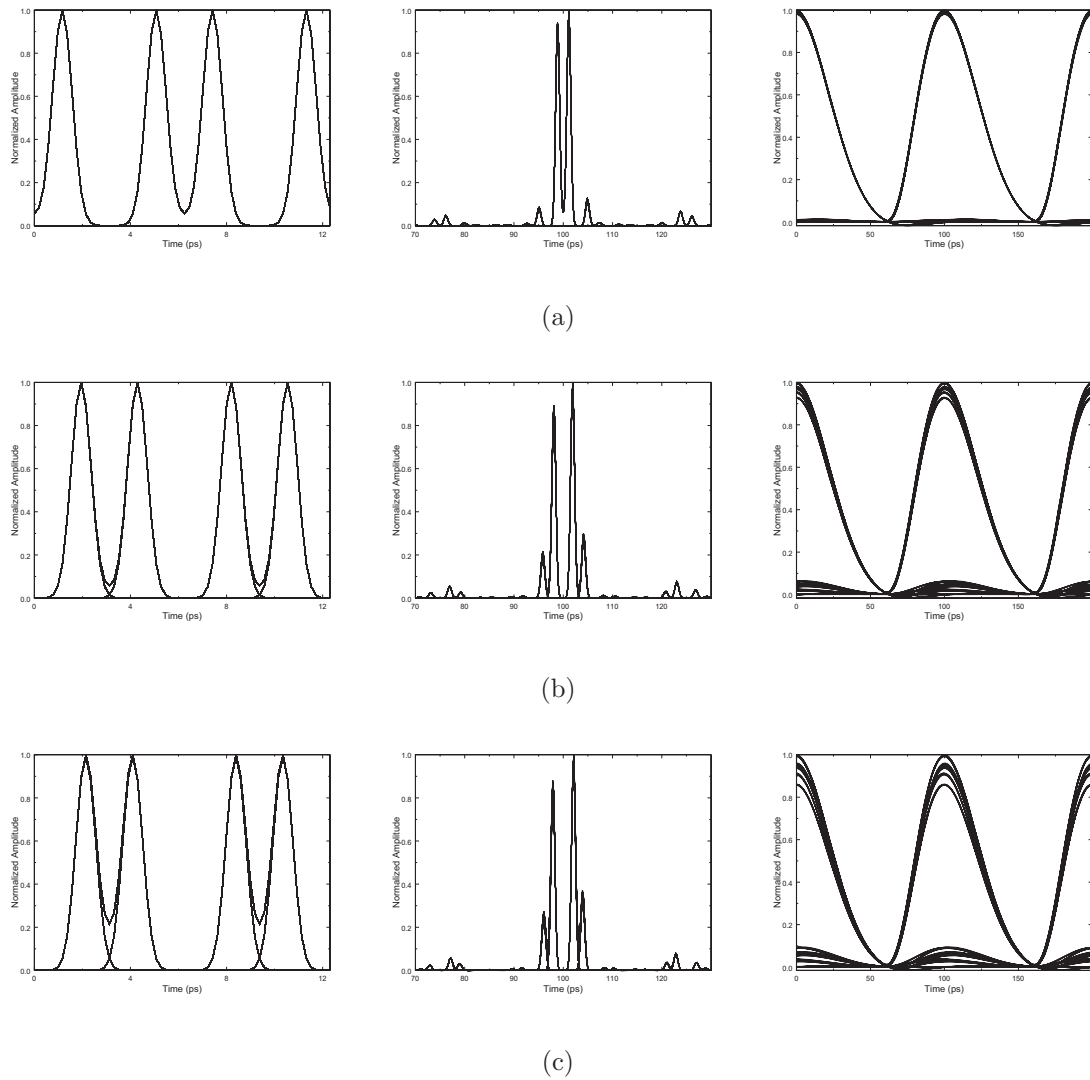
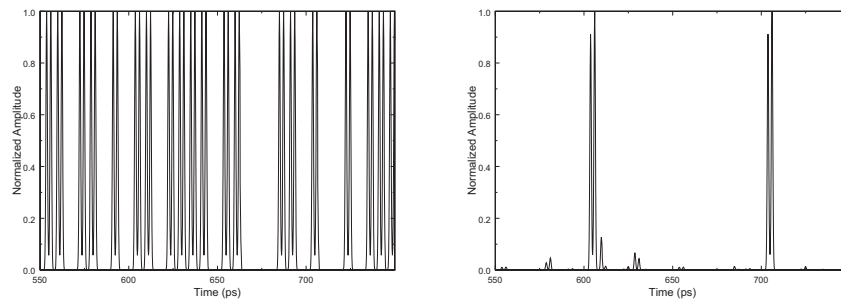
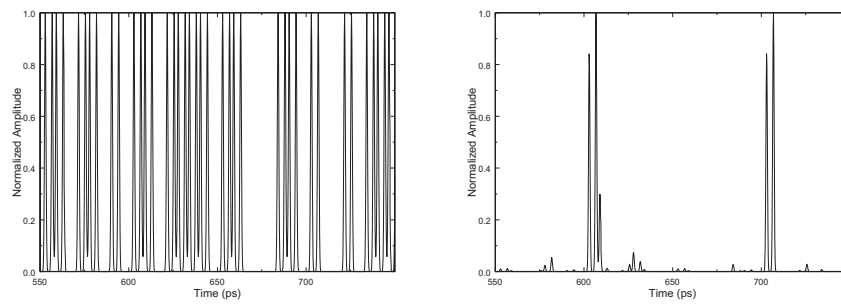


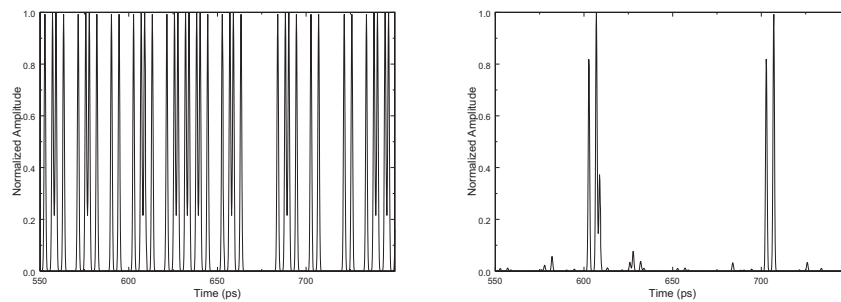
Figure 4.24: From left to right: optical eye-diagrams taken before the demultiplexer, after the demultiplexer, followed by the electrical eye-diagram, for a shift of the perpendicularly travelling mode by: (a) 0.78 ps, (b) 1.95 ps, (c) 2.73 ps.



(a)



(b)



(c)

Figure 4.25: From left to right: optical time-domain OTDM signal taken before and after the demultiplexer, for a shift of the perpendicularly travelling mode by: (a) 0.78 ps, (b) 1.95 ps, (c) 2.73 ps.

into an amplitude distortion in the electrical domain after being filtered through the pre-amplified receiver. A larger shift of the orthogonal modes would eventually lead to eye-closure. This is due to the alignment of the EAM gates relative to the OTDM signal. Each EAM gate is aligned to the split pulses in the same manner as if they had not been split through PMD. The peak (where bits are totally passed) of each EAM gate lies directly in between the resulting split pulses.

## 4.6 Non-Linear Effects

### 4.6.1 Introduction

The method used to simulate the effects of non-linear responses in an optical fiber were previously discussed in Chapter 2. It was also stated, and shown by the above discussion, that by effectively reducing the optical pulse power, the effects of such nonlinearities (i.e. self phase modulation (SPM)) may be minimized. However, typical optical systems, especially long-haul networks, contain periodically placed optical amplifiers that will increase the transmitted power at the input of each span. This is done to compensate for fiber losses. While increasing the optical power through amplifiers does not always lead to the necessity of characterizing non-linear effects, the effects from nonlinearities limit the amount of power that should be chosen as an input to an optical fiber.

### 4.6.2 System Tolerance

During simulation, a step size length of 500 m was determined by running the simulator for multiple step sizes. Recall that the accuracy of the fixed step size method

is only improved upon by decreasing this value. The distance of 500 m was settled upon when the change in EOP was negligible after reducing it further. Reducing the step size further posed a trade-off between marginally improved accuracy and computation time in the simulator.

During previous simulations, an input power of 10 dBm was used and the non-linear term of the propagation equation neglected. The effect and onset of nonlinearities, such as SPM, may cause system performance to behave unfavourably; especially in the presence of dispersion. In the absence of dispersion, the effects of intra-channel four wave mixing (FWM) and intra-channel cross-phase modulation (XPM) may also contribute negatively to system performance. In the following discussion and simulation, these effects are neglected.

The effect that non-linearities impose on the resulting dispersion tolerance are of importance, as OTDM signals are considered dispersion limited. Large transmission powers that may arise due to the periodic placement of amplifiers can result in elevated levels of degradation. This is especially true when traversing DCFs as their effective areas are substantially smaller than those of SMFs. Recall from Eq. (3.25) the inverse proportionality effective area has to change in refractive index; a smaller value of  $A_{eff}$  will result in a larger change. This effect is typically subsided due to the lower power realized at the input to the DCF (neglecting any amplification).

In a practical field implementation, the periodic amplifiers mentioned above would be placed between the SMF and DCF spans as shown in Figure 4.26. However, in considering the penalties brought on by non-linear behaviour within the optical fiber, there exists a limit as to how much gain may be applied without degrading the system performance substantially. To adequately show these effects, a simulation was devised

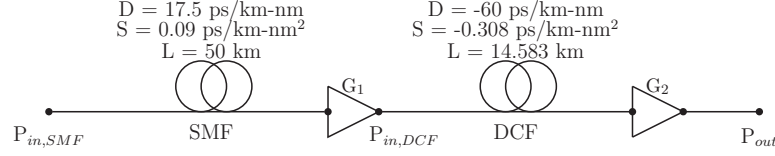


Figure 4.26: Diagram outlining the placement of amplifiers in a typical fiber transmission link.

in which an amplifier was placed both between the SMF and DCF, and after the DCF. Typically, the values of  $G_1$  and  $G_2$  are chosen such that  $P_{in,SMF} = P_{out}$ .

Table 4.11 outlines the operating conditions in performing the above described simulation. The input powers to both the SMF and DCF were chosen as to avoid possible negative values of  $G_1$  and  $G_2$ .

As SMF and DCF have known attenuation coefficients of 0.22 dB/km and 0.33 dB/km,  $G_1$  may be described as,

$$G_1(dB) = P_{in,DCF} - P_{in,SMF} + \left(0.22 \frac{dB}{km}\right) L_{SMF} \quad (4.5)$$

and  $G_2$  as,

$$G_2(dB) = P_{out} - P_{in,DCF} + \left(0.33 \frac{dB}{km}\right) L_{DCF} \quad (4.6)$$

to satisfy the  $P_{in,SMF} = P_{out}$  condition, where  $L_{SMF}$  and  $L_{DCF}$  are the respective fiber lengths. Contour plots were constructed in Figure 4.27 and Figure 4.28 to show what values of  $G_1$  and  $G_2$  are necessary to achieve the desired fiber input and output powers. From Eq. (4.5) and Eq. (4.6), it can be shown that,

$$G_1 + G_2 = \left(0.22 \frac{dB}{km}\right) L_{SMF} + \left(0.33 \frac{dB}{km}\right) L_{DCF} \quad (4.7)$$

which is conveyed by Figures 4.27 and 4.28.

| Parameter            | Value      | Units                    |
|----------------------|------------|--------------------------|
| SMF fiber length     | 50         | km                       |
| SMF dispersion       | 17.5       | ps/(km-nm)               |
| SMF dispersion slope | 0.09       | ps/(km-nm <sup>2</sup> ) |
| SMF input power      | 7.6 – 15.1 | dBm                      |
| DCF fiber length     | 14.583     | km                       |
| DCF dispersion       | -60.0      | ps/(km-nm)               |
| DCF dispersion slope | -0.308     | ps/(km-nm <sup>2</sup> ) |
| DCF input power      | 5.0 – 12.5 | dB                       |
| Step Size            | 500        | m                        |

Table 4.11: Simulation configuration in measuring penalty resulting from imperfect dispersion and dispersion slope compensation due to non-linear effects.

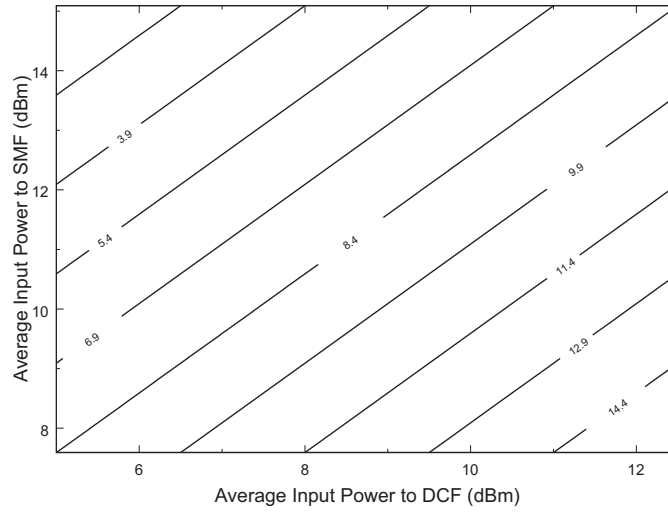


Figure 4.27: Resulting values of  $G_1$  due to changes of  $P_{in,SMF}$  and  $P_{in,DCF}$ .

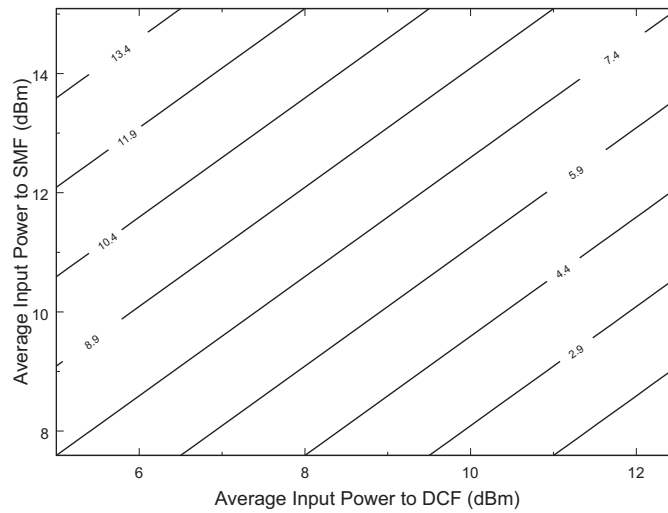


Figure 4.28: Resulting values of  $G_2$  due to changes of  $P_{in,SMF}$  and  $P_{in,DCF}$ .

From the above described simulation, the resulting contour plot may be seen in Figure 4.29. The results show that while the input power is kept low (system is in linear operation), there is a slow changing penalty relative to a B2B eye-diagram. Due to the results of Section 4.3.2, it should be clear that without the presence of  $G_1$  and  $G_2$ , the resulting EOP would be zero as the values listed in Table 4.11 for the SMF and DCF result in perfect compensation. Note that in the presence of the aforementioned intra-channel effects, additional penalty may result. The contour also shows that as the input power to either the SMF or DCF increases, dispersion and dispersion slope compensation are no longer fully realized. In defining the system tolerance toward non-linear effects, the values of  $G_1$  and  $G_2$  should be chosen such that the EOP does not exceed 1 dB. Additionally, typical systems are designed to maximize the input power to the transmission fiber (SMF), and not to that of the compensating fiber (DCF). Under these conditions, the input power to the SMF and DCF should be chosen at 15.1 dBm and 8.16 dBm respectively. The resulting values of  $G_1$  and  $G_2$  are 4.1 dB and 11.75 dB.

The above result is important in designing OTDM systems as researchers are interested in compensating for fiber losses as much as possible through the use of amplifiers such as erbium-doped fiber amplifiers (EDFAs). While dispersive effects may be imperfectly compensated, EDFAs placed between the SMF and DCF spans would give the desired effect. This results in a trade-off between compensating for said losses, and signal degradation by non-linear effects such as SPM. Furthermore, these results are also applicable to WDM systems. However, further degradation would occur for lower input powers due to XPM. The penalty would also increase more rapidly compared to the single channel case.

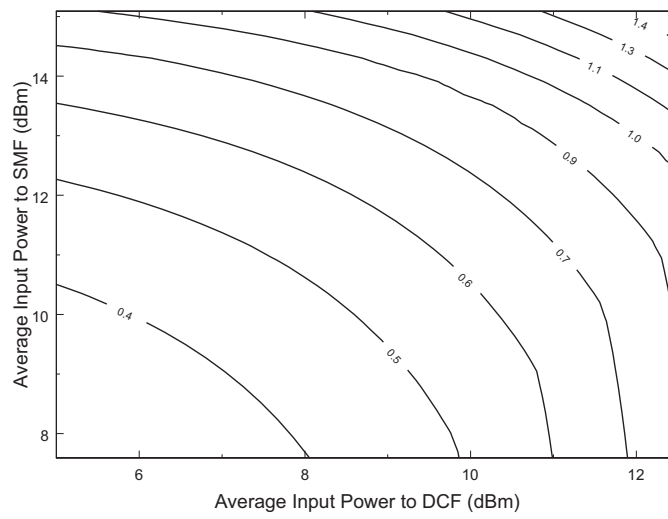


Figure 4.29: Penalty (EOP) due to changes in both SMF and DCF input powers.

# Chapter 5

## Conclusions

### 5.1 Thesis Contributions

The material outlined in this thesis has contributed to an understanding of the governing tolerances associated with optical time division multiplexing (OTDM) signal transmission. An extraordinary amount of care was taken to effectively model the system, from transmission through to reception, including: the generation of optimal pulse shape, the maintenance of a pseudo-random bit sequence (PRBS), the optimization of the gating devices, and penalty measurement accuracy. The simulations performed concluded the tolerance an OTDM signal exhibits towards: first and second order dispersion, timing jitter, polarization mode dispersion (PMD), and non-linear effects. These values are of particular importance in OTDM system design as they are the major contributors to system performance degradation.

It has been shown that the dispersion tolerance of such as system is  $\pm 1.7$  ps/nm, and the slope tolerance is  $\pm 2.2$  ps/nm<sup>2</sup> over 50 km of fiber when neglecting non-linear effects. In the design of dispersion compensating systems by means of dispersion

compensating fiber (DCF), it was shown the DCF must be within 0.2% of the optimal calculated value to avoid unreasonable values of penalty. In regards to timing jitter, it was concluded that the effect on the electro-absorption modulator (EAM) gates would be a limiting factor in transmission. An offset of the switching window between -2.192 ps to 1.772 ps has been determined to be tolerable. PMD simulations have shown that a maximum shift of 2.15 ps between parallel and perpendicularly travelling modes is allowable to maintain less than 1 dB of penalty. Lastly, the effects of fiber non-linearities were simulated outlining their effects as an additional source of pulse broadening; especially in the presence of dispersion and dispersion slope. Using typical amplifier placement within a optical fiber span, it was determined that the gain resulting from the amplifier located after the single-mode fiber (SMF) span should be chosen to be 4.1 dB. Coincidentally, the gain resulting from the amplifier placed after the DCF should be chosen to be 11.75 dB. These values were determined by maximizing the launch power into the transmission fiber while maintaining less than 1-dB of eye-opening penalty (EOP).

With the knowledge of these defining sources of system penalty, the design of a physical system implementation may be achieved with greater ease and understanding. Furthermore, the sources of penalties that may be observed can be related to the causes presented in this document through the use of eye-diagrams and their explanations.

## 5.2 The Future of OTDM

As observed from the results of this thesis, much improvement may be needed to facilitate a widespread deployment of OTDM systems. Technologies such as adaptive dispersion, and dispersion slope compensation (by use of tunable gratings[36, 37]), as well as adaptive PMD compensation (using the configuration described in [38]), may be useful as the degree at which these impairments affect the signal is temperature dependant. Coding methods or different modulation formats (such as carrier-suppressed return-to-zero (CS-RZ) or RZ-differential-phase-shift-keying (RZ-DPSK)[39, 40]), and/or pre-compensation techniques (in which the signal is pre-distorted[41]) may also provide additional security against the generation of bit errors.

As high bandwidth demands are expected to increase further, OTDM technologies will undoubtedly be coupled with the techniques of wavelength division multiplexing (WDM) networks. Recently, all optical techniques have been developed in which OTDM-to-WDM signal conversion is made possible by use of cross-absorption modulation in EAMs[42]. By merging these two methods, capacities larger than one terabit per second may be realized. As the combination of OTDM and WDM may form the future of high speed optical communications, the details presented in this thesis are of much use for further development and research.

# Bibliography

- [1] U. Feiste, R. Ludwig, C. Schubert, J. Berger, C. Schmidt, H. Weber, B. Schmauss, A. Munk, B. Buchold, D. Briggmann, F. Kueppers, and J. Rumpf, “160 Gbit/s field transmission over 116km standard single mode fiber using 160 Gbit/s OTDM and 40 Gbit/s ETDM demultiplexer,” *IEE Proc. Optoelectron.*, vol. 148, no. 4, pp. 171–175, Aug. 2001.
- [2] G. P. Agrawal, *Fiber-optic communication systems*, 3rd ed. New York: John Wiley & Sons, Inc., 2002.
- [3] A. Gnauck, G. Charlet, P. Tran, P. Winzer, C. Doerr, J. Centanni, E. Burrows, T. Kawanishi, T. Sakamoto, and K. Higuma, “25.7-tb/s WDM transmission of polarization-multiplexed rz-dqpsk signals,” *IEEE Journ. of Lightwave Technol.*, vol. 26, no. 1, pp. 79–84, Jan. 2008.
- [4] H. Chou, Z. Hu, J. Bowers, D. Blumenthal, K. Nishimura, R. Inohara, and M. Usami, “Simultaneous 160-Gb/s demultiplexing and clock recovery by utilizing microwave harmonic frequencies in a travelling-wave electroabsorption modulator,” *IEEE Photon. Technol. Lett.*, vol. 16, no. 2, pp. 608–610, Feb. 2004.

- [5] I. Shake, H. Takara, K. Uchiyama, I. Ogawa, T. Kitoh, T. Kitagawa, M. Okamoto, K. Magari, Y. Suzuki, and T. Morioka, "160 Gbit/s full OTDM demultiplexing based on FWM of SOA array integrated on planer lightwave circuit," in *Proc. 27th Eur. Conf. on Opt. Comm.*, 2001, pp. 182–183.
- [6] T. Miyazaki and F. Kubota, "Simultaneous demultiplexing and clock recovery for 160-Gb/s OTDM signal using a symmetric MachZehnder switch in electrooptic feedback loop," *IEEE Photon. Technol. Lett.*, vol. 15, no. 7, pp. 1008–1010, July 2003.
- [7] J. Turkiewicz, E. Tangdiongga, G. Lehmann, H. Rohde, W. Schairer, Y. Zhou, E. Sikora, A. Lord, D. Payne, G. Khoe, and H. de Waardt, "160 Gb/s OTDM networking using deployed fiber," *IEEE Journ. of Lightwave Technol.*, vol. 3, no. 1, pp. 225–235, Jan. 2005.
- [8] K. Tajima, S. Nakamura, and Y. Sugimoto, "Ultrafast polarization-discriminating Mach-Zehnder all-optical switch," *IEEE Appl. Phys. Lett.*, vol. 67, no. 25, pp. 3709–3711, 1995.
- [9] N. Patel, K. Rauschenbach, and K. Hall, "40 gb/s demultiplexing using an ultrafast nonlinear interferometer (UNI)," *IEEE Photon. Technol. Lett.*, vol. 8, no. 12, pp. 1695–1697, Dec. 1996.
- [10] C. Schubert, S. Diez, J. Berger, R. Ludwig, U. Feiste, H. Weber, G. Toptchiyski, K. Petermann, and V. Krajinovic, "160-Gb/s all-optical demultiplexing using a gain-transparent ultrafast-nonlinear interferometer (GT-UNI)," *IEEE Photon. Technol. Lett.*, vol. 13, no. 5, pp. 475–477, May 2001.

- [11] J. Zhang, M. Yao, Q. Xu, H. Zhang, C. Peng, and Y. Gao, "Interferometric noise in optical time division multiplexing transmission system," *IEEE Journ. of Lightwave Technol.*, vol. 20, no. 8, pp. 1329–1334, Aug. 2002.
- [12] H. Chou and J. Bowers, "High-speed otdm and wdm networks using traveling-wave electroabsorption modulators," *IEEE Journ. of Selected Topics in Quantum Electronics*, vol. 13, no. 1, pp. 58–69, Jan. 2007.
- [13] D. Tong, K. Deng, B. Mikkelsen, G. Raybon, K. Dreyer, and J. Johnson, "160 Gbit/s clock recovery using electroabsorption modulator-based phase locked loop," *IEEE Electron. Lett.*, vol. 36, no. 23, pp. 1951–1952, Nov. 2000.
- [14] J. Turiewicz, E. Tangdionga, G. Khoe, and H. de Waardt, "Clock recovery and demultiplexing performance of 160-Gb/s OTDM field experiments," *IEEE Photon. Technol. Lett.*, vol. 16, no. 6, pp. 1555–1557, June 2004.
- [15] J. Auge, M. Cavallari, M. Jones, P. Kean, D. Watley, and A. Hadjifotiou, "Single channel 160 GB/s OTDM propagation over 480 km of standard fiber using a 40 GHz semiconductor mode-locked laser pulse source," in *Proc. Optical Fiber Communication Conf. (OFC)*, 2002, pp. TuA3–4 – TuA3–5.
- [16] J. Qiu, G. Zhou, J. Wu, and J. Lin, "8 x 10 gb/s otdm signal demultiplexing by using self-cascaded electro-absorption modulator (eam) after transmitting over 300 km," *IEEE Photon. Technol. Lett.*, vol. 18, no. 23, pp. 2541–2543, Dec. 2006.
- [17] B. Mikkelsen, G. Raybon, R. Essiambre, A. Stentz, T. Nielsen, D. Peckham, L. Hsu, L. Gruner-Nielsen, K. Dreyer, and J. Johnson, "320-Gb/s single-channel

- pseudolinear transmission over 200 km of nonzero-dispersion fiber,” *IEEE Photon. Technol. Lett.*, vol. 12, no. 10, pp. 1400–1402, Oct. 2000.
- [18] J. Yu, K. Kojima, and N. Chand, “Simultaneous demultiplexing and clock recovery of 80 Gb/s OTDM signals using a tandem electro-absorption modulator,” in *Proc. Optical Fiber Communication Conf. (OFC)*, 2001, pp. 358–359.
- [19] *Eye measurements on optical RZ signals*, Printed, Tektronix, 2002.
- [20] J. Downie, “Relationship of Q penalty to eye-closure penalty for NRZ and RZ signals with signal-dependent noise,” *IEEE Journ. of Lightwave Technol.*, vol. 23, no. 6, pp. 2031–2038, June 2005.
- [21] J. G. Proakis, *Digital Communications*. New York: McGraw-Hill, 2001.
- [22] R. Ludwig, U. Feiste, C. Schmidt, C. Schubert, J. Berger, E. Hilliger, M. Kroh, T. Yamamoto, and C. Weinert, “Enabling transmission at 160 Gbit/s,” in *Proc. Optical Fiber Communication Conf. (OFC)*, 2002, pp. TuA1-1 – TuA1-2.
- [23] B. Konrad, K. Petermann, J. Berger, C. W. R. Ludwig, H. Weber, and B. Schmauss, “Impact of fiber chromatic dispersion in high-speed TDM transmission systems,” *IEEE Journ. of Lightwave Technol.*, vol. 20, no. 12, pp. 2129–2135, Dec. 2002.
- [24] B. Konrad and K. Petermann, “Optimum fiber dispersion in high-speed TDM systems,” *IEEE Photon. Technol. Lett.*, vol. 13, no. 4, pp. 299–301, Apr. 2001.
- [25] G. P. Agrawal, *Nonlinear fiber optics*, 3rd ed. San Diego: Academic Press, Inc., 2001.

- [26] O. Sinkin, R. Holzlohner, J. Zweck, and C. Menyuk, "Optimization of the split-step Fourier method in modeling optical fiber communications systems," *IEEE Journ. of Lightwave Technol.*, vol. 21, no. 1, pp. 61–68, Jan. 2003.
- [27] O. Mitomi, S. Nojima, I. Kotaka, K. Wakita, K. Kawano, and M. Naganuma, "Chirping characteristic and frequency response of MQW optical intensity modulator," *IEEE Journ. of Lightwave Technol.*, vol. 10, no. 1, pp. 71–77, Jan. 1992.
- [28] Y. S. Kang, S. B. Kim, Y. D. Chung, and J. Kim, "Low insertion loss electroabsorption modulator based on dual waveguide structure with spot size converter," in *Proc. Optical Fiber Communication Conf. (OFC)*, 2005, pp. TuBB2–406 – TuBB2–407.
- [29] P. Reyes, N. Litchinitser, M. Sumetsky, and P. Westbrook, "160-Gb/s tunable dispersion slope compensator using a chirped fiber Bragg grating and a quadratic heater," *IEEE Photon. Technol. Lett.*, vol. 17, no. 4, pp. 831–833, Apr. 2005.
- [30] R. Stephens, "Analyzing jitter at high data rates," *IEEE Opt. Comm.*, pp. S6–S10, Feb. 2004.
- [31] I. Monfils, "All-optical clock recovery in a q-switching self-pulsating dfb laser," Ph.D. dissertation, Queen's University, 2007.
- [32] D. Lee, "Analysis of jitter in phase locked loops," *IEEE Trans. Circuits Syst.*, vol. 49, no. 11, pp. 704–711, Nov. 2002.
- [33] C. D. Poole and J. Nagel, *Optical fiber telecommunications volume IIIA - Chapter 6: Polarization effects in lightwave systems*. Lucent Technologies, 1997.

- [34] S. Vorbeck and R. Leppa, “Dispersion and dispersion slope tolerance of 160-Gb/s systems, considering the temperature dependence of chromatic dispersion,” *IEEE Photon. Technol. Lett.*, vol. 15, no. 10, pp. 1470–1472, Oct. 2003.
- [35] C. Pease and D. Babic, “Practical measurement of timing jitter contributed by a clock-and-data recovery circuit,” *IEEE Trans. Circuits Syst.*, vol. 52, no. 1, pp. 119–126, Jan. 2005.
- [36] S. Vorbeck and R. Leppa, “Dispersion and dispersion slope tolerance of 160-gb/s systems, considering the temperature dependence of chromatic dispersion,” *IEEE Photon. Technol. Lett.*, vol. 15, no. 10, pp. 1470–1472, Oct. 2003.
- [37] T. Inui, T. Komukai, M. Nakazawa, K. Suzuki, K. Tamura, K. Uchiyama, and T. Morioka, “Adaptive dispersion slope equalizer using a nonlinearly chirped fiber bragg grating pair with a novel dispersion detection technique,” *IEEE Photon. Technol. Lett.*, vol. 14, no. 4, pp. 549–551, Apr. 2002.
- [38] S. Kieckbusch, S. Ferber, H. Rosenfeldt, R. Ludwig, C. Boerner, A. Ehrhardt, E. Brinkmeyer, and H. Weber, “Automatic pmd compensator in a 160-gb/s otdm transmission over deployed fiber using rz-dpsk modulation format,” *IEEE Journ. of Lightwave Technol.*, vol. 23, no. 1, pp. 165–171, Jan. 2005.
- [39] J. Seoane, A. Clausen, L. Oxenlowe, M. Galili, T. Tokle, and P. Jeppesen, “Enabling technologies for otdm networks at 160 gbit/s and beyond,” in *Proc. Lasers and Electro-Optics Society (LEOS)*, 2005, pp. MG1–81 – MG1–82.

- [40] H. Murai, M. Kagawa, H. Tsuji, and K. Fujii, "Ea modulator based optical time division multiplexing/demultiplexing techniques for 160-gb/s signal transmission," *IEEE Journ. of Lightwave Technol.*, vol. 13, no. 1, pp. 70–79, Jan. 2007.
- [41] I. Papagiannakis, D. Klonidis, V. Curri, P. Poggiolini, G. Bosco, R. Killey, M. Omella, J. Prat, D. Fonseca, A. Teixeira, A. Cartaxo, R. Freund, E. G. A. Bogris, A. Birbas, and I. Tomkos, "Electronic distortion compensation in the mitigation of optical transmission impairments: the view of joint project on mitigation of optical transmission impairments by electronic means ephoton/one1 project," *IET Optoelectronics*, vol. 3, no. 2, pp. 73–85, Mar. 2009.
- [42] G. Lei, C. Shu, and M. Fok, "All-optical otdm-to-wdm signal conversion using cross-absorption modulation with time- and wavelength-interleaved short pulses," *IEEE Photon. Technol. Lett.*, vol. 22, no. 8, pp. 571–573, Apr. 2010.